FILE COPY
NO. 2-W

CASE FILE
COPY

N 62 65800

ARR No. 4K09

NATIONAL ADVISORY COMMITTEE FOR AERONAUTICS

WARTIME REPORT

ORIGINALLY ISSUED
April 1945 as
Advance Restricted Report 4K09

MEASUREMENTS IN FLIGHT OF THE PRESSURE DISTRIBUTION ON THE RIGHT WING OF A P-39N-1 AIRPLANE AT SEVERAL VALUES OF MACH NUMBER

By Lawrence A. Clousing, William N. Turner
and L. Stewart Rolls

Ames Aeronautical Laboratory
Moffett Field, California

NACA FILE COPY
To be returned to
the files of the National
Advisory Committee
for Aeronautics
Washington, D. C.

WASHINGTON

NACA WARTIME REPORTS are reprints of papers originally issued to provide rapid distribution of advance research results to an authorized group requiring them for the war effort. They were previously held under a security status but are now unclassified. Some of these reports were not technically edited. All have been reproduced without change in order to expedite general distribution.

NACA ARR No. 4K09

NATIONAL ADVISORY COMMITTEE FOR AERONAUTICS

ADVANCE RESTRICTED REPORT

MEASUREMENTS IN FLIGHT OF THE PRESSURE DISTRIBUTION ON THE RIGHT WING OF A P-39N-1 AIRPLANE AT SEVERAL VALUES OF MACH NUMBER

By Lawrence A. Clousing, William N. Turner, and L. Stewart Rolls

SUMMARY

Pressure-distribution measurements were made on the right wing of a P-39N-1 airplane at values of Mach number up to 0.80. The results showed that a considerable portion of the lift was carried by components of the airplane other than the wings, and that the proportion of lift carried by the wings may vary considerably with Mach number, thus changing the bending moment at the wing root whether or not there is a shift in the lateral position of the center of pressure. It was also shown that the center of pressure does not necessarily move outward at high Mach numbers, even though the wing-thickness ratio decreases toward the wing tip. The wing pitching-moment coefficient increased sharply in a negative direction at a Mach number slightly higher than the critical Mach number. The lift-curve slope increased with Mach number up to values of Mach number which, in some instances, were considerably above the critical value. Pressures inside the wing were small and negative.

INTRODUCTION

Measurements in flight of the pressure distribution on the wings of airplanes were conducted by the NACA several years ago (references 1 to 3) for the purpose of establishing the air loads obtained in various maneuvers. Because of the relatively low speeds attainable with these airplanes, information on the effects of high Mach and Reynolds numbers, needed by designers of present-day airplanes, was not obtained.

The speeds reached by modern aircraft are often so high that compression shocks develop in the air flow over the wing (and other parts of the airplane), resulting in changes in the air-load distribution. Wind-tunnel tests have shown that the center of pressure on a wing moves backward as the shock stall develops. In addition, because of the spanwise variation in thickness ratio of most present-day airplane wings, it has been generally considered that the inboard sections would stall first, causing the center of pressure to move outward also, thus increasing, perhaps to a dangerous degree, the bending moment at the wing root for a given value of lift.

As actual data had not been obtained in flight on the nature of such a variation, the Air Technical Service Command, U.S. Army Air Forces, requested that these tests be undertaken. Measurements were made of the pressure distribution in flight on the right wing of a P-39N-1 airplane. It was possible to make measurements up to a Mach number of approximately 0.80, the highest value attainable with this airplane when dived vertically from its operating ceiling of about 34,000 feet to a minimum altitude of about 10,000 feet.

DESCRIPTION OF THE AIRPLANE

The Bell P-39N-1 airplane is a single-engine, single-place, low-wing, cantilever monoplane equipped with partial-span split flaps and tricycle retractable landing gear. Figures 1 and 2 are photographs of the airplane as instrumented for the flight tests. Figure 3 is a general arrangement drawing of the airplane. The specifications of the airplane, which were taken mainly from reference 4, are as follows:

Airplane, general

Span	34.0 ft
Length	30.167 ft
Height	9.271 ft

Wing

Airfoil section, root (22 in. outboard of airplane center line)	NACA 0015
Airfoil section, tip (projected, 204 in. outboard of airplane center line)	NACA 23009
Area, total, including ailerons and section projected through the fuselage	213.22 sq ft

Chord, root (22 in. outboard of airplane center line)	8.22 ft
Chord, tip (projected, 204 in. outboard of airplane center line)	4.17 ft
Chord, mean aerodynamic	6.72 ft
Dihedral, at 30 percent upper ordinate	4.0°
Incidence, with respect to thrust line	2.0°
Sweepback, leading edge	4.58°

Horizontal tail

Span	13.00 ft
Area	40.99 sq ft
Distance, normal-gross-weight center of gravity to one-third maximum chord point	14.95 ft

Weight

Empty	5761 lb
Normal gross	7629 lb
As flown	7730 to 7460 lb

Center-of-gravity positions

Normal gross weight, gear up	0.285 M.A.C.
As flown	0.288 to 0.291 M.A.C.

Engine

Type . . . . . Allison V-1710-85

Ratings, without ram:

	bhp	Manifold pressure (in. Hg)	rpm	Altitude (ft)	Time limit (min)
Take-off	1200	51.5	3000	Sea level	5
Military	1125	44.5	3000	15,500	15
Normal	1000	39.0	2600	14,000	None

Engine/propeller speed ratio 2.23:1

Propeller

Diameter	11.58 ft
Type	Aeroproducts three-blade hollow-steel selective automatic pitch

Blade model	A-20-156-17
Maximum pitch limits, nominal	23° to 63°
Maximum pitch limits, measured	28.7° to 65.3°
Direction of rotation, as seen by pilot	Clockwise

Curves of the wing thickness and geometric twist as measured on the airplane are shown in figures 4 and 5. The wing incidence, especially, is seen to vary somewhat from the specifications.

INSTRUMENTATION

Standard NACA photographically recording instruments were used to measure the following variables as a function of time: indicated airspeed, pressure altitude, approximate angle of attack, normal acceleration, engine manifold pressure, engine speed, propeller-blade angle, and air pressure over the wing. Free-air temperature, for use in evaluating Reynolds number, was determined from an indicator connected to a resistance bulb protruding below the right wing. The installation was calibrated for error due to the temperature rise caused by air compression at the bulb.

A free-swiveling airspeed head was mounted on a boom about 4 feet ahead of the leading edge of the right wing at a spanwise station about 7 feet inboard from the wing tip. The head consisted of two separate static-pressure tubes (for separate connections to the airspeed recorder and altitude recorder) with a single total-pressure tube between them. The airspeed and altitude recorders were mounted in the wing at the base of the boom. Calibration indicated that the lag in this system was negligible.

The recording and service static heads were calibrated for position error by comparing the readings of the respective altimeters with the known pressure altitude as the airplane was flown at several speeds past a reference height. It was assumed that the total pressure was measured correctly. The service system's airspeed error so determined is shown in figure 6. Calibration of the recording head in the Ames 16-foot wind tunnel showed that the error in recorded airspeed due to the difference in Mach number between the highest value obtained in the flight calibration (0.50) and the highest value obtained in the flight tests (0.80) was less than 1 percent.

Indicated airspeed as used in this report was computed according to the formula by which standard airspeed meters are graduated (gives true airspeed at standard sea-level conditions). The formula may be written as follows:

$$V_i = 1703\left[\left(\frac{H-p}{p_o} + 1\right)^{0.286} - 1\right]^{1/2}$$

where

V_i correct indicated airspeed, miles per hour

H free-stream total pressure

p free-stream static pressure

p_o standard atmospheric pressure at sea level

A 60-cell pressure recorder was used to measure the wing pressures. The recorder was mounted in the rear section of the fuselage between the oil tank and the baggage compartment. The pressures were measured at flush orifices at the locations listed in table I and shown in figure 7. The difference, shown in table I, between the measured leading-edge radius of the wing sections and that specified for the particular thickness ratio should be noted. An attempt was made to locate all upper-surface orifices directly above their lower-surface counterparts, so that accurate resultant pressures (the algebraic difference of the pressures at the top and bottom surfaces) at each orifice station could be measured. Interference of structural details prevented complete attainment of this condition in some instances. It is believed that the resulting errors, however, were not large enough to affect appreciably the final results of the investigation. Most of the tubing connecting the orifices with the pressure recorder was 9/64-inch-inside-diameter aluminum tubing or 3/16-inch-inside-diameter rubber tubing. In a few instances, space restrictions required the use of short lengths of 3/32-inch-inside-diameter rubber tubing. Space restrictions also required the use of 7/64-inch-inside-diameter rubber tubing inside the ailerons. The pressure-lag characteristics of typical lines were investigated and the lag was found to be negligible for the rates of pressure change encountered in this investigation. The lag tests are discussed in the appendix. Resultant pressures were measured at all stations except C-1, C-3, C-6, C-10, and F. At the stations mentioned in row C, individual surface pressures were measured with respect to the uncorrected

static pressure at a vent in each side of the fuselage just ahead of the rear baggage compartment door. (See fig. 3.) Calibration of the static vents in the fuselage showed that the maximum departure from free-stream static pressure was about 2 percent of the dynamic pressure. Station F was merely an open-end tube inside the wing. The internal static pressure thus measured also was referred to the pressure at the fuselage static vents.

The approximate angle of attack of the airplane was measured by a standard NACA yaw vane mounted horizontally on the end of a boom located 3.3 feet ahead of the leading edge of the left wing and 6.7 feet inboard from the wing tip. Corrections for upwash at the vane at various Mach numbers and for deflection of the boom were made.

TEST PROCEDURE

In order to cover the available range of Mach and Reynolds numbers, tests were run throughout the speed and altitude ranges attainable by the airplane, and included measurements taken in vertical dives from the airplane's ceiling (about 34,000 ft) and the subsequent pull-outs.

With other conditions approximately constant, the lift coefficient was varied by gradually increasing the normal acceleration of the airplane. The change in effective wing camber introduced by the resulting curved flight path was considered small enough to be negligible. In interpreting the test results, it also should be realized that a certain amount of wing-skin wrinkling (with its resultant effect on the pressure distribution) and wing twisting was unavoidably present in flight. Photographs illustrating the relative amount of wing-skin wrinkling obtained in various flight conditions are shown in figure 8. The grid shown in the photographs is made up of straight white lines painted on the wing surface just ahead of the inboard end of the right aileron. (See fig. 2.) The camera used, a standard 16-millimeter, 12-volt, gun-sight-aiming-point camera, was mounted in the canopy behind the pilot's head. Using the slope of the grid lines in figure 8(a) as a zero reference, the twist of the wing at the grid station in the several conditions of flight represented in figure 8 was as follows:

Figure number	Indicated airspeed (mph)	Mach number	Acceleration factor	Twist (deg)
8(a)	0	0	1	0
8(b)	150	.36	.5	.4
8(c)	444	.77	.7	0
8(d)	454	.73	5.5	.7

Power off tests were run with the engine fully throttled and the propeller in the high-pitch setting. Power-on tests were run with power settings of 39 inches of mercury manifold pressure and 2600 rpm up to the critical altitude; at higher altitudes the power was set at full throttle with 3000 rpm. In some of the dives from high altitudes the latter power control settings were not changed even though the airplane was dived past the critical altitude. Curves showing the actual values of engine speed, propeller-blade angle, and brake horsepower (as determined by reference to the engine-power charts) resulting from these power settings are shown in figures 9, 10, and 11. The apparent brake horsepower values shown for the power-off setting were obtained by extrapolating the engine-power curves to include the low values of manifold pressure measured during these test runs.

The effects of the varying power may mask somewhat the effects on pressure distribution of the variations in Mach number, especially at the lower speeds. During the course of the tests, it was found that the landing gear would not stay fully retracted in straight high-speed flight. An additional protrusion was caused by the centrifugal force in accelerated flight, the total extension sometimes exceeding an inch. A special lock was then installed which held the landing gear rigidly in the retracted position, and repeat data were taken over the entire Mach number range. The data with wheels locked, however, agreed with those obtained with wheels unlocked.

RESULTS AND DISCUSSION

The results are divided into three separate parts presenting (1) the variation of wing loads and moments with Mach number, (2) the magnitude of the internal wing pressure, and (3) the variation of the slope of the wing lift curve with Mach number. The results are discussed in that order.

Variation of Wing Loads and Moments with Mach Number

For each test run, the resultant pressure as measured at each orifice station was reduced to coefficient form and plotted as a function of the lift coefficient. The power-on curves for orifice B-3 are shown in figure 12 as an example. The resultant-pressure coefficient is defined as follows:

$$P_R = \frac{p_L - p_U}{q}$$

where

P_R resultant-pressure coefficient

p_L pressure on lower surface

p_U pressure on upper surface

q free-stream dynamic pressure

The airplane lift coefficient was determined by use of the relation

$$C_L = \frac{WA_Z}{qS}$$

where

W airplane weight at time of test run, pounds

A_Z acceleration factor (reading of an accelerometer, in terms of units of the acceleration due to gravity, normal to the thrust line)

q free-stream dynamic pressure, pounds per square foot

S total wing area, including area projected through the fuselage, 213.22 square feet

The formula is actually that for the coefficient of force normal to the airplane thrust axis. The error involved, however, is less than 1 percent. The Mach numbers corresponding to these data also were plotted and are shown in figure 13. The pressure coefficients were then cross-plotted, as shown in figure 14, as a function of Mach number for values of the

total airplane lift coefficient of 0.1, 0,2, 0.5, and 1.0. These cross-plotted curves were then used to derive the data subsequently presented. Examination of the data showed no consistent variation of pressure coefficient with Reynolds number alone that exceeded the scatter of the data. The Reynolds number notations, therefore, are not shown on the final curves. The Reynolds number range covered in the tests was from 7,000,000 to 28,000,000.

From the data in figure 14 and the similar curves for the other orifices, the chordwise and spanwise lift distributions were then plotted for each 0.025 increment of Mach number throughout the test range. Because of the large number of plots so obtained, only those for each 0.1 increment of Mach number, plus the highest Mach number, are shown for each of the four values of lift coefficient used in this report. These curves are shown in figures 15 and 16. The coefficients noted on these figures, as obtained by integration of the pressure-distribution plots, are defined as follows:

$C_{L'}$ wing-panel lift coefficient (L'/qS)

$C_{M'}$ wing-panel pitching-moment coefficient (M'/qSc)

$C_{B'}$ wing-panel bending-moment coefficient (B'/qSb)

where

L' lift on the right wing panel, pounds

q free-stream dynamic pressure, pounds per square foot

S total wing area, including area projected through the fuselage, 213.22 square feet

M' pitching moment of the right wing panel about the 0.25 mean aerodynamic chord point, foot-pounds

c length of the mean aerodynamic chord, 6.72 feet

B' bending moment at the root of the right wing panel (22 in. outboard of the airplane center line), foot-pounds

b total wing span, 34.0 feet

As in the case for the total airplane, the lift is assumed to be substandially equal to the normal force.

The same physical dimensions of the airplane were used in computing the wing-panel coefficients as would be used in computing the total airplane coefficients so that the proportion of the total loads carried by the wing panel would be immediately apparent.

A consistent decrease in pitching moment at the 8-foot spanwise station was noted in figures 15 and 16. No reason for this irregularity could be found. The station is 2.3 feet outboard of the tip of the propeller arc and about 2 feet inboard of the gun-blast tubes and airspeed boom. No unusual irregularities in the section at this station were apparent.

Owing to the relatively few orifices used along the chord of the wing, the pressure peaks near the leading edge could not be established accurately from the experimental data in all cases. However, for the purposes of the analysis carried out in this report, it is apparent that the error resulting from failure to establish leading-edge peak pressures is negligible, inasmuch as it is known that such peak pressures exist only over an exceedingly small portion of the wing chord.

Summary curves showing the variation of the coefficients and of the lateral distance to the center of pressure with Mach number are plotted in figures 17 to 20. (The lateral distance d from the wing-panel root to the center of pressure was determined by use of the relation $d = bC_B'/C_L'$.) The curves were faired from the integration of the distributions plotted for each 0.025 increment of Mach number. The points so obtained are shown on the curves, contrary to the usual practice with derived data, in order to show the experimental scatter of the data. Only the distributions for each 0.1 increment of Mach number are shown in this report. The results are discussed in the subsequent paragraphs. The terms "critical Mach number" and "Mach number of divergence," as used in the discussion, are defined as follows:

1. Critical Mach number: The flight Mach number at which sonic velocity is reached locally in the air flow over the wing

2. Mach number of divergence: The flight Mach number at which the variation of an airplane or wing characteristic with Mach number starts to diverge from its low-speed trend

In the discussion, the results will sometimes be analyzed in the light of the relation between the critical Mach numbers

of the root and tip wing sections, calculated values of which are shown in figure 21. This figure shows the inherently poor high-speed qualities of the NACA 23000-series airfoils, since, at lift coefficients below 0.15, the 15-percent-thick symmetrical airfoil actually has a higher critical Mach number than the much thinner NACA 23009 airfoil.

Wing-panel lift coefficient.- The right wing panel comprises about 43 percent of the total wing area, which includes the section projected through the fuselage by parallel lines connecting the ends of the root chords. Figure 17 shows that the load carried by the right wing panel is generally much less than 43 percent of the total load, exceeding this value only at $C_L = 0.1$ with power off at low and moderate values of Mach number, and at $C_L = 0.5$ with power on and off at moderate values of Mach number. The remainder of the lift is, of course, carried not only by the opposite wing and wing center section, but by the propeller, tail, and fuselage as well.

With power off, the wing-panel lift coefficient gradually increases as the Mach number increases to moderate values, and then gradually decreases. The variation of the wing-panel lift coefficient with Mach number would be expected to depend on the relation between the effects of Mach number on the lift characteristics of the wing and the effects of Mach number on the other lifting components of the airplane. The latter effects are not easily predicted, and no detailed analysis is attempted here. It is apparent, however, that the relative effectiveness of these other components increases at the higher Mach numbers.

In general, the power affects the right-wing-panel lift coefficient as would be expected (i.e., the engine torque tends to roll the airplane to the left, and balance, then, dictates a lower lift coefficient for the right than for the left wing). It would also be expected that the difference between power-on and power-off data would decrease with speed; this effect, however, is seen to hold entirely true only at the lowest lift coefficient. At lift coefficients of 0.1 and 0.2 it is seen that the wing-panel lift coefficient required with power on exceeds that required with power off for Mach numbers greater than 0.70 and 0.74, respectively. It is possible that this effect may be caused by decreased lifting effectiveness of the propeller, the higher rotational speed with power on resulting in shock losses over a large portion of the blades. At the highest lift coefficient considered ($C_L = 1.0$), the relatively large decrease in the wing-panel lift coefficient required with power on may indicate a rather

high lifting effectiveness of the pitched propeller at moderate values of Mach number.

Wing-panel bending-moment coefficient.- The curves of wing-panel bending-moment coefficient (fig. 18) bear a marked similarity in shape to the curves of wing-panel lift coefficient, suggesting that changes in the wing-panel bending-moment coefficient were due more to actual changes in the magnitude of the load carried by the wing rather than to a lateral shift of the position of the center of pressure. In fact, the preceding discussion concerning the wing-panel lift coefficient can be applied equally well to the discussion of the wing-panel bending-moment coefficient.

Lateral distance to center of pressure.- The curves of figure 19 show that, for power-off conditions, the lateral distance from the wing root to the center of pressure varied very little with Mach number. The greatest movement occurred at a lift coefficient of 0.1 where the center of pressure, while tending to move inward, varied irregularly over a distance of $1\frac{1}{2}$ feet as the Mach number was increased from 0.3 to 0.78. At a lift coefficient of 0.2, the lateral center-of-pressure location remained essentially constant over the Mach number range of 0.4 to 0.62 and then moved inward approximately 0.4 foot as the Mach number was further increased, while at a lift coefficient of 0.5 a negligible movement of the center of pressure for a Mach number range of 0.4 to 0.7 was experienced. At a lift coefficient of 1.0, the trend of movement of the lateral center of pressure was outward over the range of Mach numbers tested (0.25 to 0.65).

At the lowest lift coefficient, the reason for the failure of the center of pressure to move outward at high Mach numbers may be explained by the fact that the root section, NACA 0015, has a higher critical Mach number than does the tip section, NACA 23009 (fig. 21). Although the relation between the critical Mach numbers of the two sections changes at the higher lift coefficients, the difference is not large, and the failure of the center of pressure to exhibit a marked outward movement at high values of Mach number probably can be ascribed to this fact. In addition, the small amount of geometric twist in the wing of this airplane (about -0.7° from root to tip) results in an aerodynamic twist of about 0.4°. (The zero-lift angle of the NACA 23009 section is about -1.1°.) This twist tends to increase the lift coefficient and, consequently, lower the critical speed at the tip at values of C_L above 0.2, thus further inhibiting any tendency of the center of pressure to move outward at high values of Mach number.

A proposal has been made that all high-speed airplane wings be constructed of constant section with constant percentage thickness along the span in order to eliminate lateral shifts of the center of pressure at high Mach numbers. The

results presented herein show that such a requirement would unnecessarily restrict designers, as only insignificant lateral shifts of the center of pressure occurred on a wing with greatly differing section shape and thickness at root and tip. A more logical and less restricting requirement need specify only that the critical Mach number be maintained reasonably constant along the span.

The shift between the power-on and power-off curves of figure 19 for the lift coefficient of 0.1 is in the direction that would be expected from the direction of propeller rotation; the difference decreases with increase of speed as would also be expected. The reason for the lack of a similar effect of power at higher values of lift coefficient is not understood.

Wing-panel pitching-moment coefficient.- As was expected, the wing-panel pitching-moment coefficient changed sharply in a negative direction at high values of Mach number (fig. 20). The value of this Mach number of moment idvergence will be compared with the critical Mach number in a later section of the report. The change in wing pitching-moment coefficient requires increased downward tail loads for balance at high values of Mach number. The magnitude of the pitching-moment-coefficient change, however, is not too serious.

Internal Wing Pressure

In order to determine the actual air loads across the wing skin, a knowledge of the wing internal pressure is necessary, as well as of the external pressure distribution. The pressure inside the right wing of the P-39N-1 airplane was measured by recording the difference in pressure between the open end of a tube inside the wing at station F (fig. 7(a)) and the fuselage static vents. Station F is considered representative, as the interior of the wing is well vented. The internal wing pressure coefficient $\left(\frac{p_{wing} - p_{vents}}{q}\right)$ was small and, under most conditions, negative (fig. 22).

Airplane Lift-Curve Slope

The slope of the airplane lift curve $dC_L/d\alpha$ theoretically increases with Mach number. At a certain Mach number,

at or somewhat above the critical value, the flow conditions change, invalidating the theory, and the lift-curve slope decreases. The lift-curve slope of the P-39 airplane was determined from flight data by measuring the slope of the curve of C_L plotted against the angle of attack as measured by the angle-of-attack vane (horizontally mounted yaw vane). The test points were considerably scattered (fig. 23); but, when the data were faired and corrected for upwash at the vane and for deflection of the boom in accelerated flight, reasonable agreement with theory was obtained, especially at the lower Mach numbers and higher lift coefficients. The poorer agreement of the faired test data with theory at high Mach number and low lift coefficient is in the region where the corrections due to boom deflection are large. It is quite possible that the boom-deflection correction applied was somewhat in error itself, as the boom had two degrees of stiffness, depending on the normal acceleration, and, in addition, no correction was attempted for the deflection caused by the air forces on the boom and head. These air forces would be appreciable at high speeds, and would act in the direction to cause better agreement with the theory if the data were corrected for their effect. It is strongly recommended that future measurements of angle of attack made by this method be done with a very rigid boom.

Except at a C_L of 1.0, the scatter of the data does not permit ascertaining whether or not the Mach number of lift divergence was reached; although at a lift coefficient of 0.2, there appears to be a fairly definite indication of divergence at a Mach number of about 0.72. At a lift coefficient of 1.0, the lift-curve slope diverges at a Mach number of 0.5, reaching a value of only 0.012 at a Mach number of 0.67. At a Mach number of 0.3, $dC_L/d\alpha$ with power on averages about 0.01 higher than the power-off value. At higher values of Mach number the difference, if any, is masked by the experimental scatter.

It is interesting to compare the Mach number of lift divergence (fig. 23) with that of moment divergence (fig. 20) and with the theoretical value of the critical Mach number for the wing. This comparison is facilitated by the following table:

Airplane C_L	M_{cr} of poorest wing section	M of lift divergence	M of moment divergence
0.1	0.62	[a]0.79+	0.69
.2	.64	.72 (?)	.68
.5	.55	[a].73+	.60
1.0	.40	.50	.55

[a]No definite indication of divergence up to the Mach number shown.

It is immediately apparent that the attainment of the critical Mach number does not prescribe immediate changes in the trends of the airplane's characteristics. Not only does the Mach number of moment divergence exceed the critical Mach number, but, except at the highest lift coefficient, the Mach number of lift divergence exceeds that of moment divergence.

CONCLUSIONS

The following conclusions are drawn from the data presented herein:

1. A considerable portion of the weight of the airplane is carried by components other than the wings. The proportion of lift carried by the wings may vary considerably with Mach number, thus changing the bending moment at the wing root whether or not there is a shift in the lateral position of the center of pressure.

2. The center of pressure on the wings does not necessarily move outward at high Mach numbers, even though the wing-thickness ratio decreases toward the tip. The important factor to consider is the variation of critical Mach number along the span. The spanwise variations of wing section and twist are additional primary factors which may be adjusted to control the variation of the lateral position of the center of pressure with Mach number. It is seen that the extreme expedient of specifying constant section and percentage thickness along the span is unnecessary.

3. The wing pitching-moment coefficient increases sharply in a negative direction at a certain value of Mach number; this value does not necessarily correspond to the critical Mach number, but may be considerably higher. The magnitude of the change encountered on the P-39N-1 airplane is not too serious.

4. The pressure inside the wing of the P-39N-1 airplane relative to the stream static pressure varies somewhat with changes in the condition of flight, being for the most part negative. The greatest departure occurs at low values of lift coefficient and high values of Mach number; at a lift coefficient of 0.1 and a Mach number of 0.79 the internal wing pressure is as much as 0.4q lower than the free-stream static pressure.

5. In the normal speed range, the lift-curve slope increases with Mach number as predicted by theory; the tendency may persist to values of Mach number substantially above the critical value before a reversal in trend becomes apparent.

Ames Aeronautical Laboratory,
National Advisory Committee for Aeronautics,
Moffett Field, Calif.

APPENDIX

LAG IN WING-PRESSURE MEASUREMENTS

Summary

Measurements of lag in duplicates of typical wing-pressure lines were made in order to determine whether or not an error of this type existed in the recorded wing pressures. The error was found to be negligible for the conditions encountered in this flight investigation.

Pressure Lines Tested

Two types of lines were tested, hereinafter designated as the wing line and the aileron line. A description of each type follows:

Wing line.- The wing line used was typical of one of the short lines extending from a cell on the pressure recorder to an orifice in row A. The several parts of the line are listed below in that order:

1. Wing orifice, 1/8-inch inside diameter, about 1 inch long

2. Aluminum tubing, 9/64-inch inside diameter, 16 inches long

3. Rubber tubing, 3/16-inch inside diameter, 8 inches long

4. Aluminum tubing, 9/64-inch inside diameter, 7 feet long

5. Rubber tubing, 3/16-inch inside diameter, 14 inches long

6. Pressure cell, volume approximately 1 cubic inch

Aileron line.- The aileron line used was typical of one of the lines extending from a cell on the pressure recorder to an aileron orifice in row E. The several parts of the line are listed below in that order:

1. Aileron orifice, about 1/16-inch inside diameter, about 1 inch long

2. Rubber tubing, 7/64-inch inside diameter, 10 feet 3 inches long

3. Aluminum tubing, 9/64-inch inside diameter, 5 feet 2 inches long

4. Rubber tubing, 3/16-inch inside diameter, 9 inches long

5. Aluminum tubing, 9/64-inch inside diameter, 7 feet 3 inches long

6. Rubber tubing, 3/16-inch inside diameter, 15 inches long

7. Pressure cell, volume approximately 1 cubic inch

Method

A laboratory test setup was made in which the pressure in a chamber was recorded through a short (about 6 in.) direct line simultaneously with that recorded through a duplicate of one of the P-39N-1 pressure lines. The pressure in the chamber could be changed various amounts at various

rates. All pressures were measured by standard diaphragm-type pressure cells the natural frequency of which is about 100 cycles per second.

Results and Discussion

A time history of typical results is shown in figure 24. The time lag in recorded pressure at 100 percent of the final pressure was sometimes difficult to measure (points a and b, fig. 24). For this reason, time lag was defined as the lag in recorded pressure at 90 percent of the final pressure (points c and d, fig. 24). The difference in maximum rate of change of applied and recorded pressures was also measured on the time histories.

The time lag and the rate-of-change difference for various rates of pressure change are summarized in figure 25. The actual time lag for the typical wing pressure line was small enough to be practically immeasurable with the apparatus employed. A small rate-of-change difference for this line, however, could be measured. It is interesting to note that the maximum rate of change of recorded pressure for the wing line was sometimes more than that of the applied pressure. This phenomenon was caused by a small initial lag which essentially disappeared before the final pressure was reached. The time lag for a typical aileron line varied from 0.09 second at an applied rate of change of pressure of 21 inches of mercury per second to 0.16 second at an applied rate of change of pressure of 140 inches of mercury per second. The rate-of-change difference for this line rose as high as 80 inches of mercury per second at an applied rate of change of pressure of 140 inches of mercury per second.

The magnitude of pressure change tested varied between values corresponding to about 2 to 12 inches of mercury. The results were found to be independent of the magnitude of the pressure change within this range. Subsequent to the laboratory tests, it was found that even the lowest rates of pressure change used (21 in. Hg/sec) were considerably greater than the highest values encountered in this flight investigation (less than 4 in. Hg/sec, obtained on leading-edge orifices in pull-ups). These high rates of pressure change also resulted in turbulent flow in the tubes. The flight rates of change of pressure were lower than the laboratory-test rates, and although laminar flow may have existed in at least parts of the tubes, it is considered doubtful that the lag ever appreciably exceeded the values shown.

Conclusions

The error in recorded pressures due to lag in the pressure lines was negligible for the conditions encountered in this flight investigation.

REFERENCES

1. Crowley, J. W., Jr.: Pressure Distribution over a Wing and Tail Rib of a VE-7 and of a TS Airplane in Flight. NACA Rep. No. 257, 1927.

2. Rhode, Richard V.: The Pressure Distribution over the Wings and Tail Surfaces of a PW-9 Pursuit Airplane in Flight. NACA Rep. No. 364, 1930.

3. Pearson, H. A.: Pressure Distribution Measurements on an O-2H Airplane in Flight. NACA Rep. No. 590, 1937.

4. Anon.: Army Air Forces Spec. No. C-619-21, dated Oct. 6, 1942, for AAF Model P-39N-1.

TABLE I.- ORDINATES OF PRESSURE ORIFICES

[All values are in percent of chord]

Orifice	Row A				Row B			
	Upper surface		Lower surface		Upper surface		Lower surface	
	Station	Ordinate	Station	Ordinate	Station	Ordinate	Station	Ordinate
1	0.30	1.16	0.30	1.16	0.43	1.38	0.58	1.58
2	.93	2.10	1.21	2.26	1.23	2.34	1.35	2.37
3	1.97	2.95	2.70	3.31	2.05	2.97	2.61	3.14
4	5.20	4.50	5.20	4.30	4.85	4.21	5.02	4.10
5	9.08	5.66	9.77	5.54	9.21	5.53	9.22	5.21
6	16.79	6.94	16.79	6.54	18.07	6.88	18.78	6.48
7	25.49	7.50	25.49	7.08	25.90	7.25	25.38	6.86
8	36.02	7.44	36.51	6.37	37.30	7.03	37.30	6.86
9	48.08	6.71	48.62	6.74	51.82	6.12	51.82	6.03
10	59.70	5.70	60.21	5.71	62.85	5.16	62.85	5.06
11	70.62	4.51	71.48	4.51	73.00	3.98	73.00	3.89
	L.E. radius 2.29 (measured) L.E. radius 2.34 (specified) T.E. thickness = 0.19				L.E. radius 2.18 (measured) L.E. radius 2.18 (specified) T.E. thickness = 0.17			

Row C

Orifice	Upper surface		Lower surface	
	Station	Ordinate	Station	Ordinate
1	0.45	1.64	0.45	1.05
2	1.29	2.61	1.29	1.89
3	2.68	3.46	2.81	2.69
4	5.27	4.62	5.50	3.57
5	10.52	6.01	10.52	4.60
6	24.93	7.42	23.73	5.84
7	37.20	7.25	35.80	5.95
8	45.95	6.71	45.95	5.58
9	53.41	6.23	53.41	5.21
10	62.41	5.43	63.69	4.32
11	76.27	3.79	76.27	2.91
	L.E. radius 2.03 (measured) L.E. radius 1.95 (specified) T.E. thickness = 0.15			

TABLE I.-- Continued

Orifice	Row D				Row E			
	Upper surface		Lower surface		Upper surface		Lower surface	
	Station	Ordinate	Station	Ordinate	Station	Ordinate	Station	Ordinate
1	0.89	2.08	1.14	1.53	0.86	2.22	1.02	1.19
2	2.10	2.88	2.34	2.13	1.99	2.78	2.26	1.69
3	4.08	3.92	4.27	2.84	5.57	4.32	5.88	2.44
4	6.73	4.86	6.92	3.45	8.21	5.07	8.21	2.68
5	12.41	6.02	12.79	4.34	16.08	6.09	16.08	3.61
6	29.27	6.82	29.27	5.61	30.86	6.26	30.86	4.27
7	48.42	6.02	48.42	5.04	51.89	5.36	51.89	3.75
8	68.62	4.34	68.62	3.42	69.32	4.13	69.32	2.57
9	84.08	2.51	84.08	1.97	80.76	2.89	80.76	1.82
10	87.30	2.01	87.30	1.62	84.88	2.28	84.80	1.47
11	92.36	1.01	92.36	1.18	93.69	1.19	93.69	.71
	L.E. radius 1.89 (measured) L.E. radius 1.64 (specified) T.E. thickness = 0.12				L.E. radius 1.73 (measured) L.E. radius 1.24 (specified) T.E. thickness = 0.19			

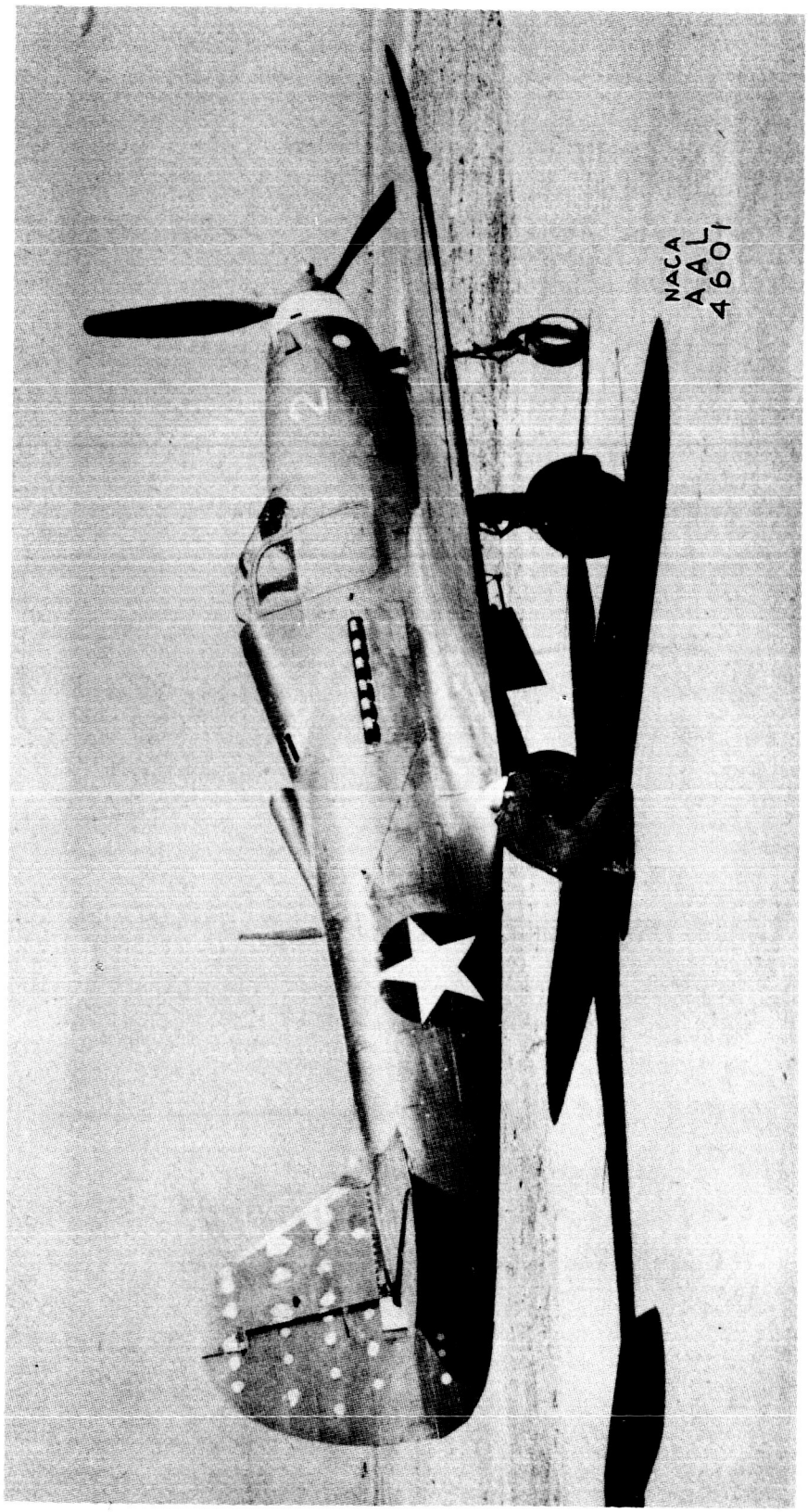

Figure 1.- Three-quarter rear view, P-39N-1 airplane.

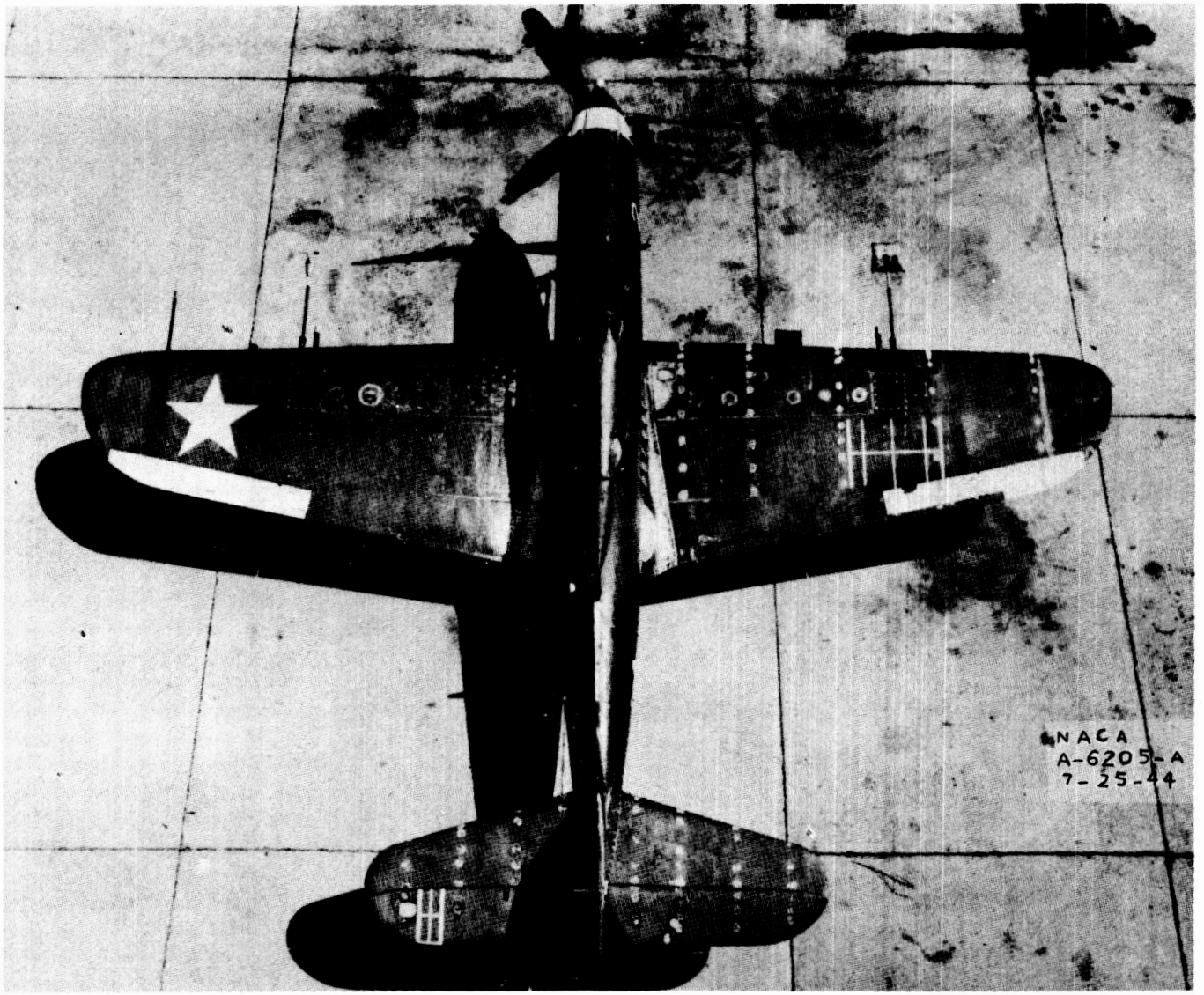

Figure 2.- Top view, P-39N-1 airplane as instrumented for flight tests.

A-13

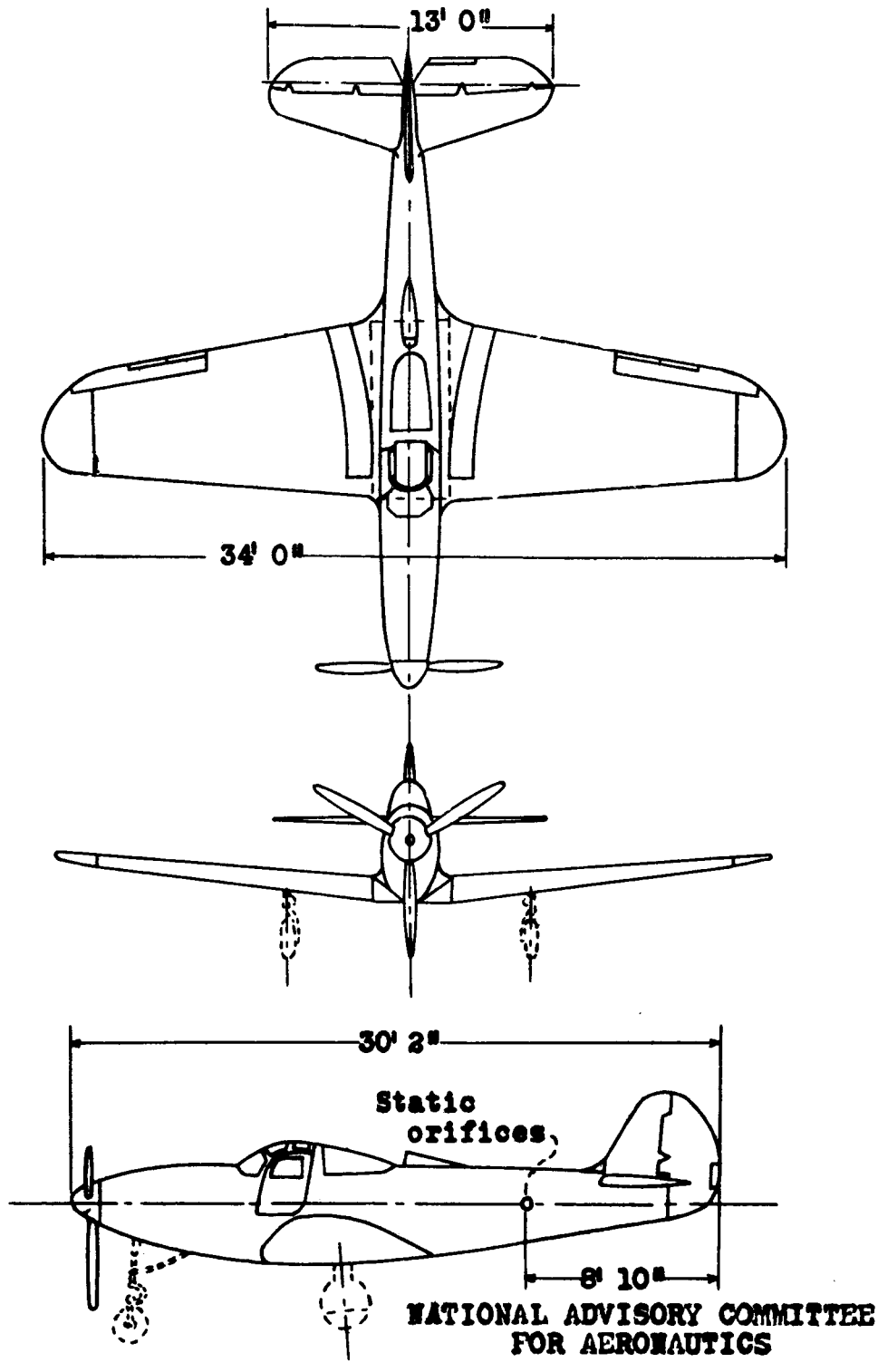

Figure 3.- Three-view drawing of the Bell P-39N-1 airplane.

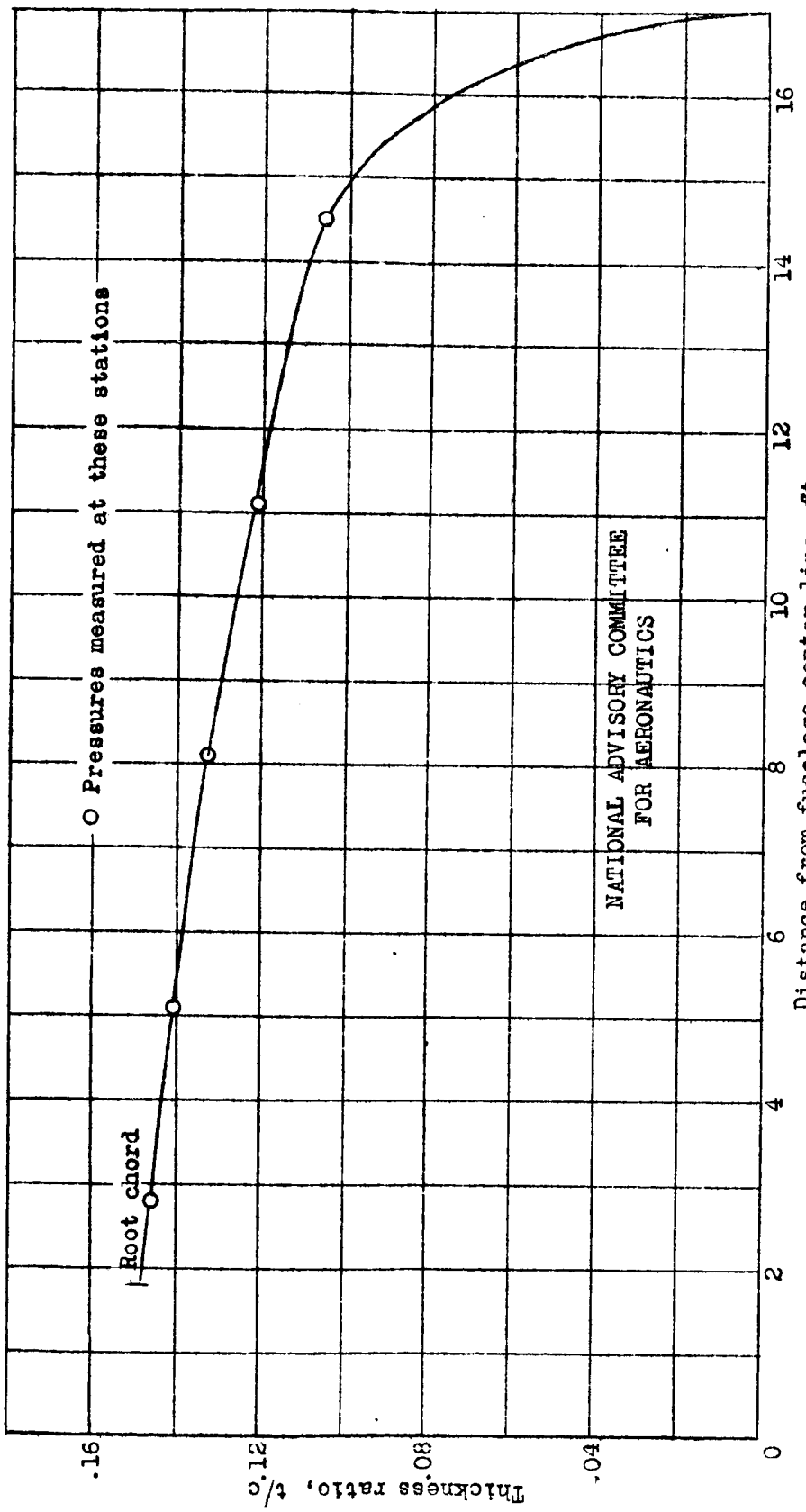

Figure 4.- Variation of thickness ratio along span of right wing. P-39N-1 airplane.

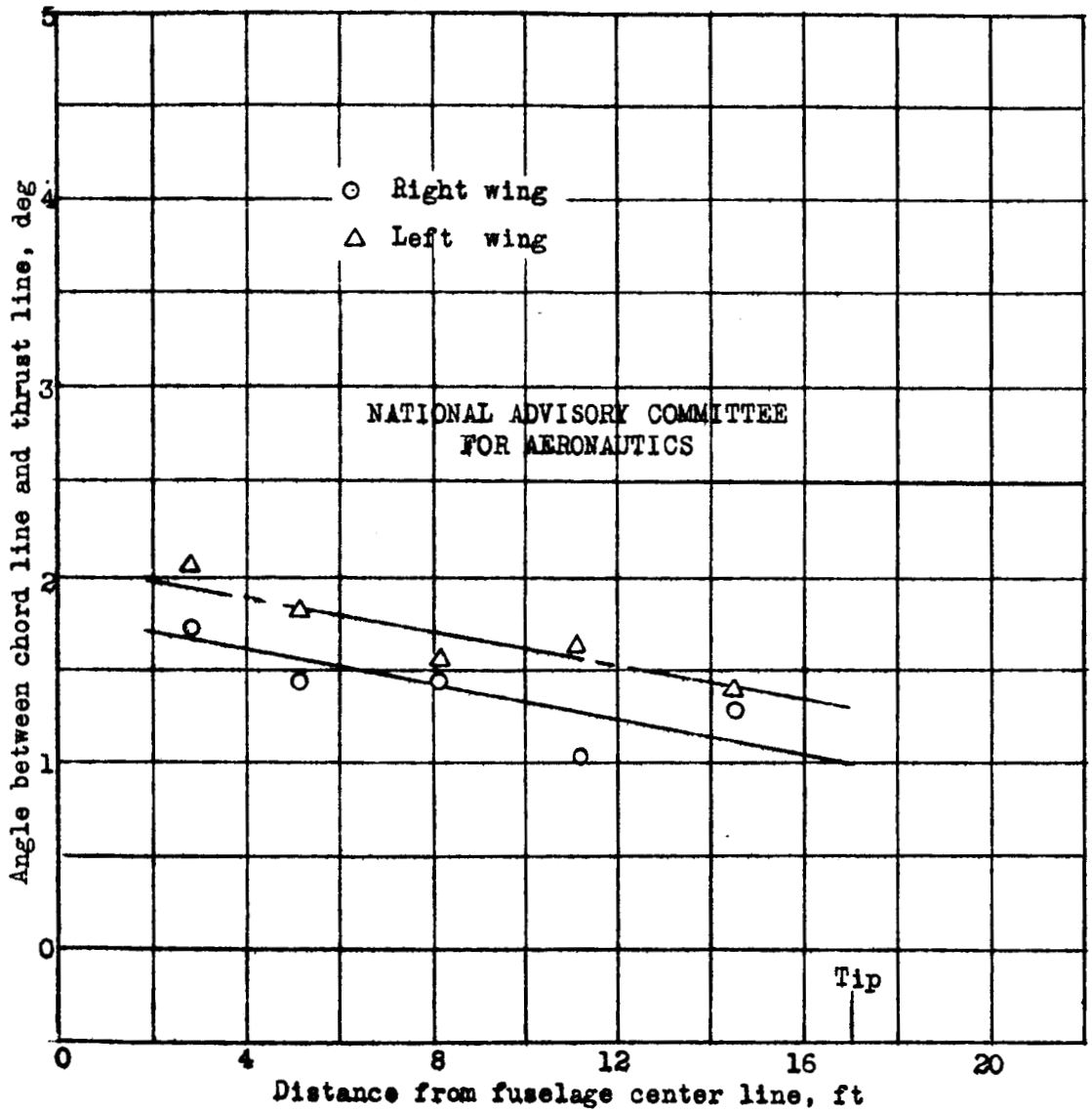

Figure 5.- Incidence and geometric twist of the wings on the P-39N-1 airplane.

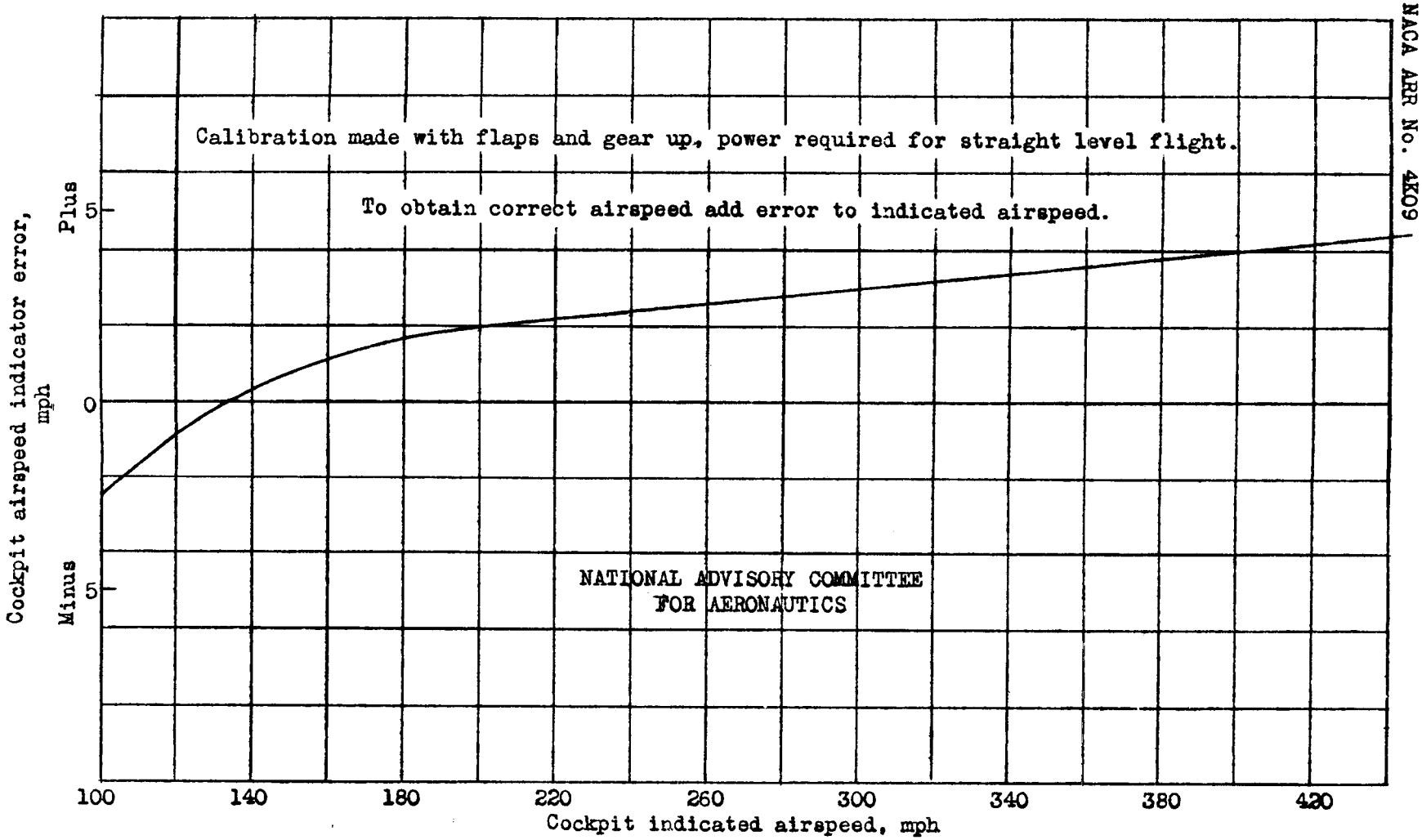

Figure 6.- Calibration of service airspeed-measuring system. P-39N-1 airplane.

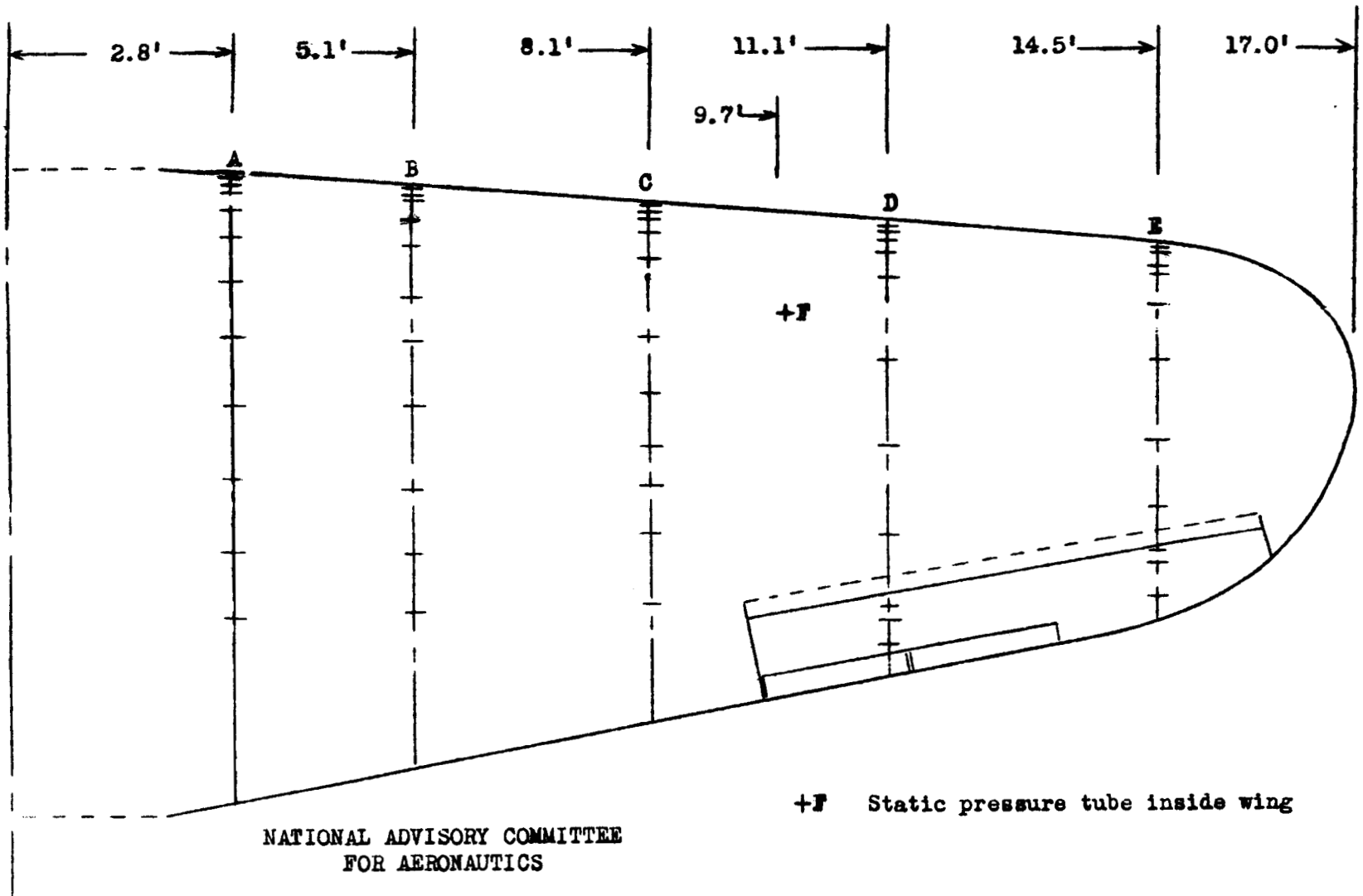

(a) Plan view

Figure 7.- Orifice locations on right wing. P-39N-1 airplane.

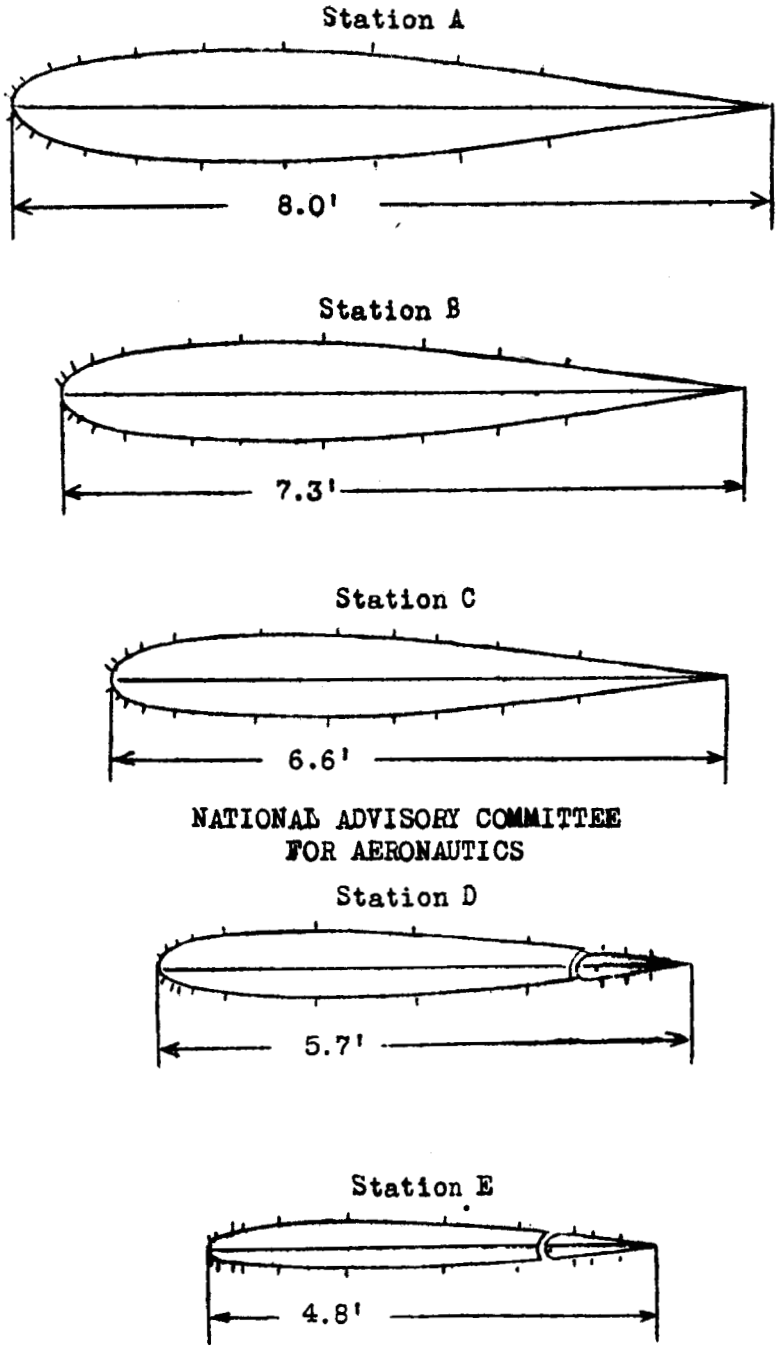

(b) Section views

Figure 7.- Concluded. P-39N-1.

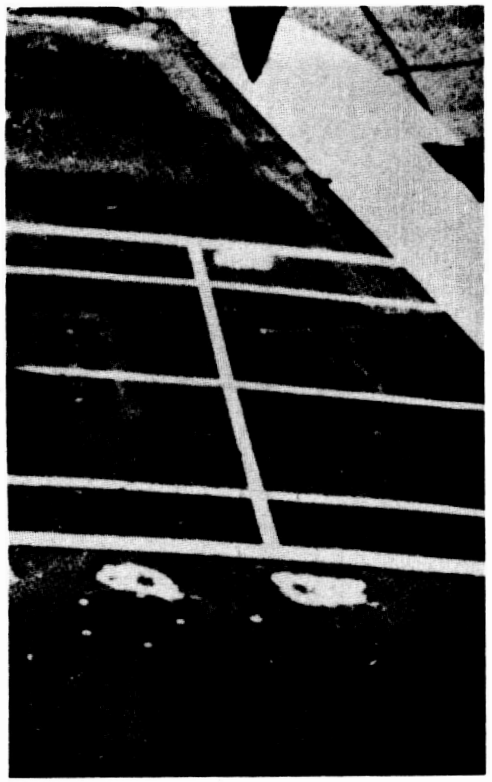

(a) On ground at zero speed.

(b) In straight flight at an indicated airspeed of 150 miles per hour.

Figure 8.- Wing-skin wrinkling under various conditions. P-39N-1 airplane.

(c) In a straight dive at an indicated airspeed of 444 miles per hour.

(d) In a dive pull-out at an indicated airspeed of 454 miles per hour and normal acceleration factor of 5.5.

Figure 8.- Concluded. P-39N-1.

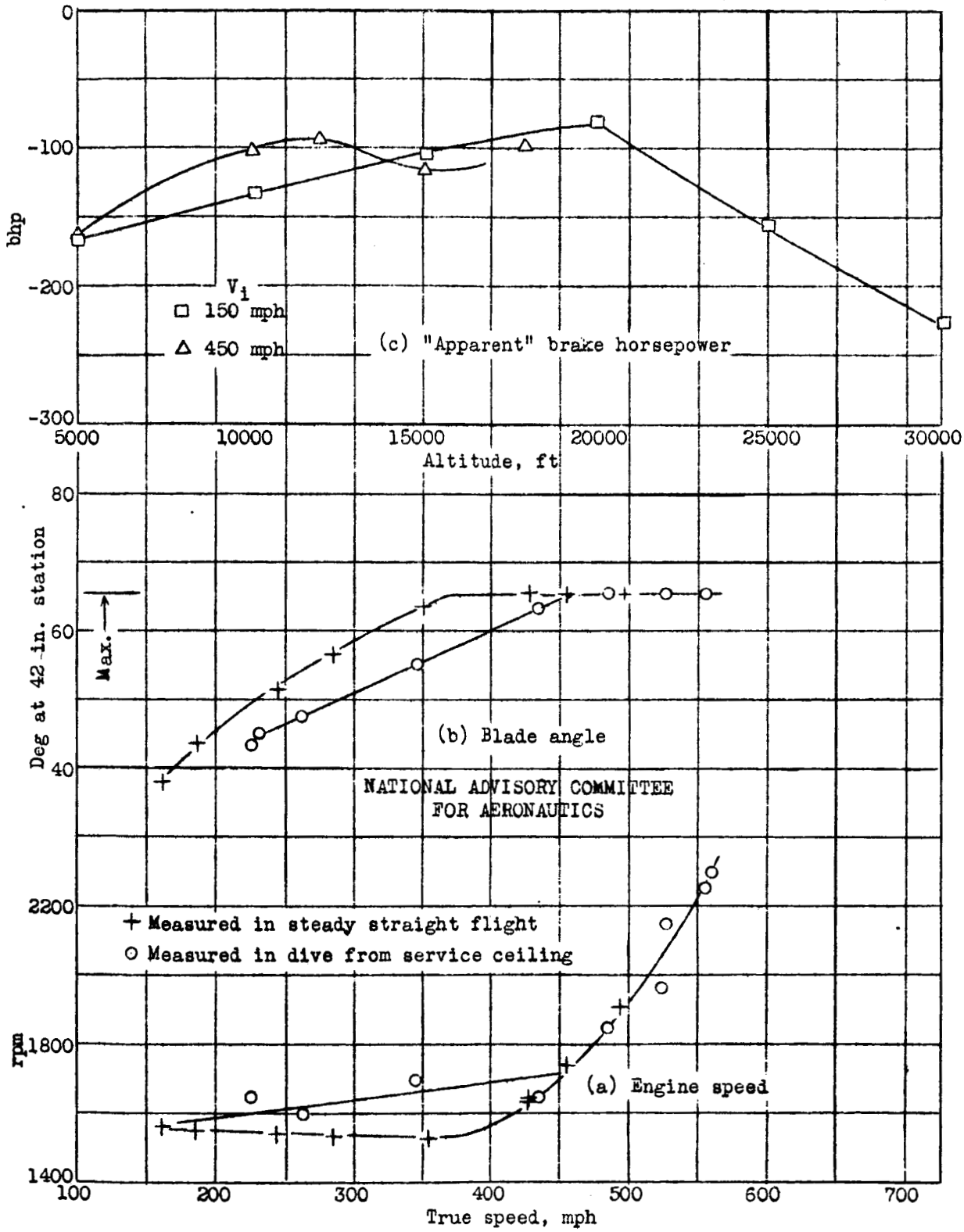

Figure 9.- Engine speed, propeller-blade angle, and brake horsepower for the engine-throttled, propeller-in-high-pitch power setting. P-39N-1 airplane.

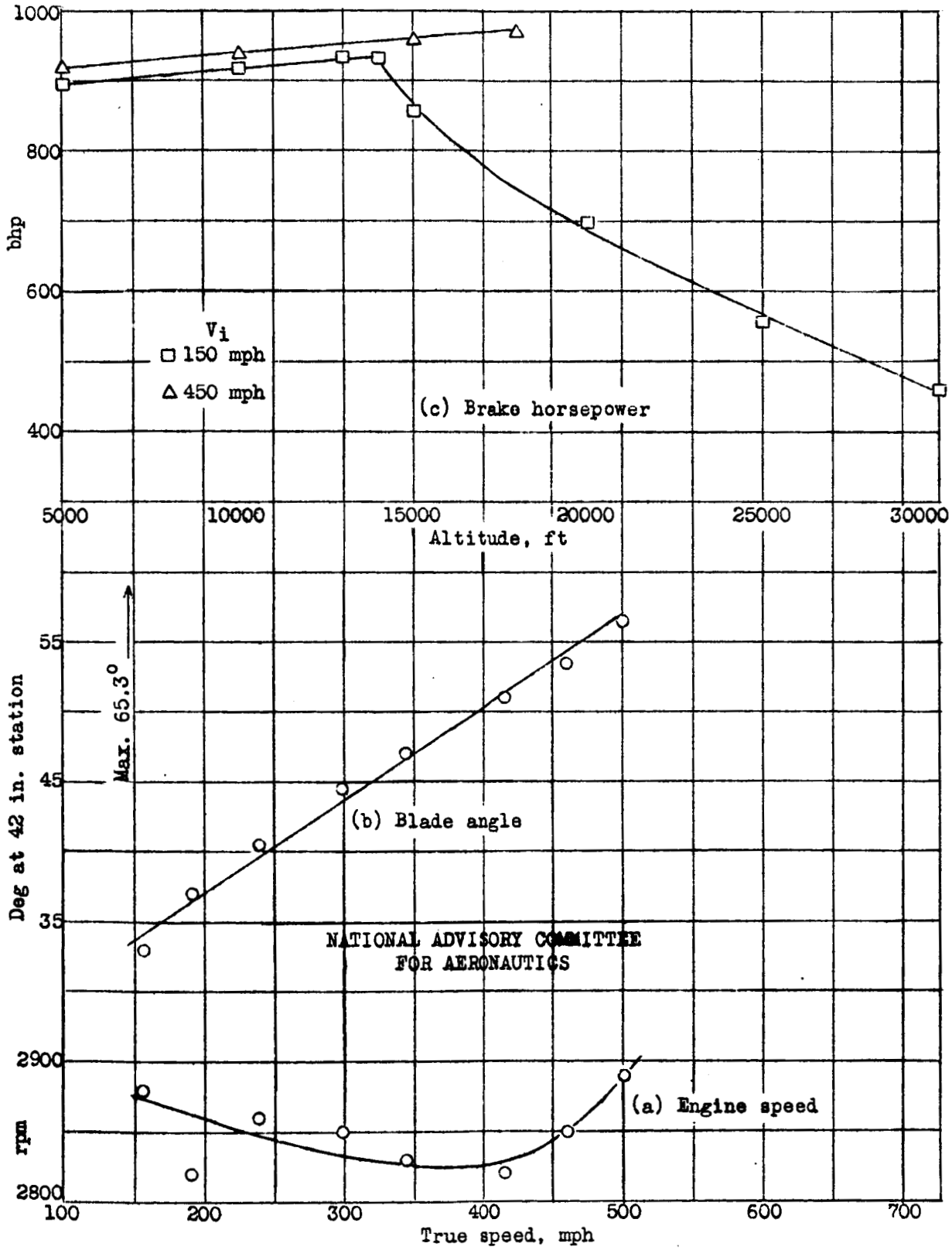

Figure 10.- Engine speed, propeller-blade angle, and brake horsepower for a power setting of 39 inches of mercury and 2600 rpm. P-39N-1 airplane.

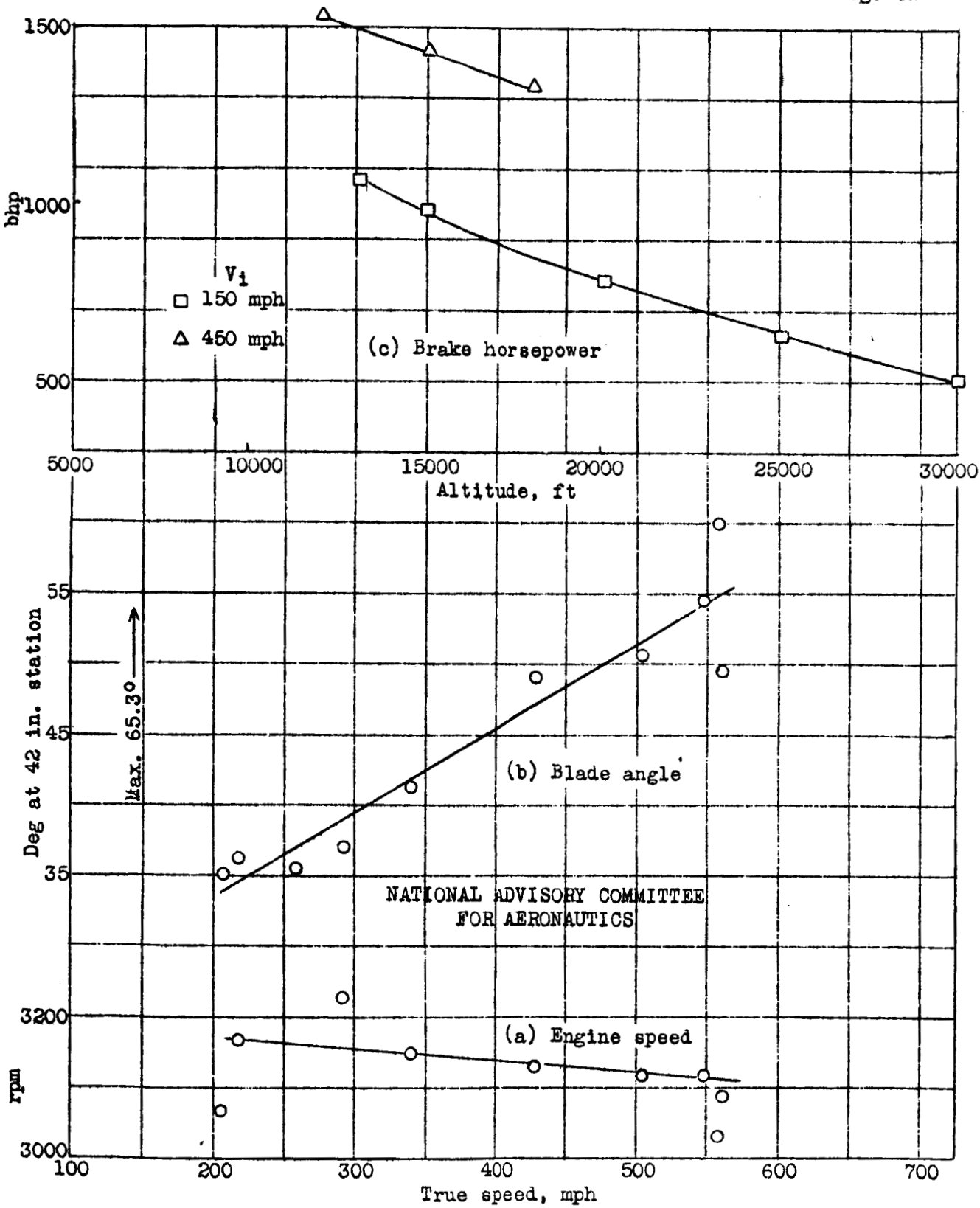

Figure 11.- Engine speed, propeller-blade angle, and brake horsepower for a power setting of full throttle and 3000 rpm. P-39N-1 airplane.

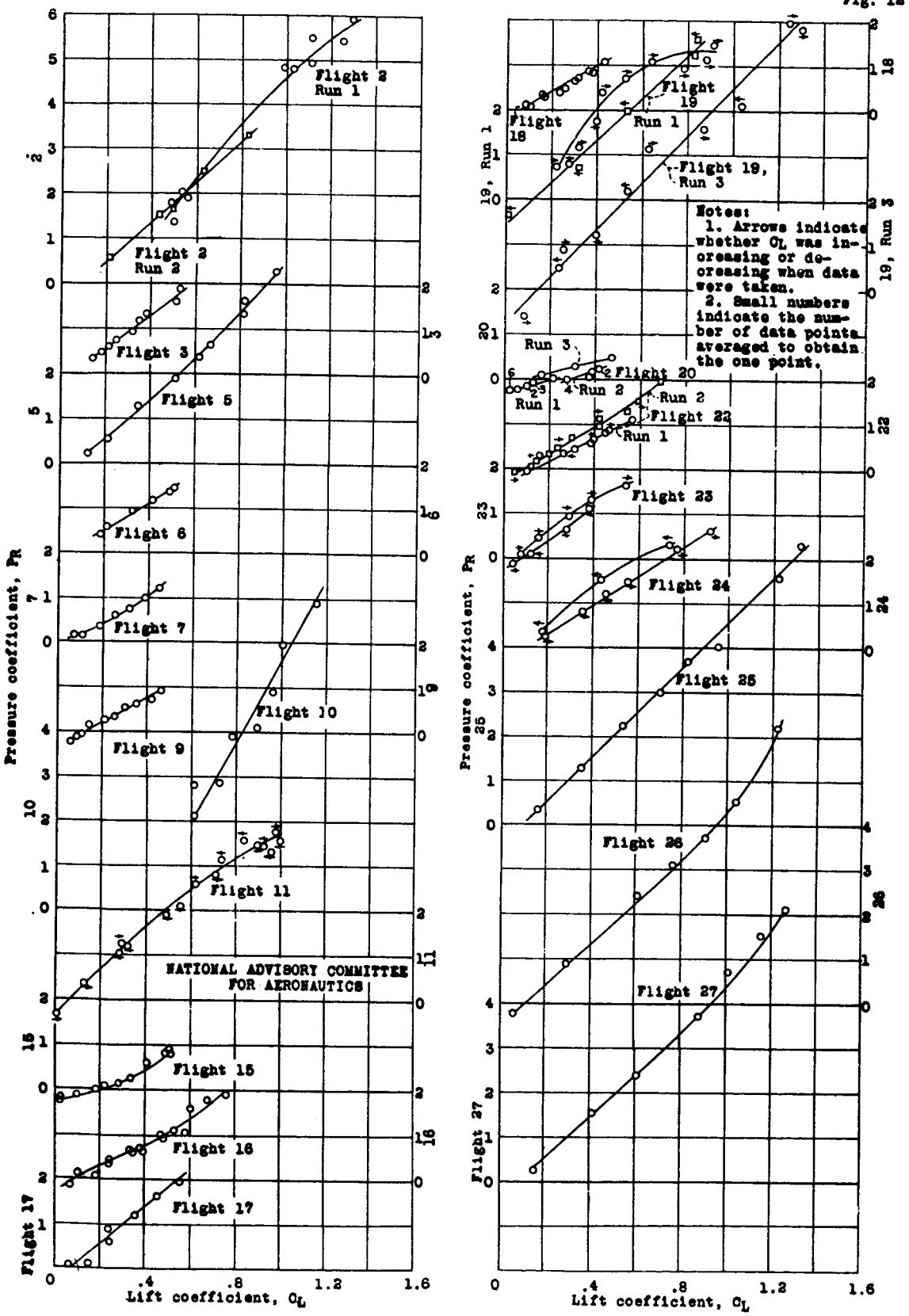

Figure 12.- Variation of resultant pressure coefficient for orifice station B-3 with airplane lift coefficient during the power-on test flights. P-39N-1 airplane.

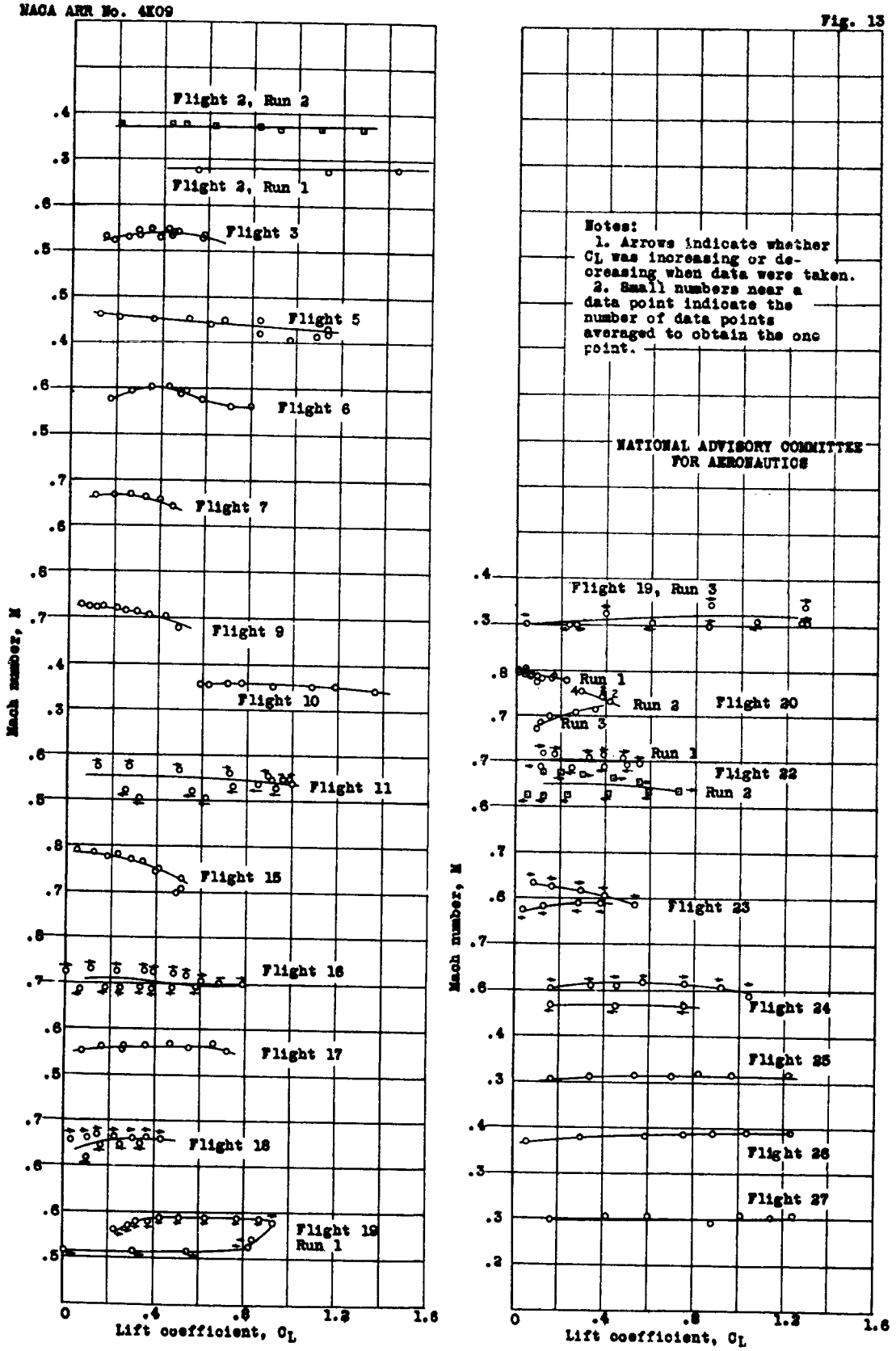

Figure 13.- Variation of Mach number with airplane lift coefficient during the power-on test flights. P-39N-1 airplane.

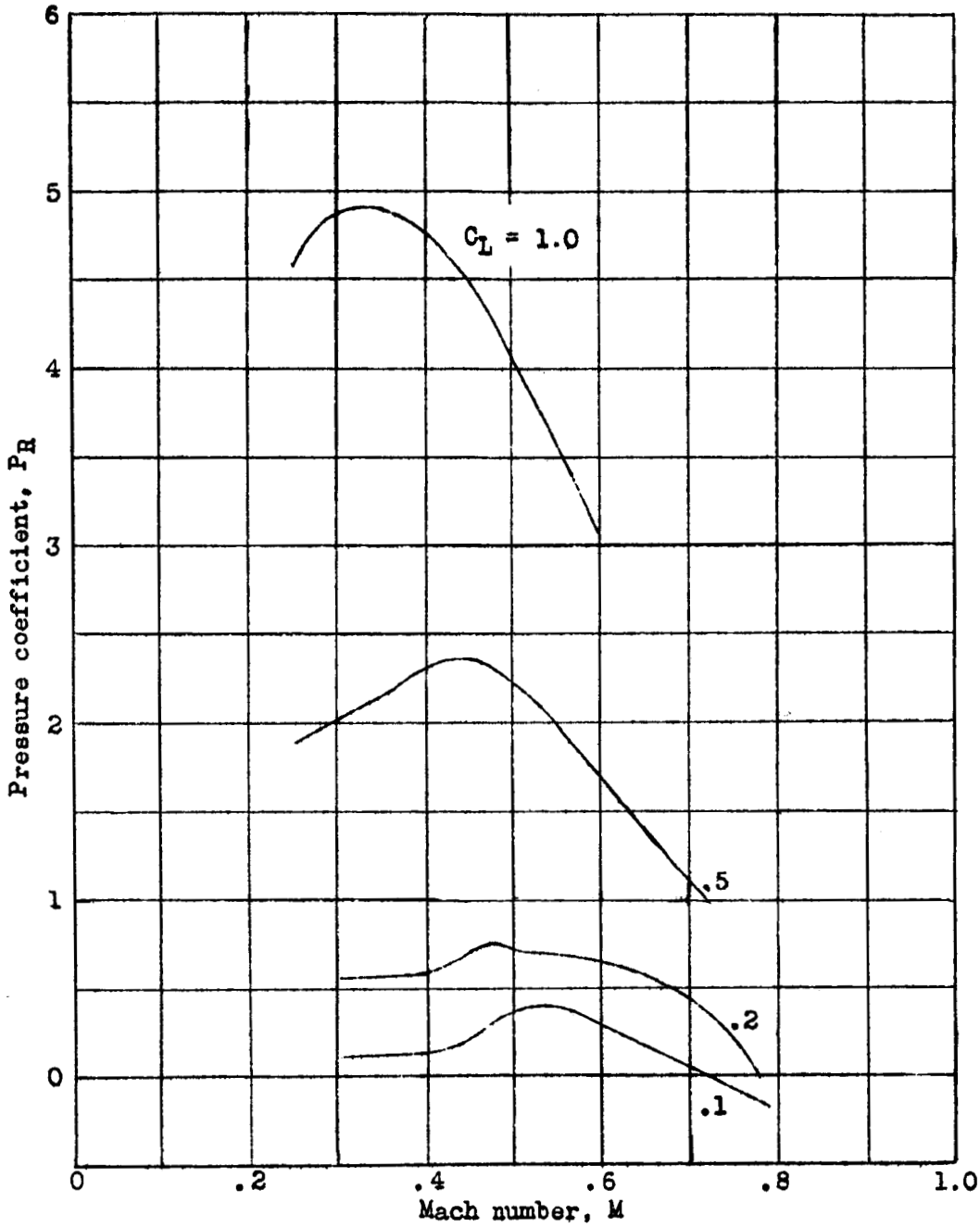

Figure 14.- Variation of resultant pressure coefficient with Mach number for orifice B-3, as measured in power-on flight. P-39N-1 airplane.

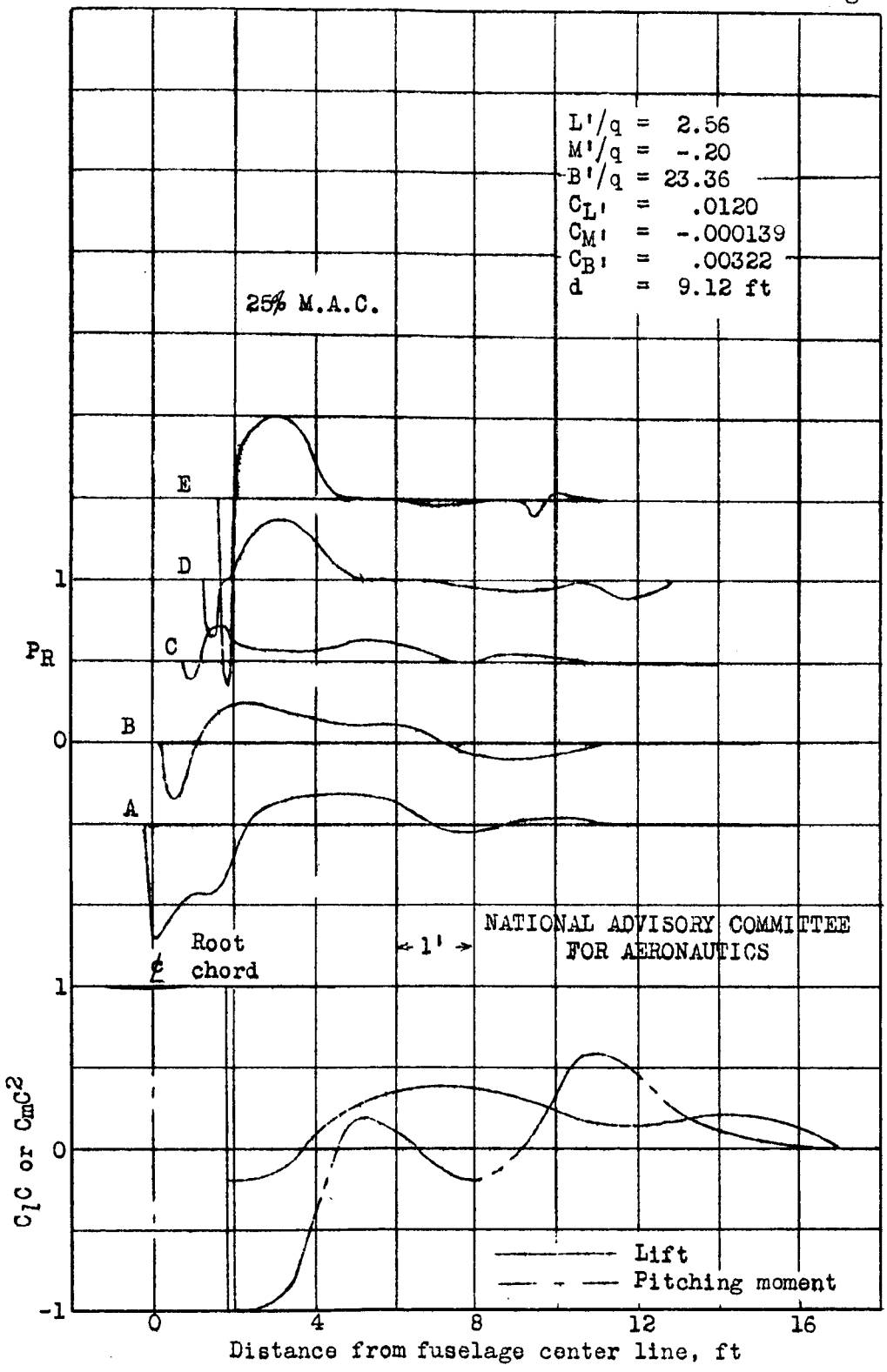

Figure 15.- Pressure distribution on the right wing in power-on flight. P-39N-1 airplane. Lift coefficient = .10, Mach number = .30.

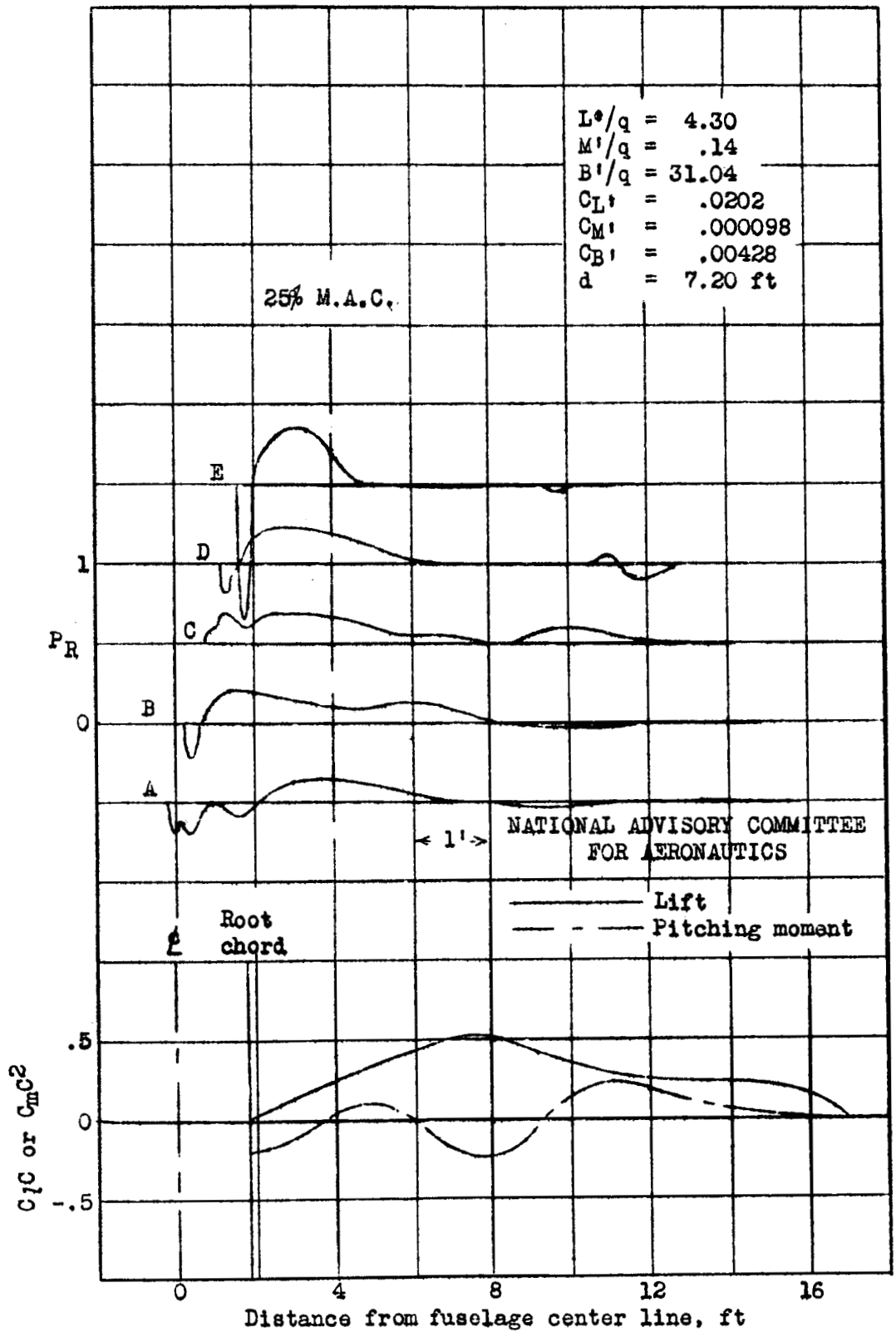

Figure 15.- Continued. (b) Lift coefficient = .10, Mach number = .40. P-39N-1.

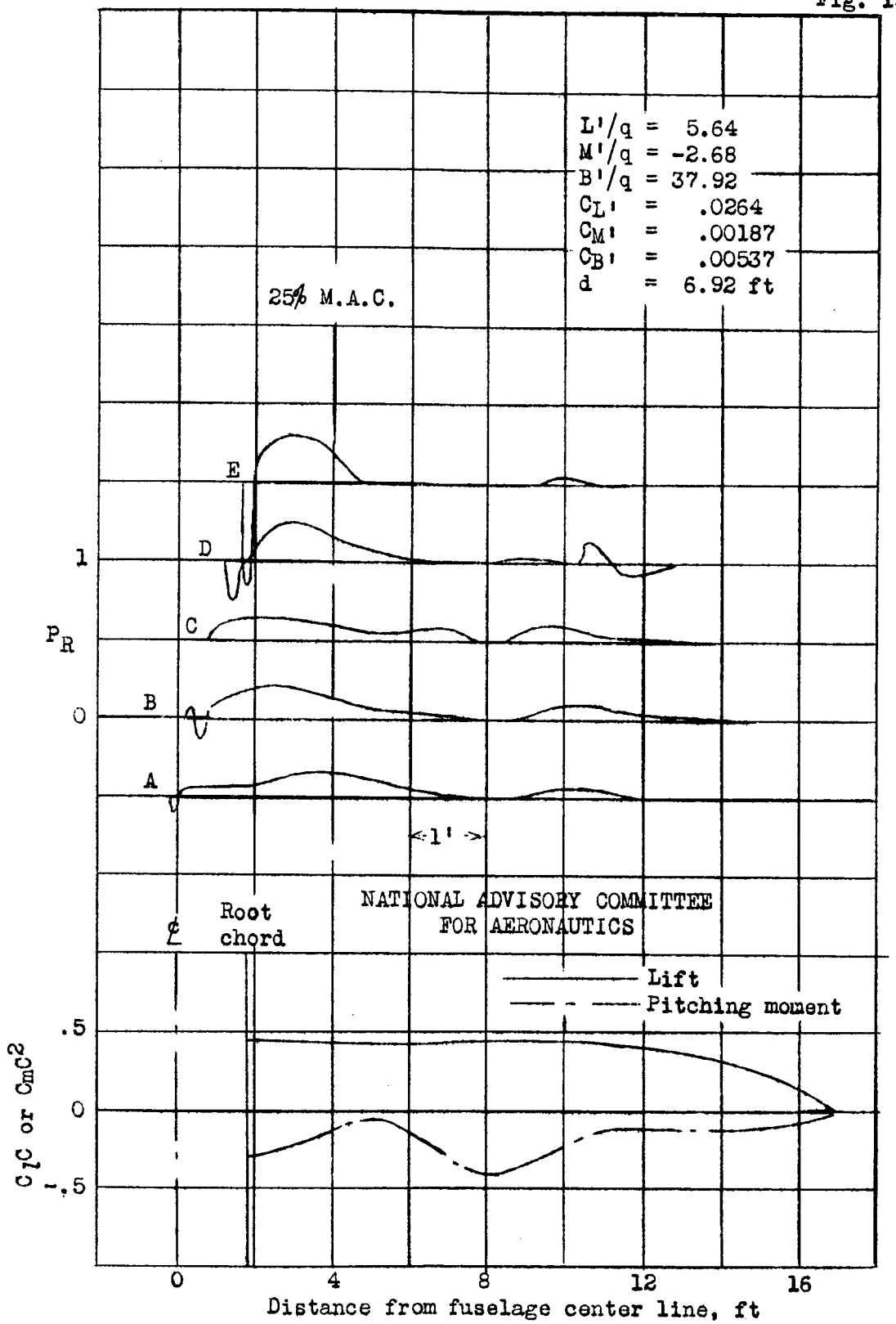

Figure 15.- Continued. (c) Lift coefficient = .10, Mach number = .50. P-39N-1.

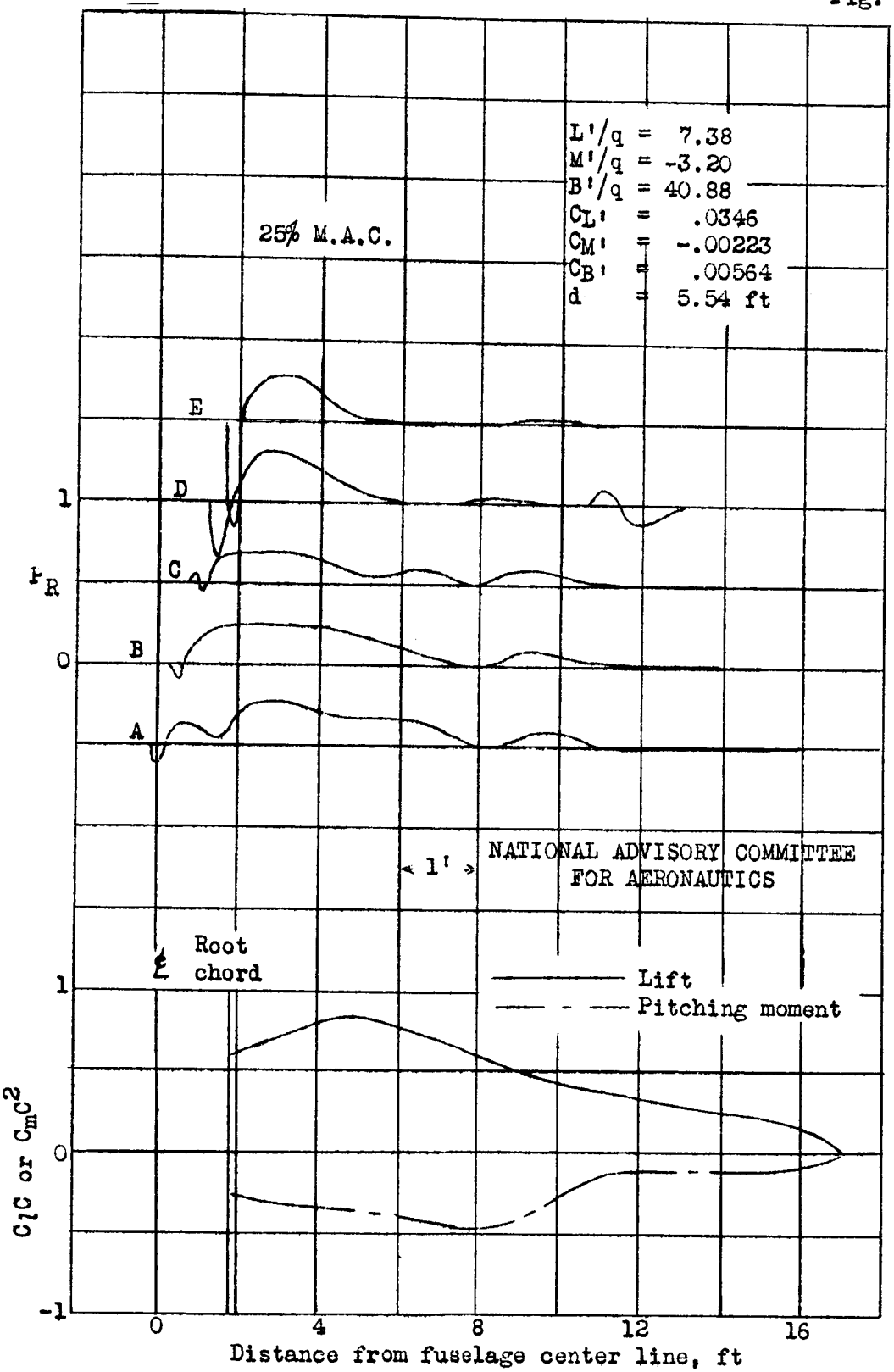

Figure 15.- Continued. (d) Lift coefficient = .10, Mach number = .60. P-39N-1.

A-13

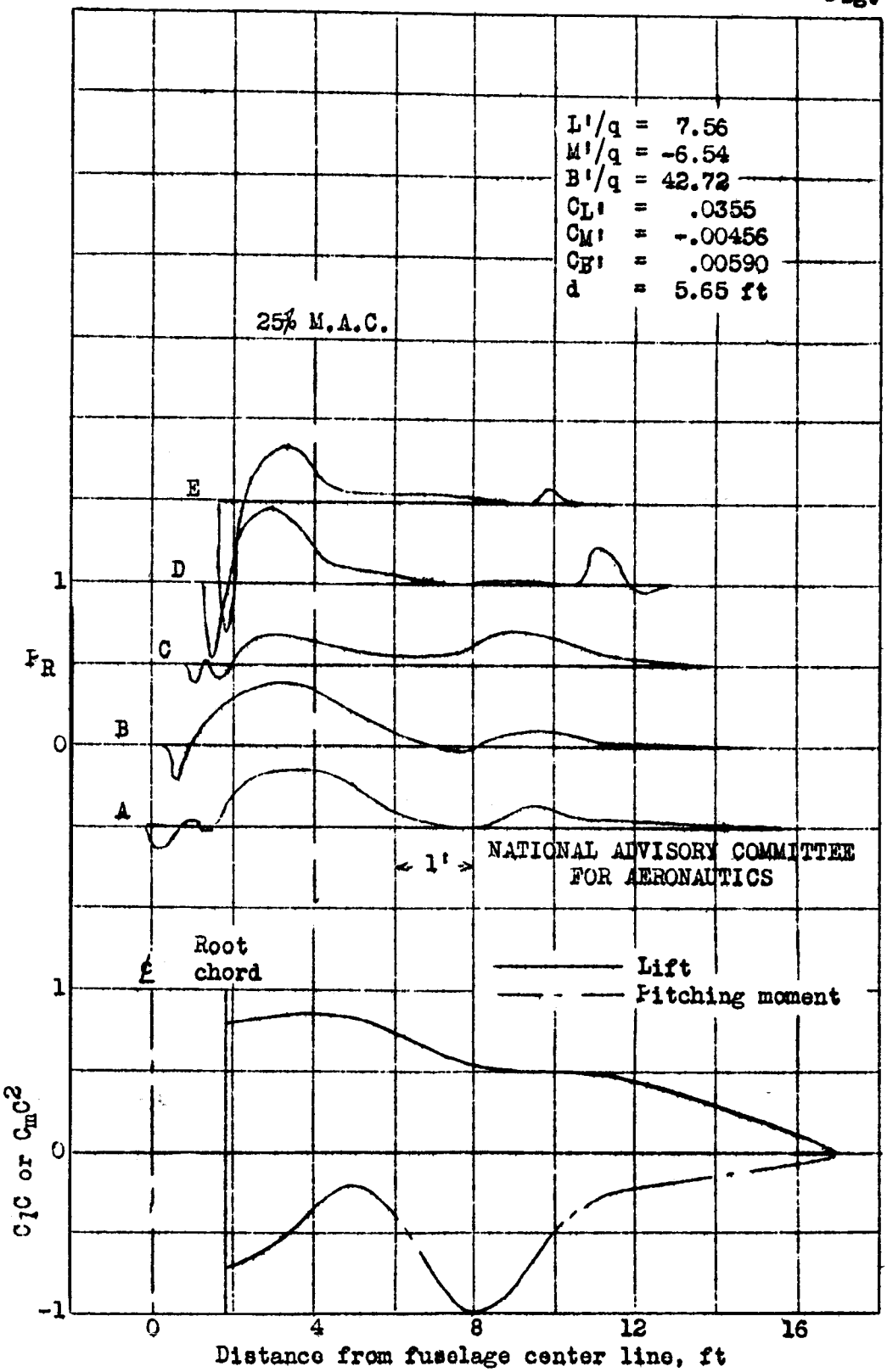

Figure 15.- Continued. (e) Lift coefficient = .10, Mach number = .70. P-39N-1.

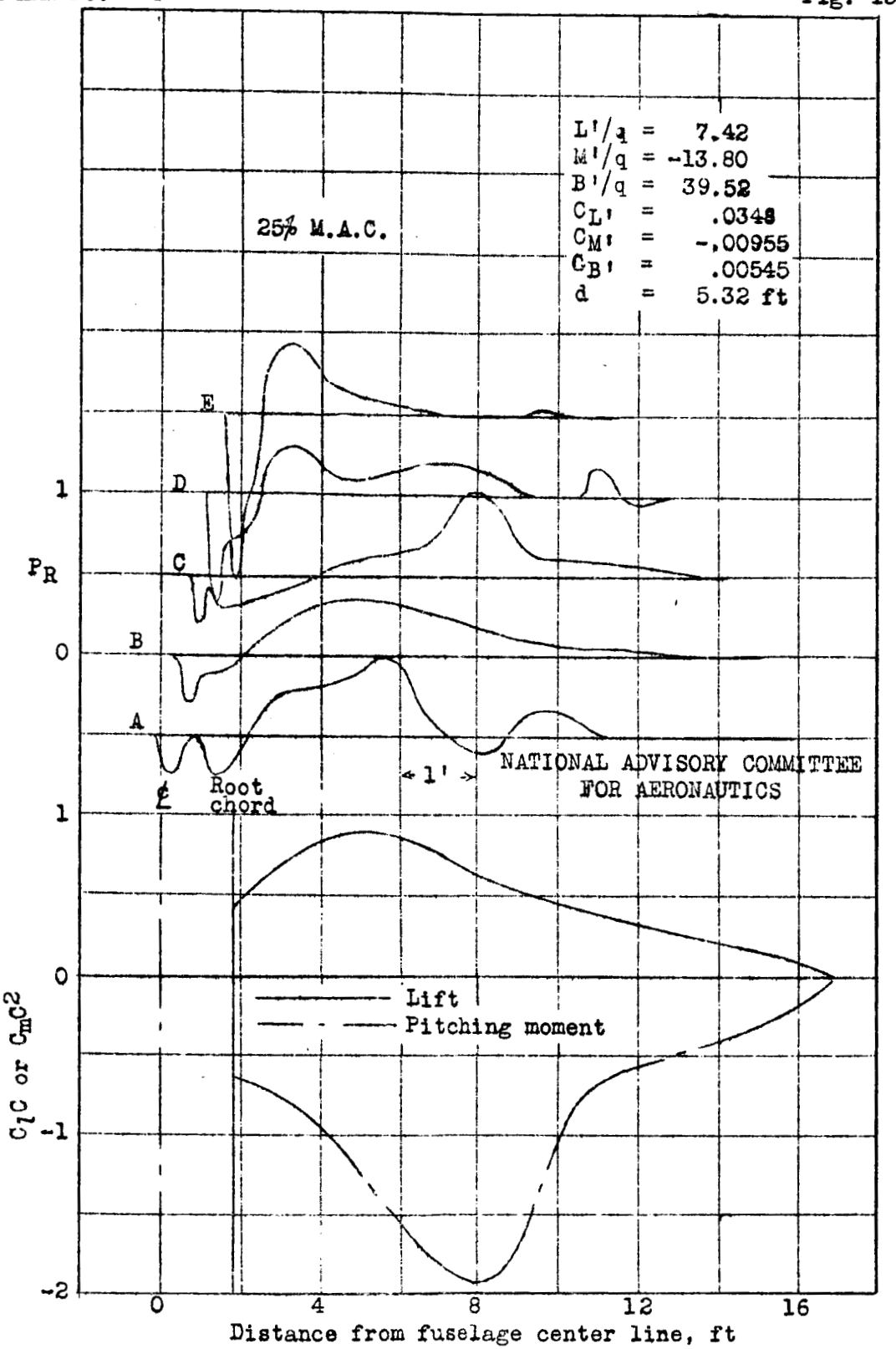

Figure 15.- Continued. (f) Lift coefficient = .10, Mach number = .78. P-39N-1.

A-13

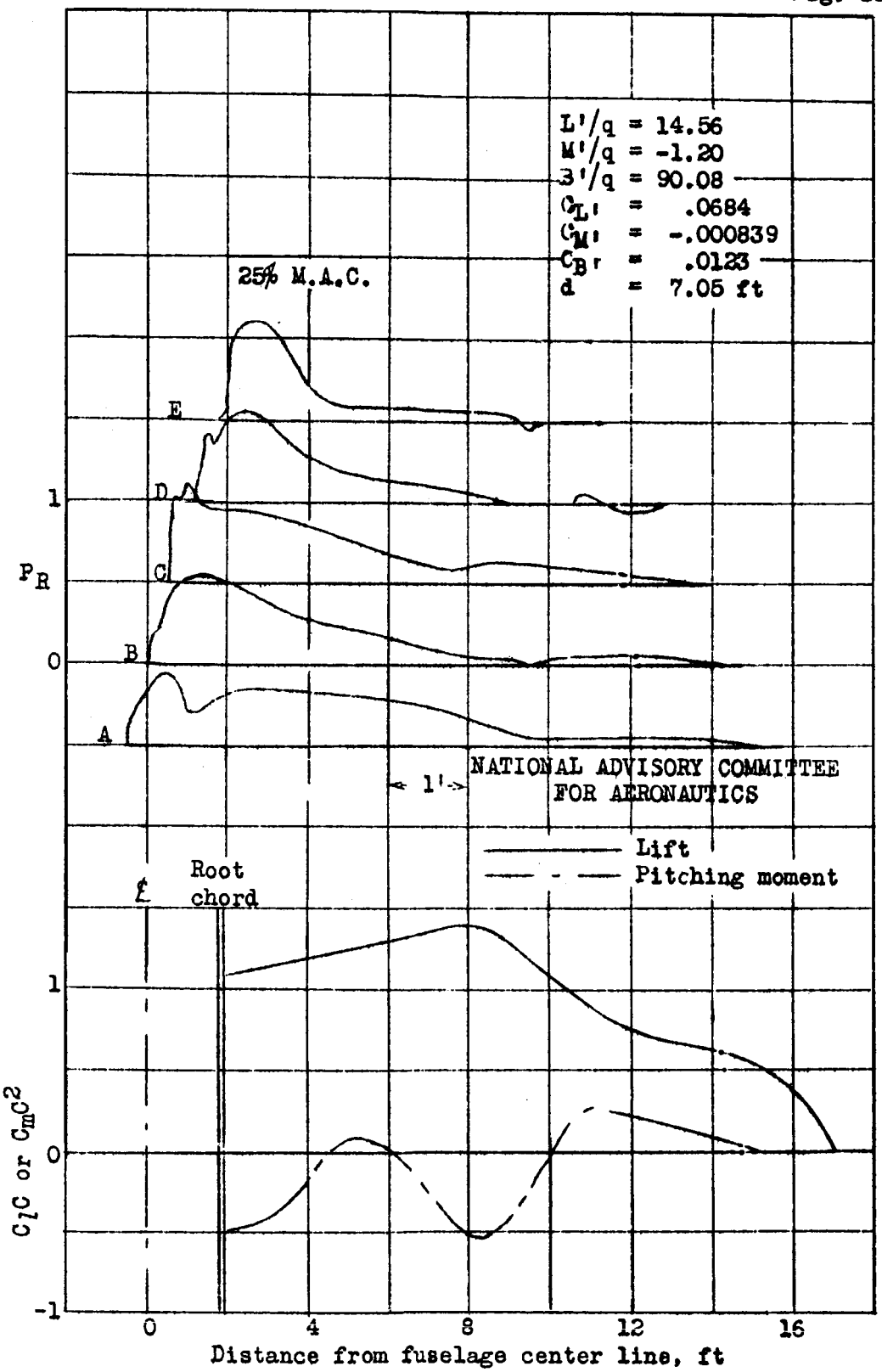

Figure 15.- Continued. (g) Lift coefficient = .20, Mach number = .30. P-39N-1.

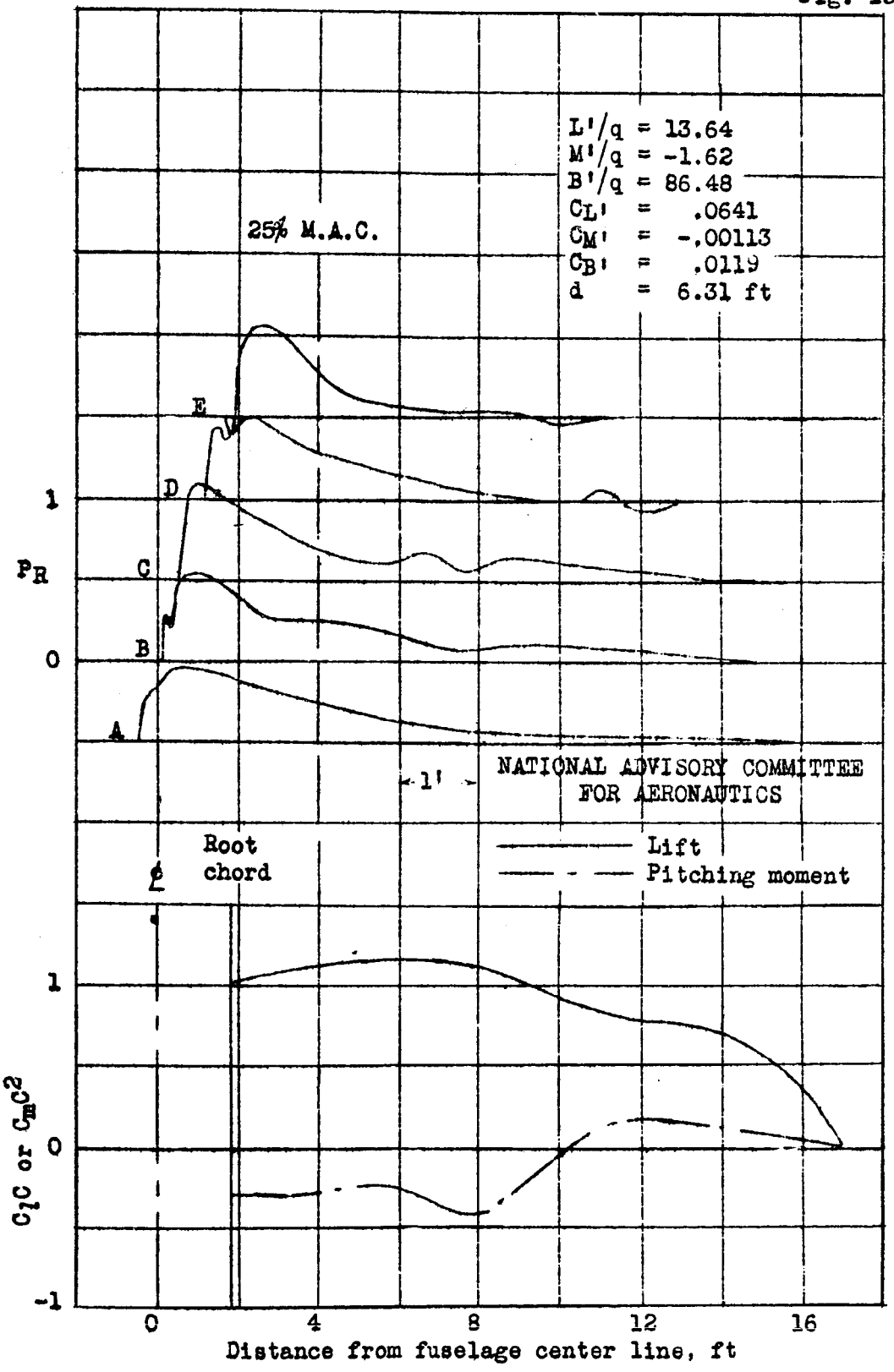

Figure 15.- Continued. (h) Lift coefficient = .20, Mach number = .40. P-39N-1.

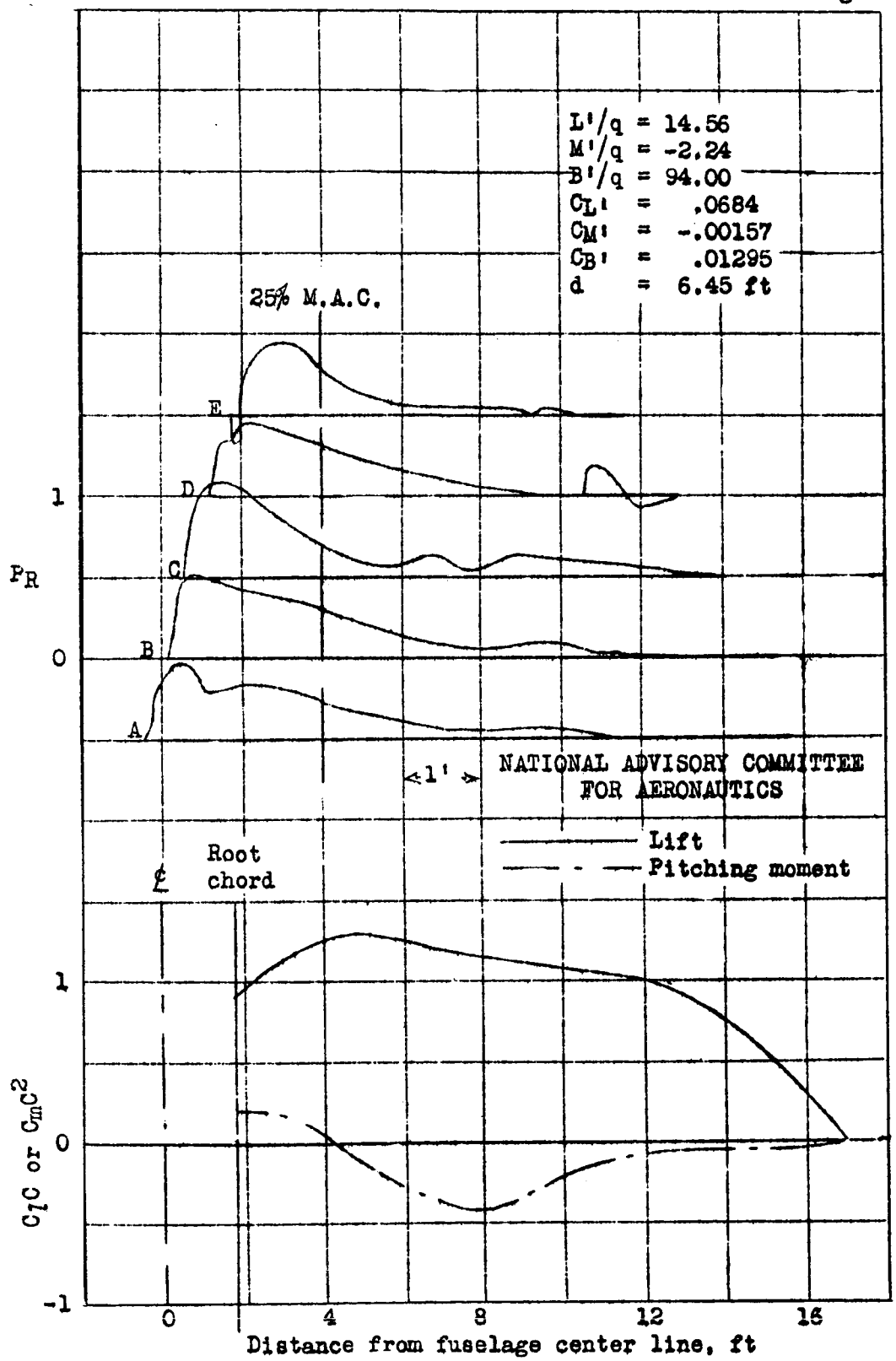

Figure 15.- Continued. (i) Lift coefficient = .20, Mach number = .50. P-39N-1.

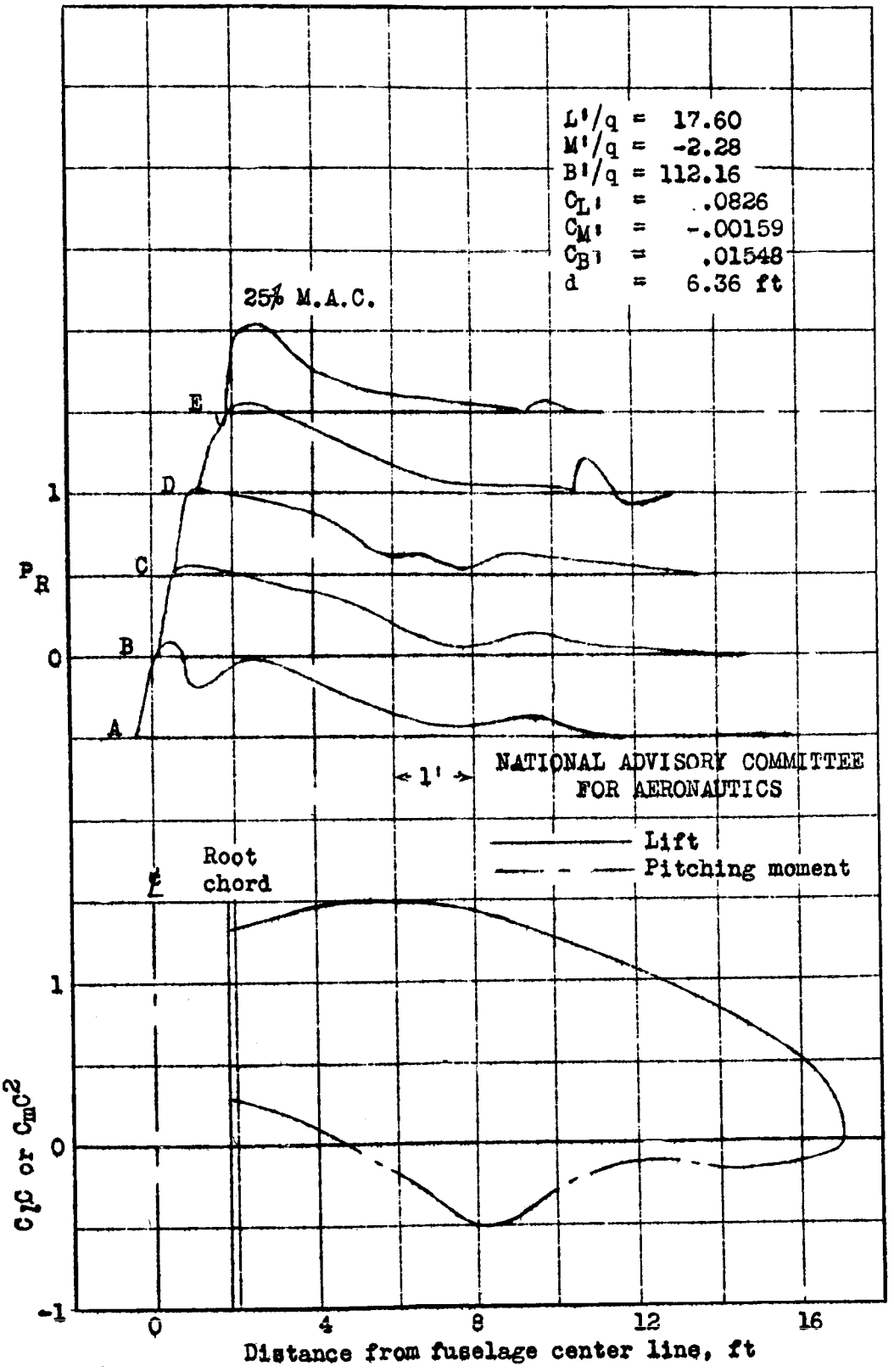

Figure 15.- Continued. (j) Lift coefficient = .20, Mach number = .60. P-39N-1.

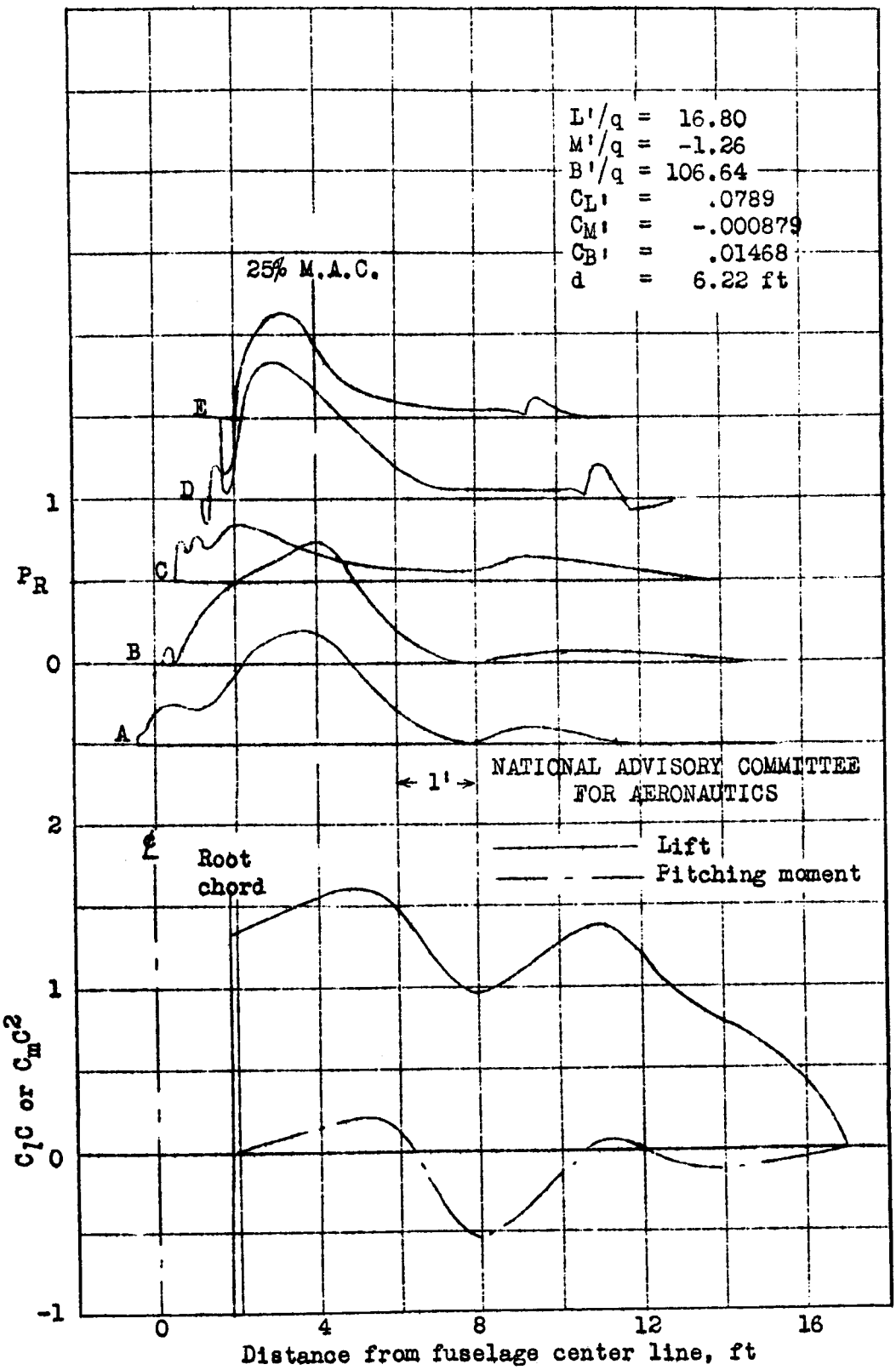

Figure 15.- Continued. (k) Lift coefficient = .20, Mach number = .70. P-39N-1.

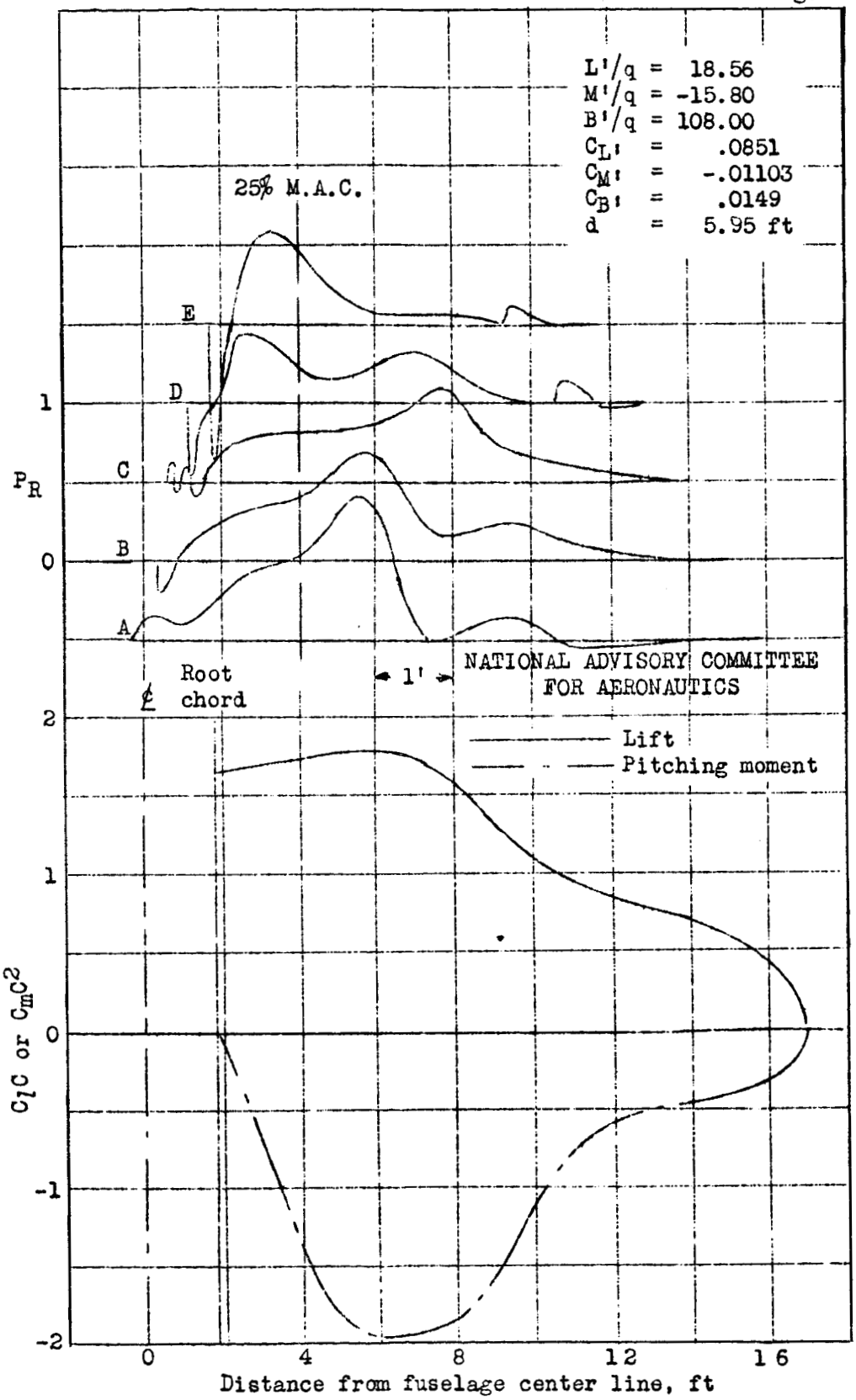

Figure 15.- Continued. (1) Lift coefficient = .20, Mach number = .78. P-39N-1.

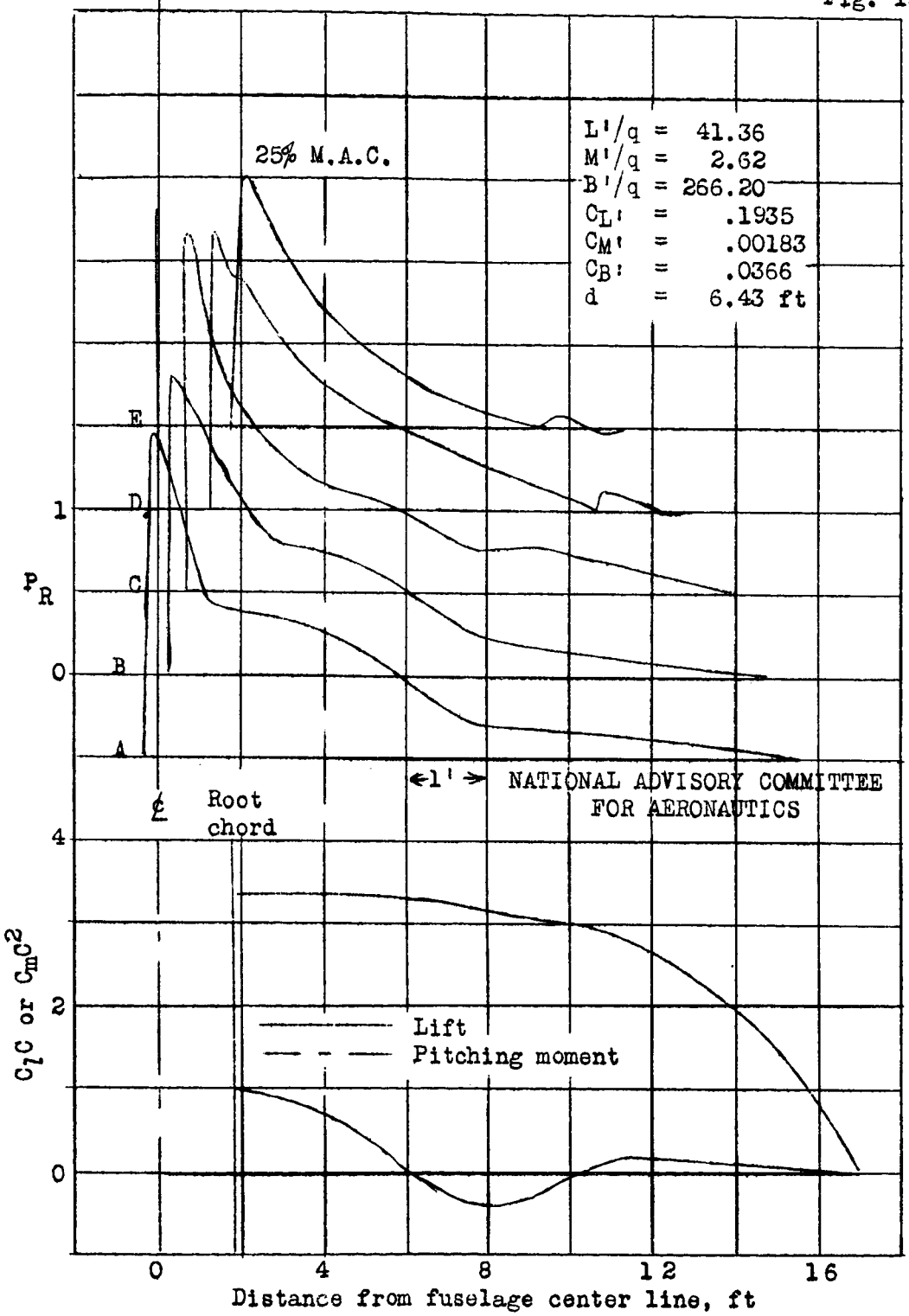

Figure 15.- Continued. (m) Lift coefficient = .50, Mach number = .30. P-39N-1.

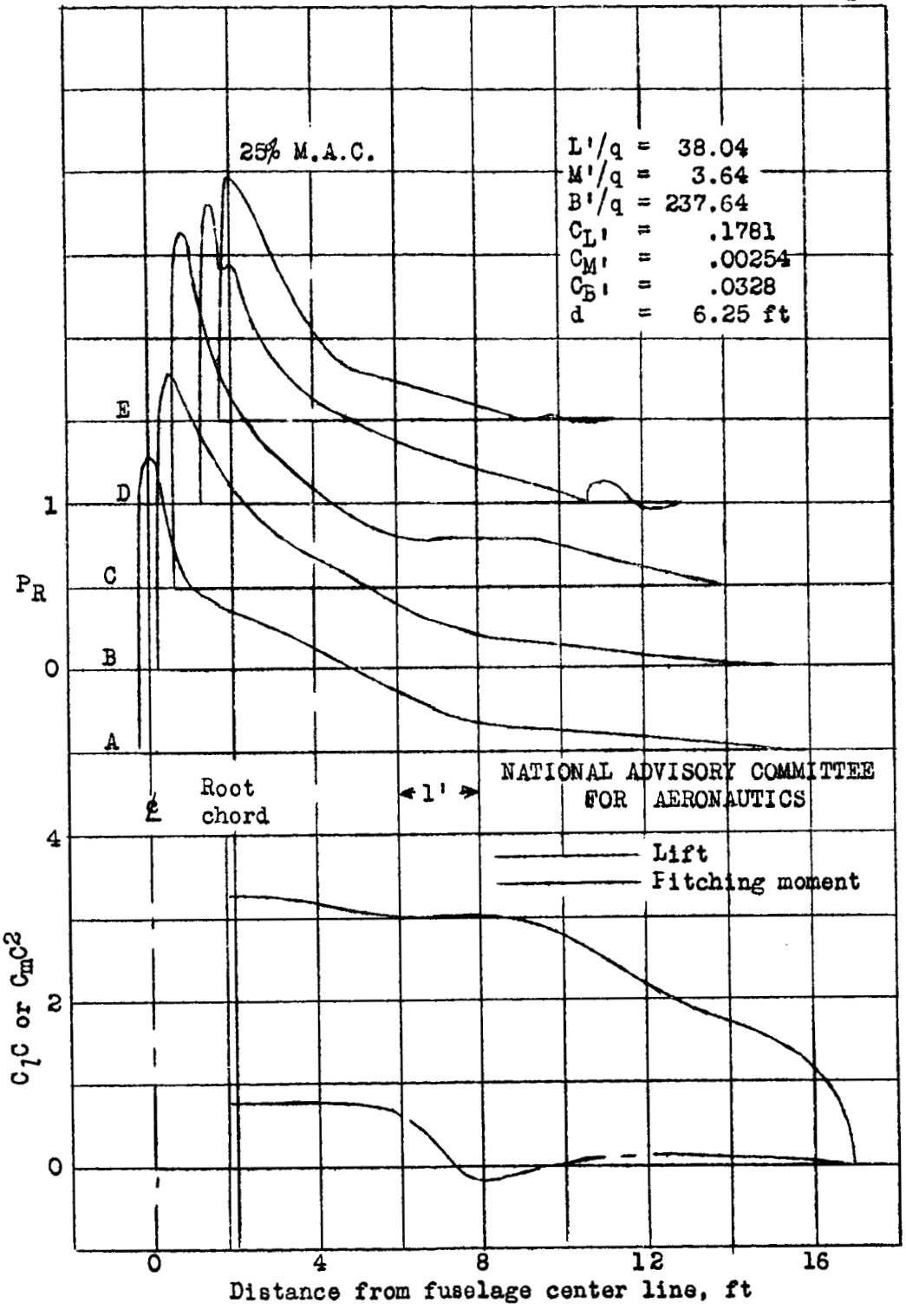

Figure 15.- Continued. (n) Lift coefficient = .50, Mach number = .40. P-39N-1.

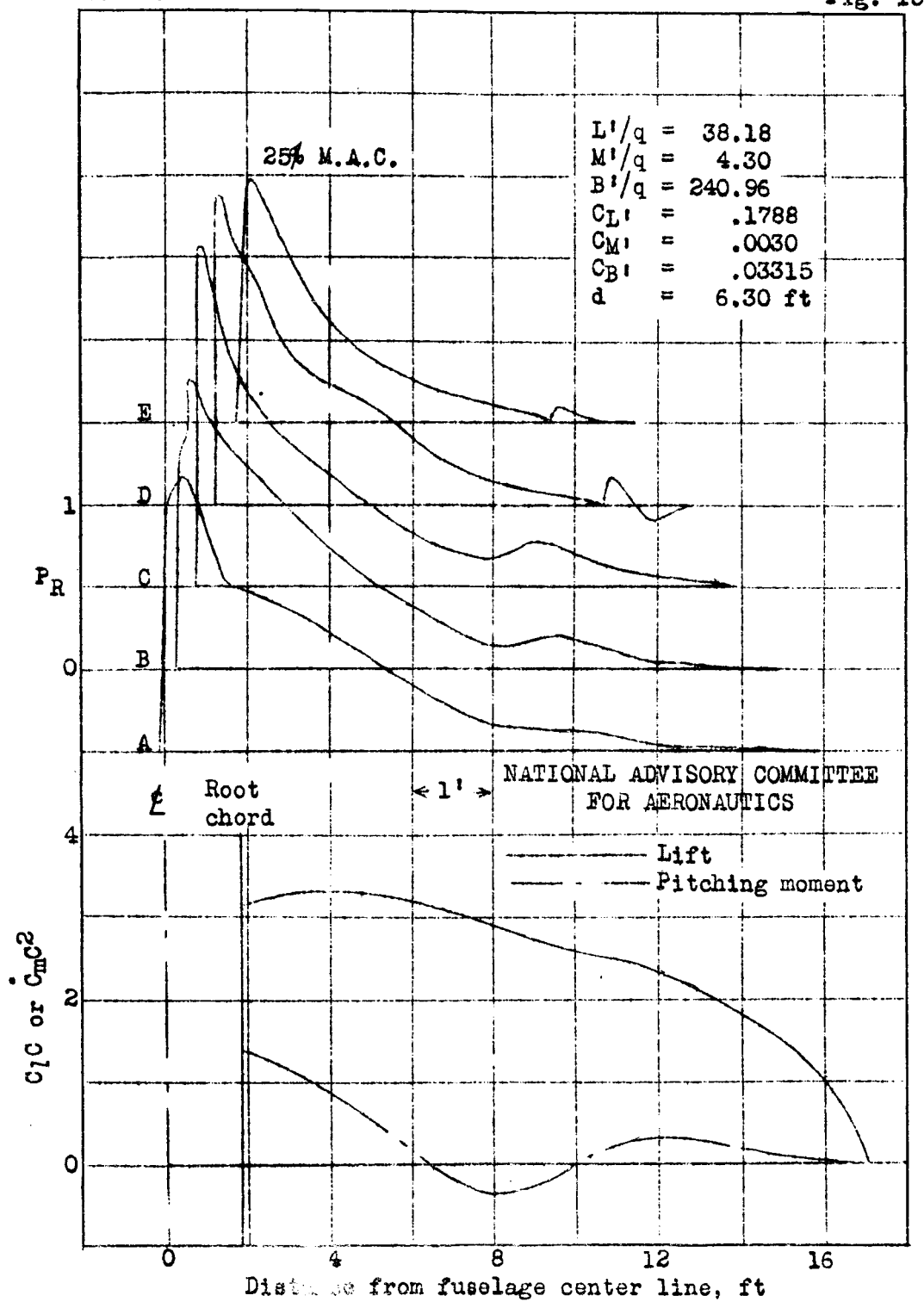

Figure 15.- Continued. (o) Lift coefficient = .50, Mach number = .50. P-39N-1.

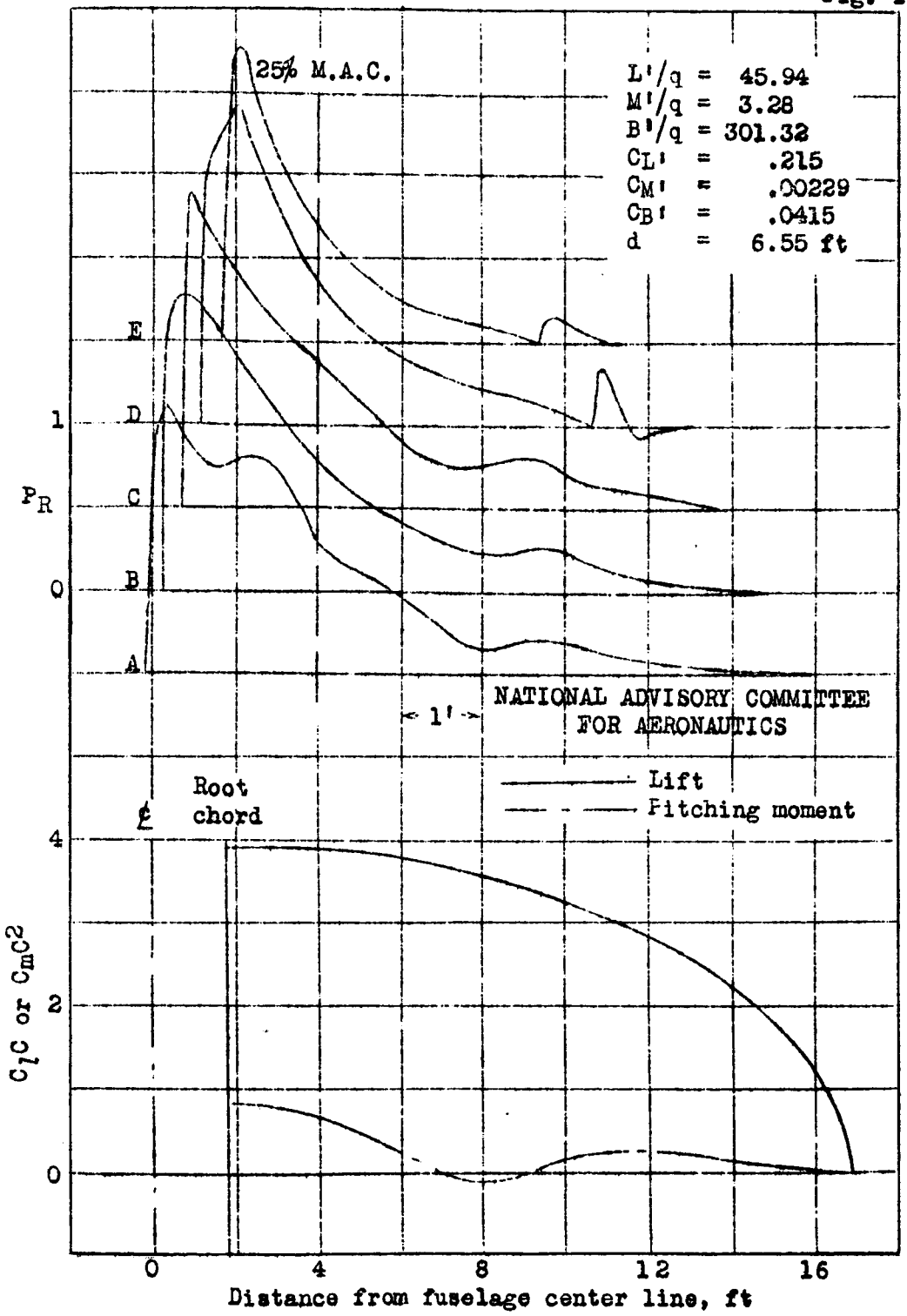

Figure 15.- Continued. (p) Lift coefficient = .50, Mach number = .60. P-39N-1.

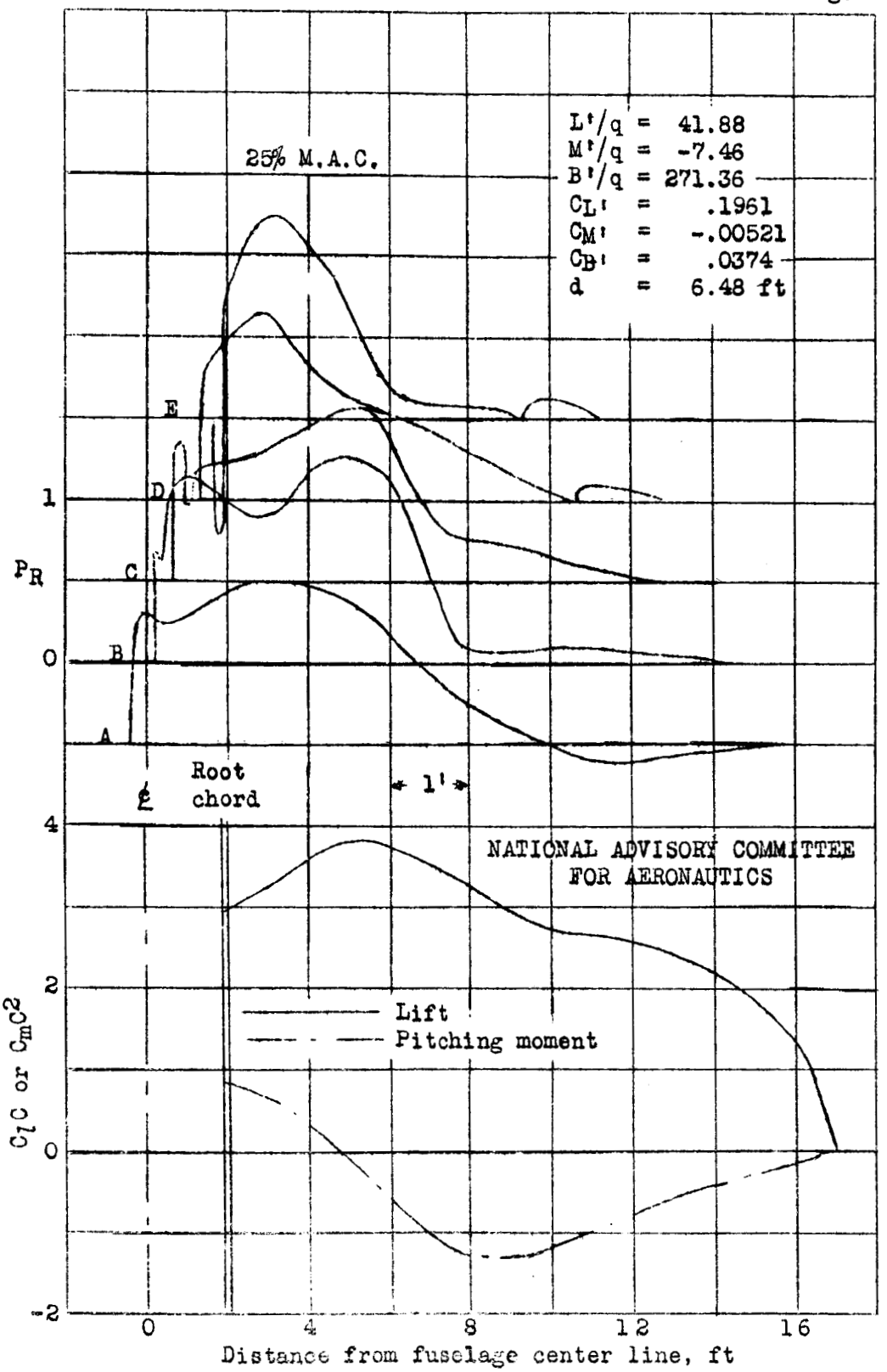

Figure 15.- Continued. (q) Lift coefficient = .50, Mach number = .73, P-39N-1.

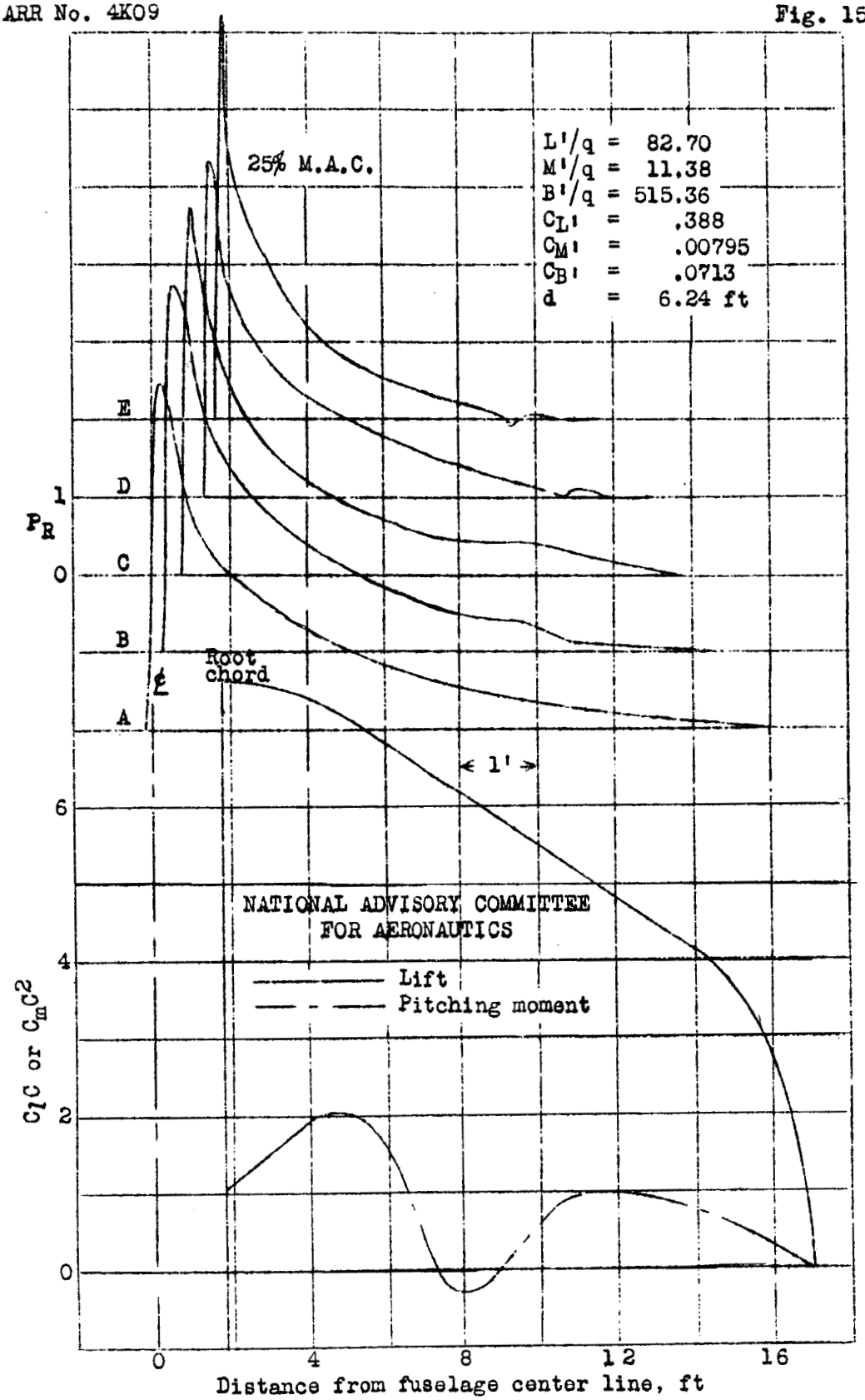

Figure 15.- Continued. (r) Lift coefficient = 1.00, Mach number = .30, P-39N-1.

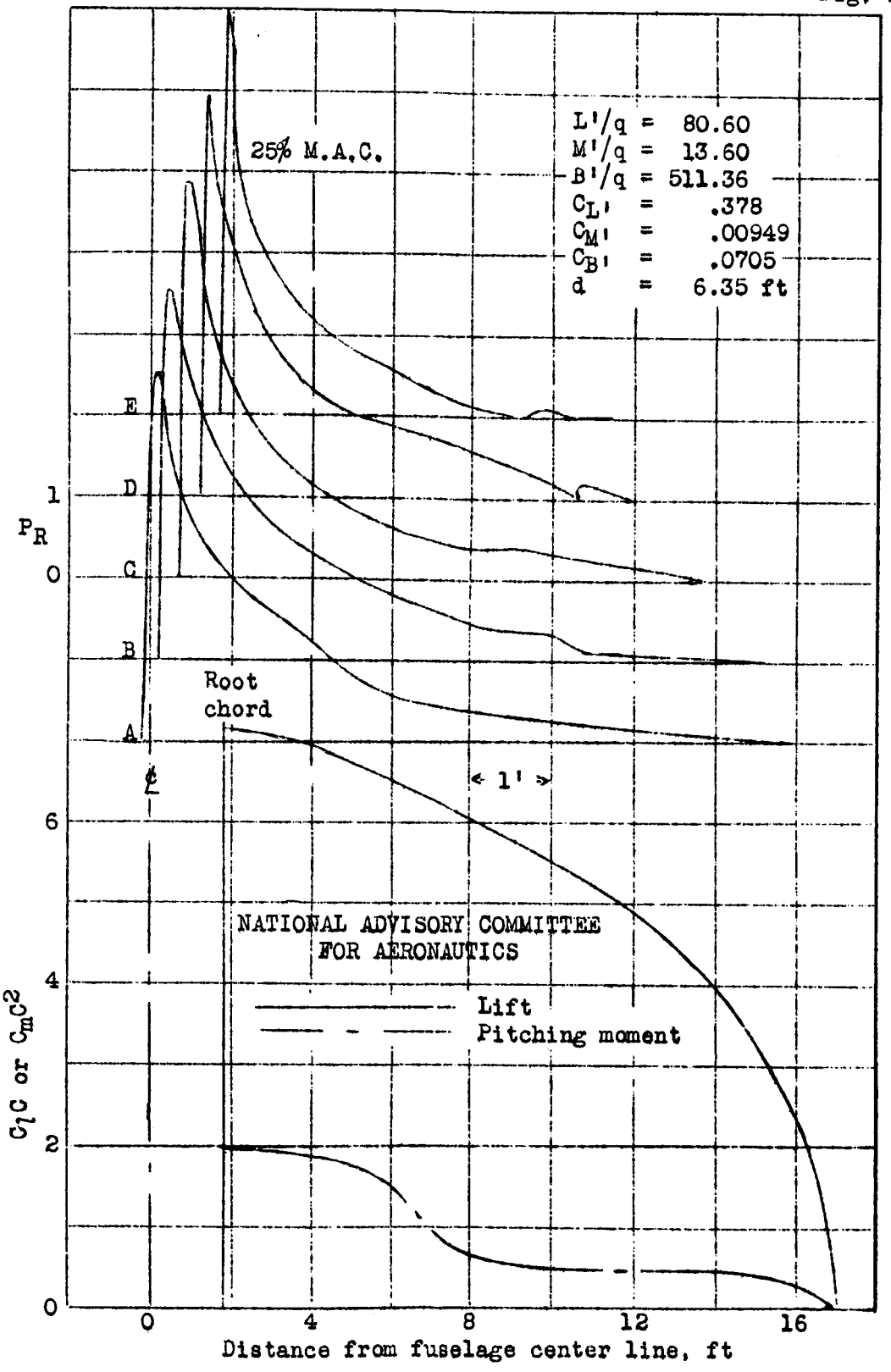

Figure 15.- Continued. (s) Lift coefficient = 1.00, Mach number = .40. P-39N-1

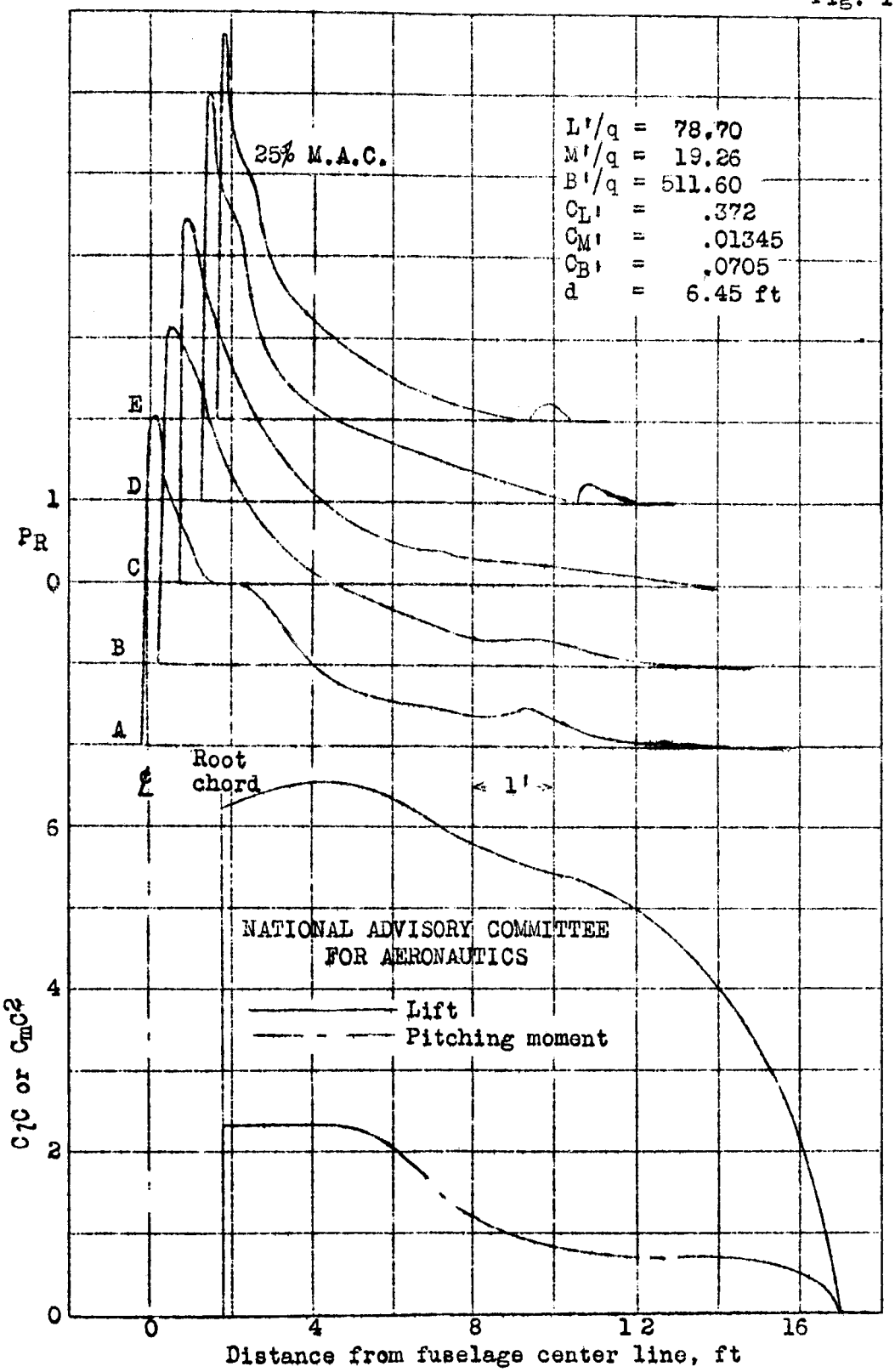

Figure 15.- Continued. (t) Lift coefficient = 1.00, Mach number = .50, P-39N-1.

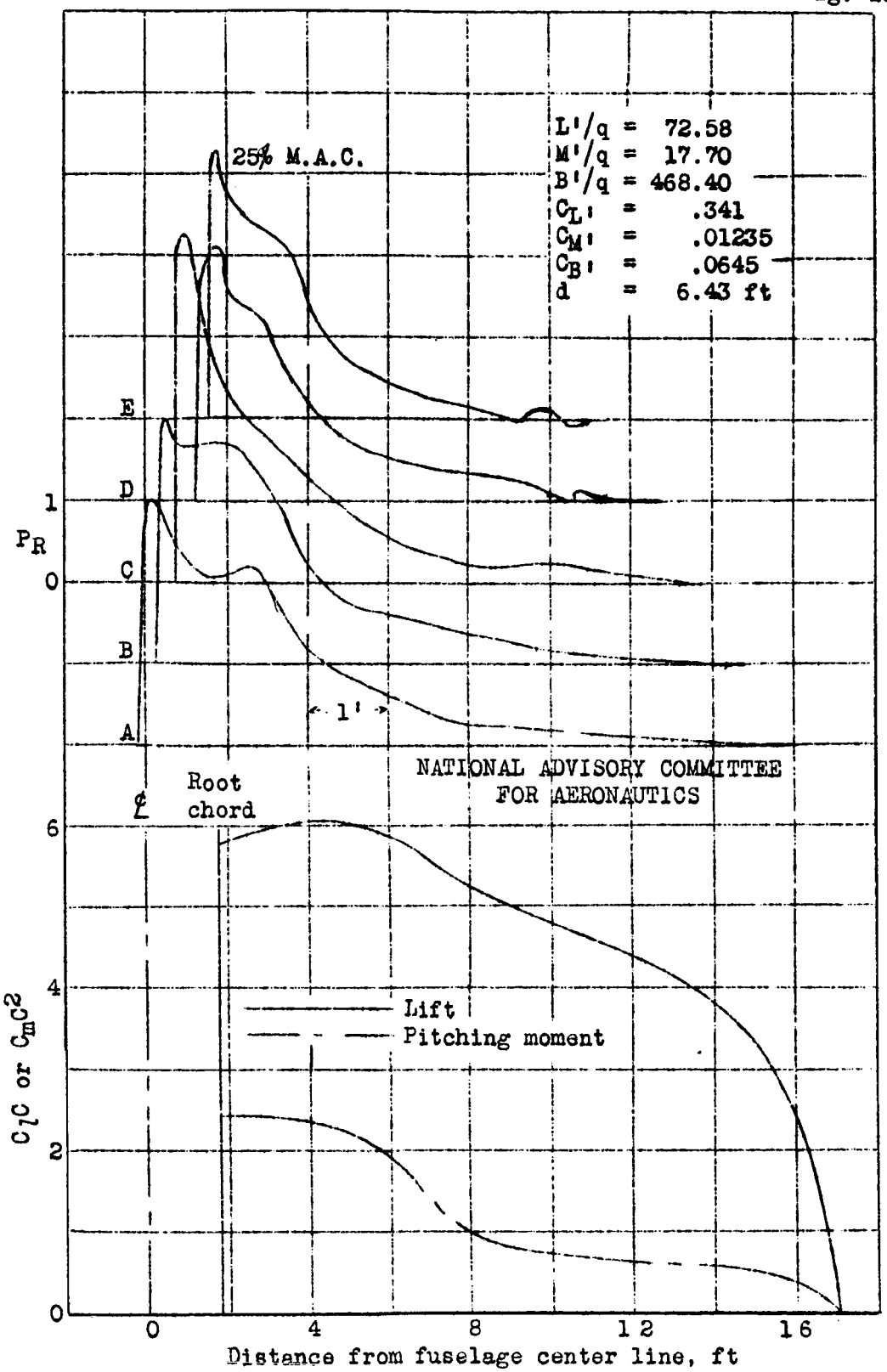

Figure 15.- Concluded. (u) Lift coefficient = 1.00, Mach number = .60. P-39N-1.

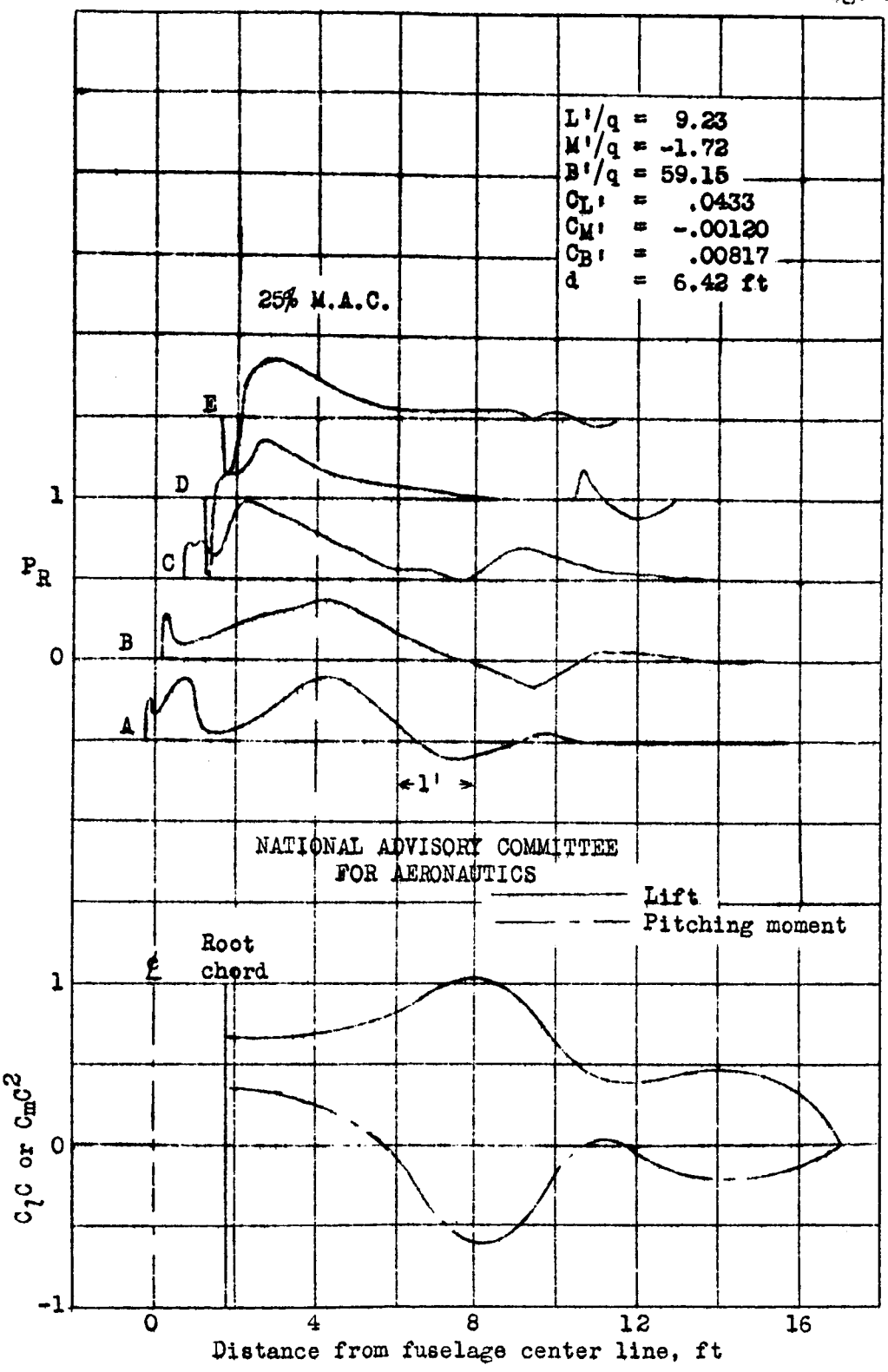

Figure 16.- Pressure distribution on the right wing in power-off flight. P-39N-1 airplane. (a) Lift coefficient = .10, Mach number = .30.

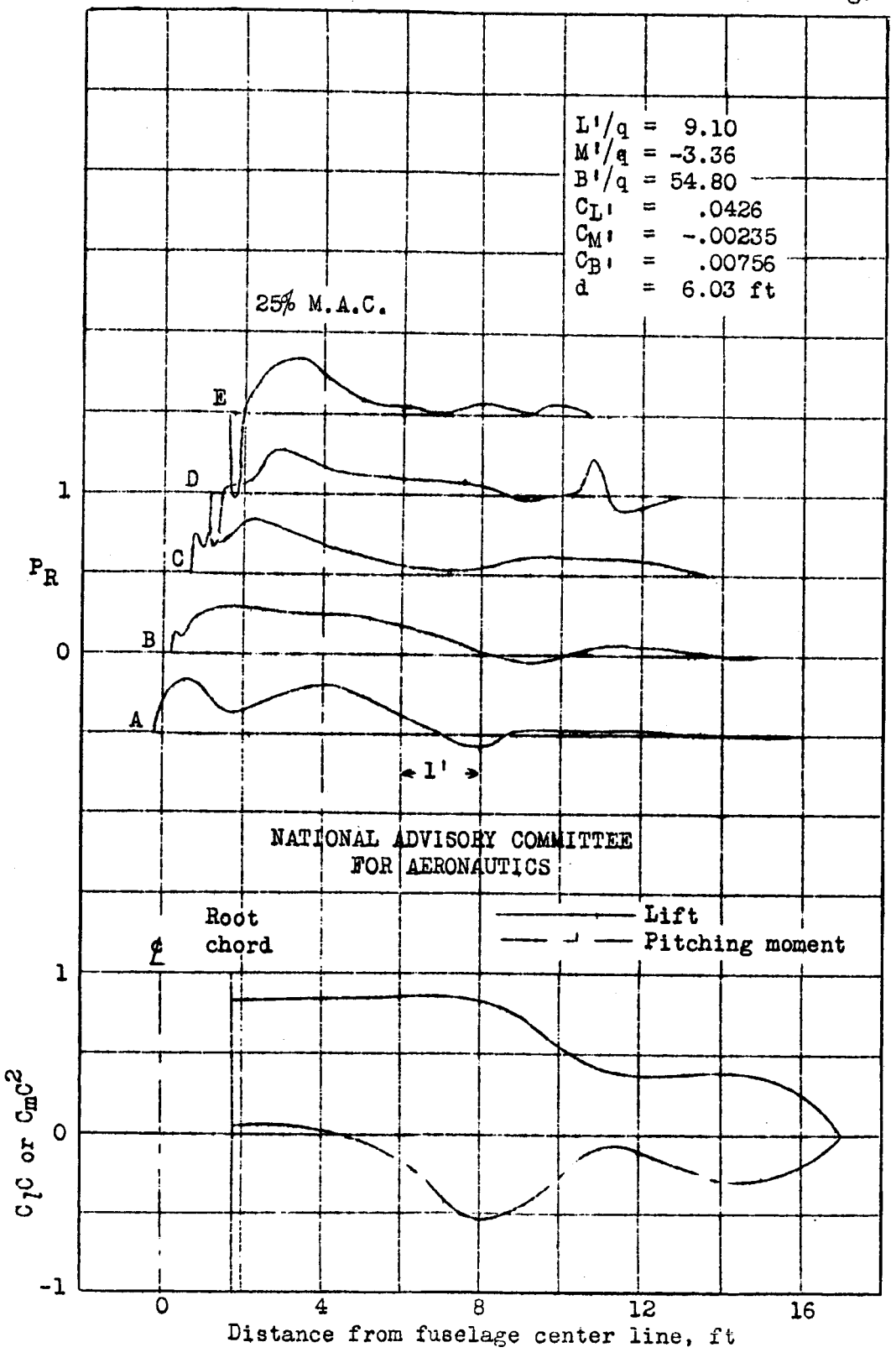

Figure 16.- Continued. (b) Lift coefficient = .10, Mach number = .40. P-39N-1.

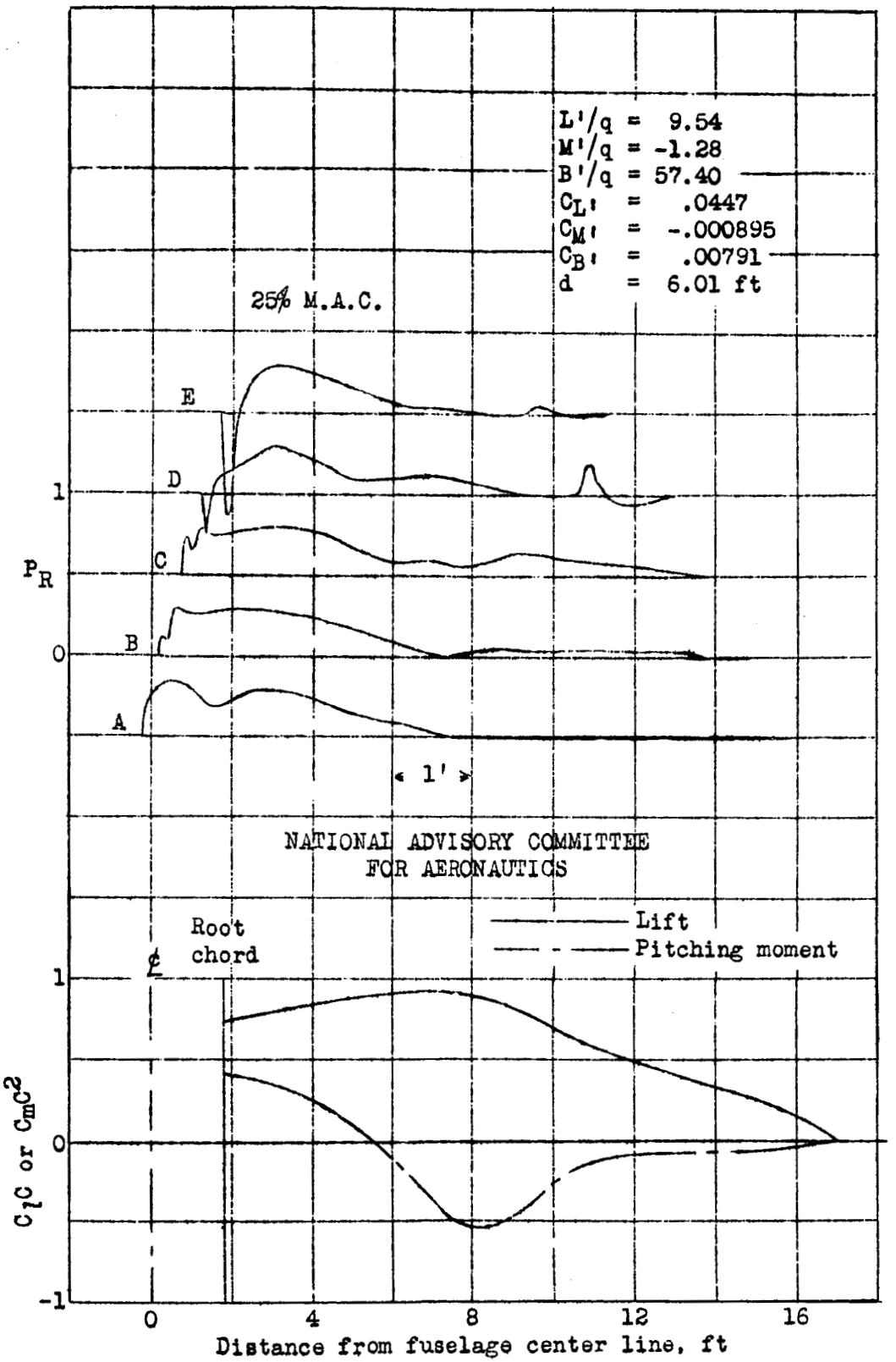

Figure 16.- Continued. (c) Lift coefficient = .10, Mach number = .50. P-39N-1.

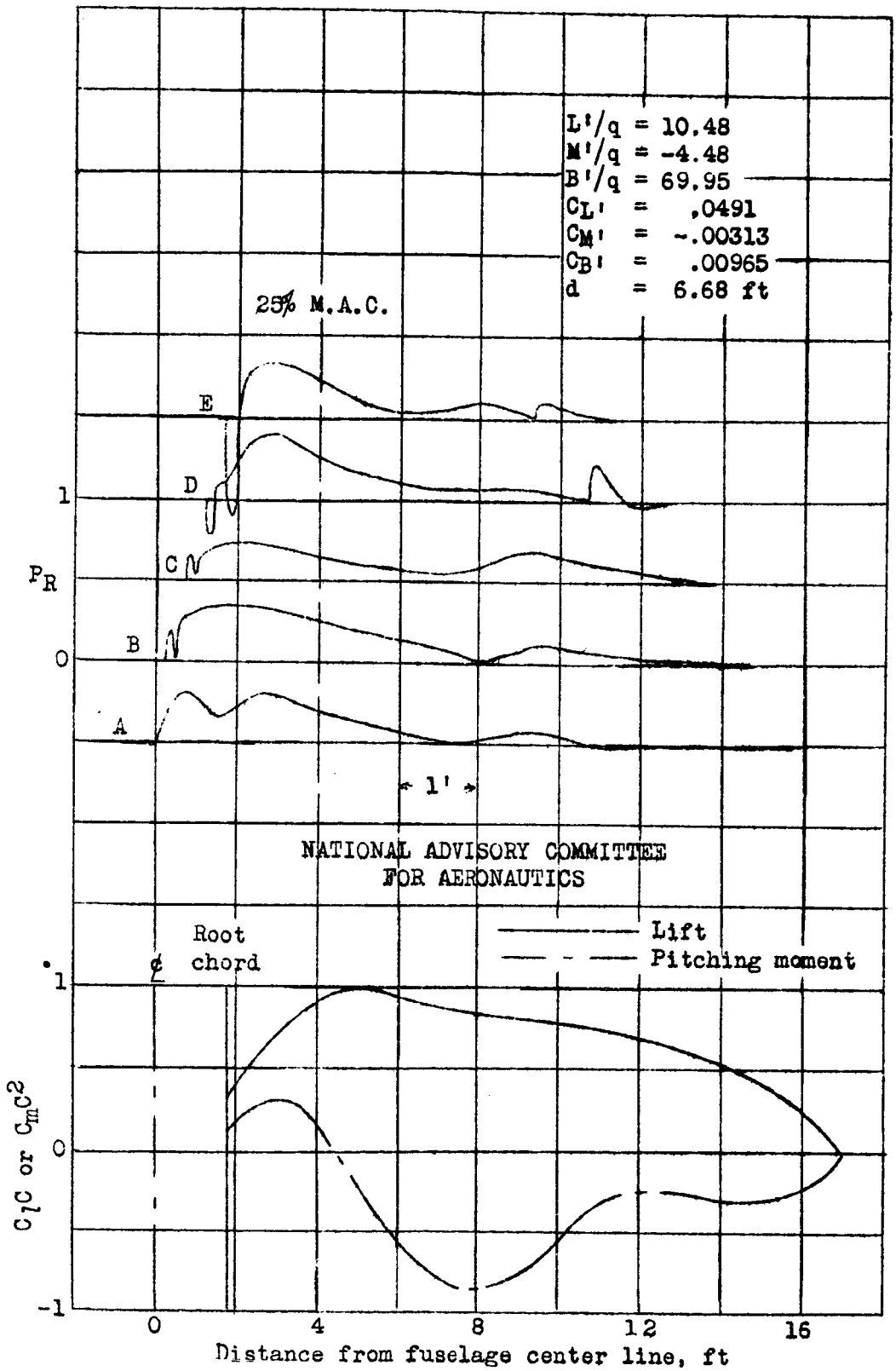

Figure 16.- Continued. (d) Lift coefficient = .10, Mach number = .60. P-39N-1.

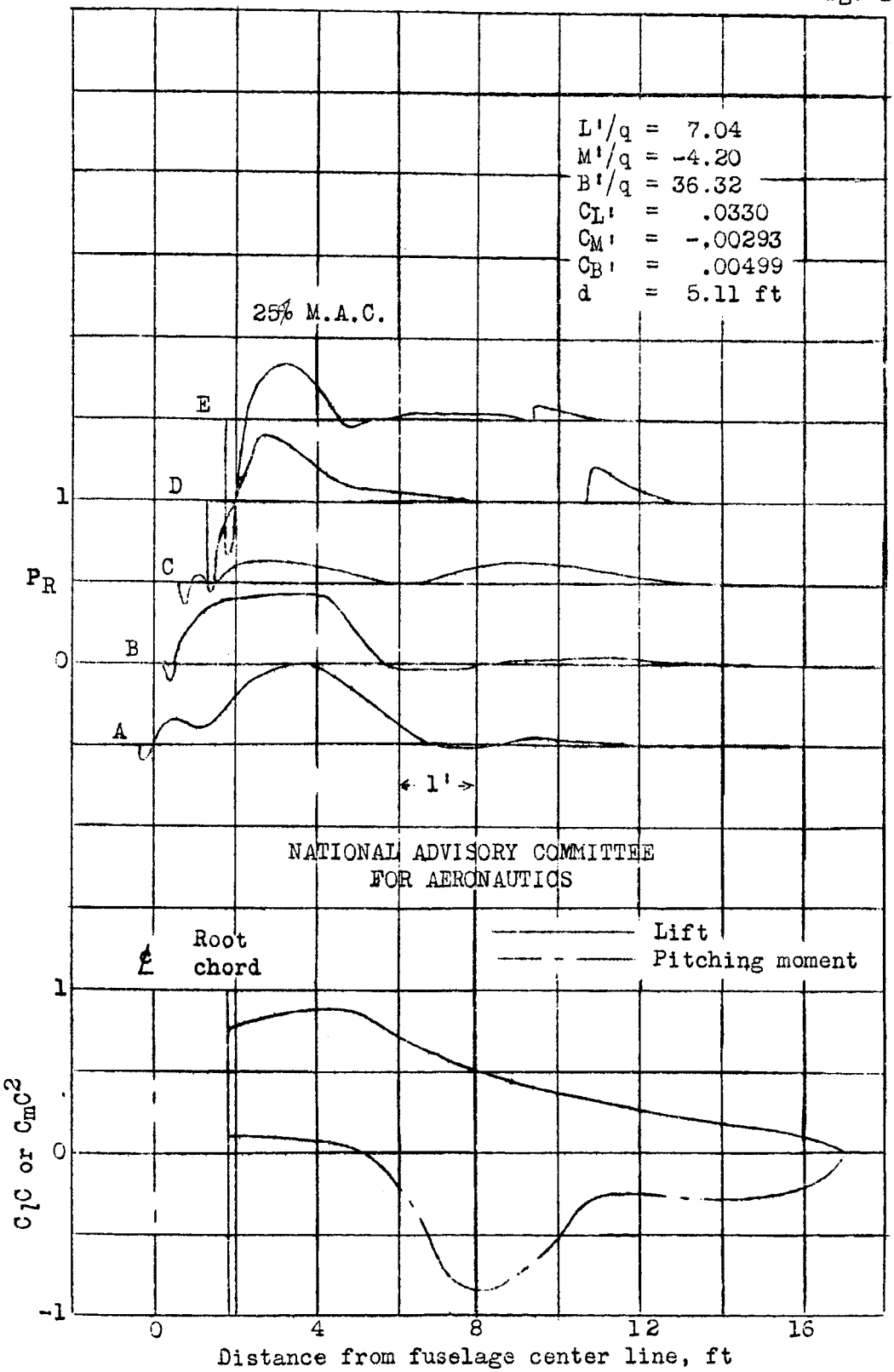

Figure 16.- Continued. (e) Lift coefficient = .10, Mach number = .70. P-39N-1.

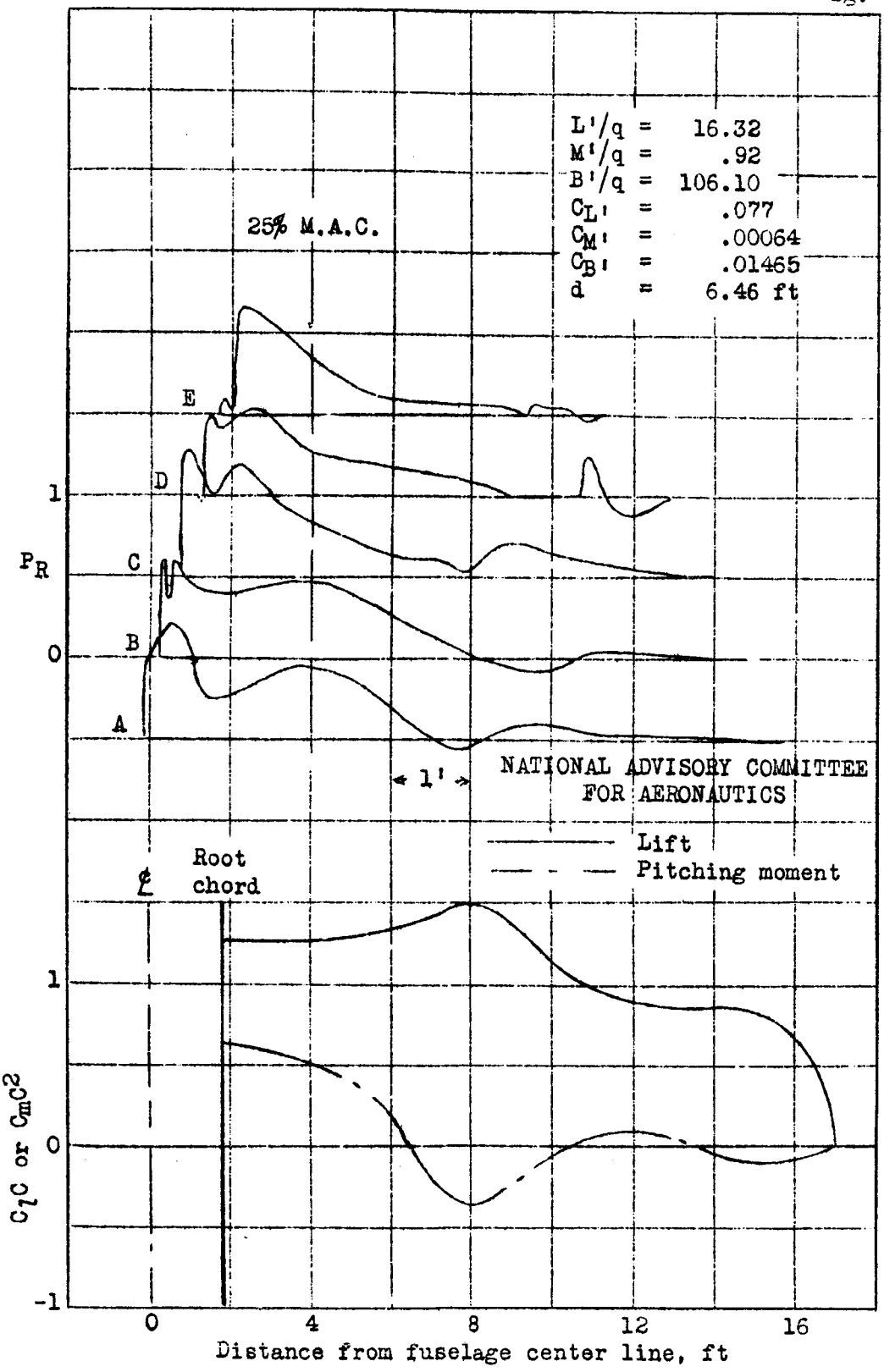

Figure 16.- Continued. (g) Lift coefficient = .20, Mach number = .30. P-39N-1.

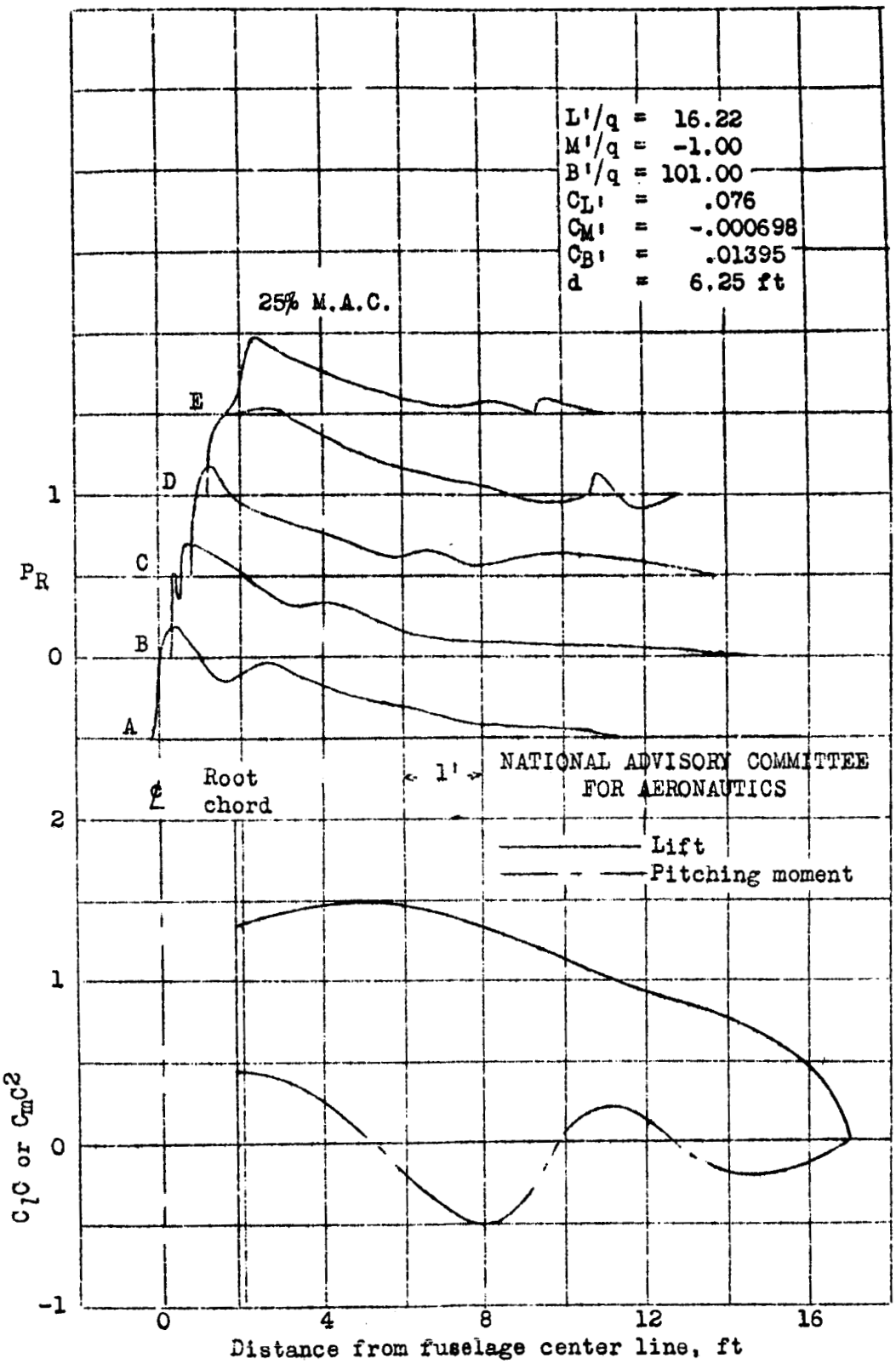

Figure 16.- Continued. (h) Lift coefficient = .20, Mach number = .40. P-39N-1.

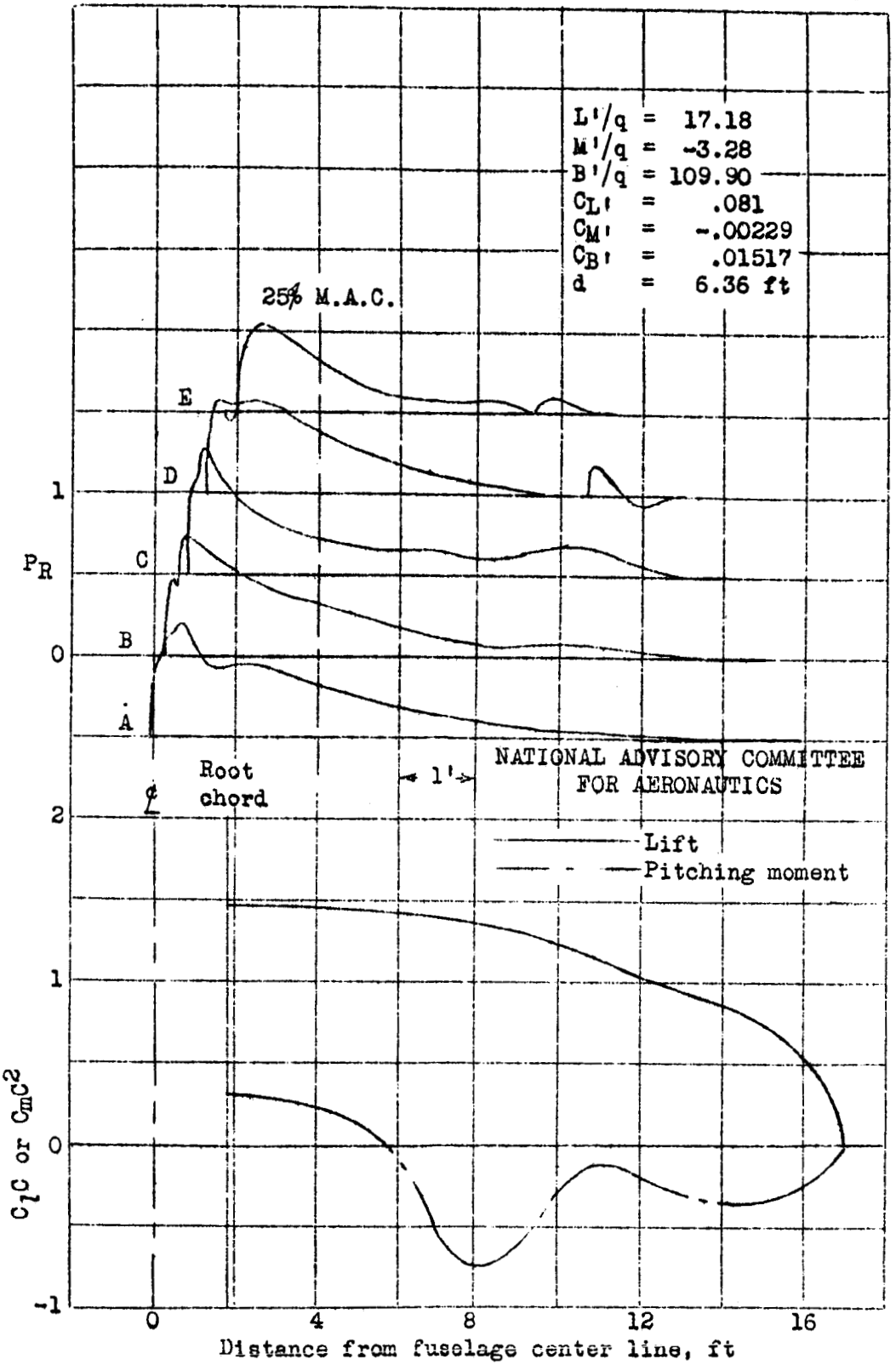

Figure 16.- Continued. (i) Lift coefficient = .20, Mach number = .50. P-39N-1.

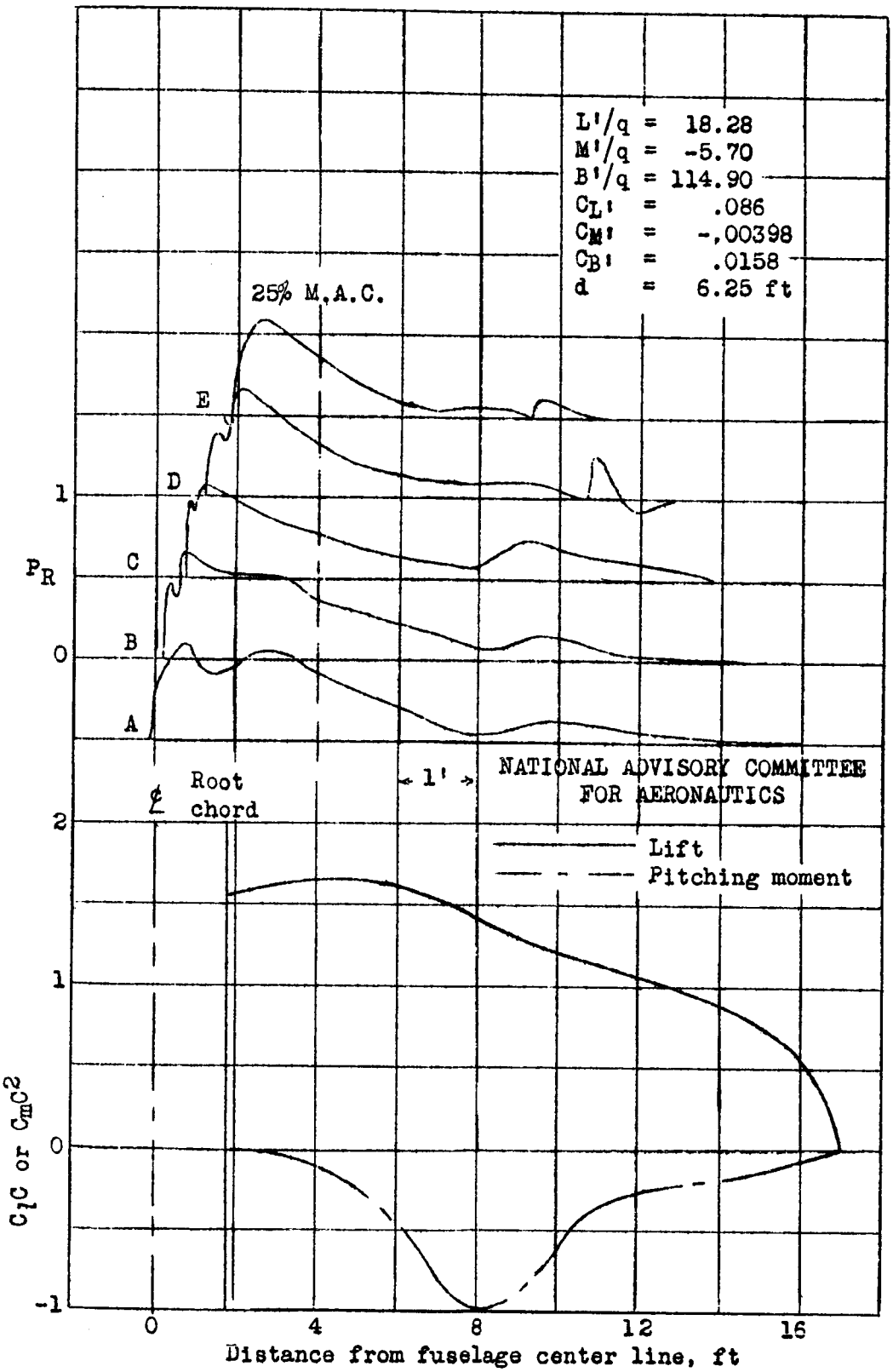

Figure 16.- Continued. (j) Lift coefficient = .20, Mach number = .60. P-39N-1.

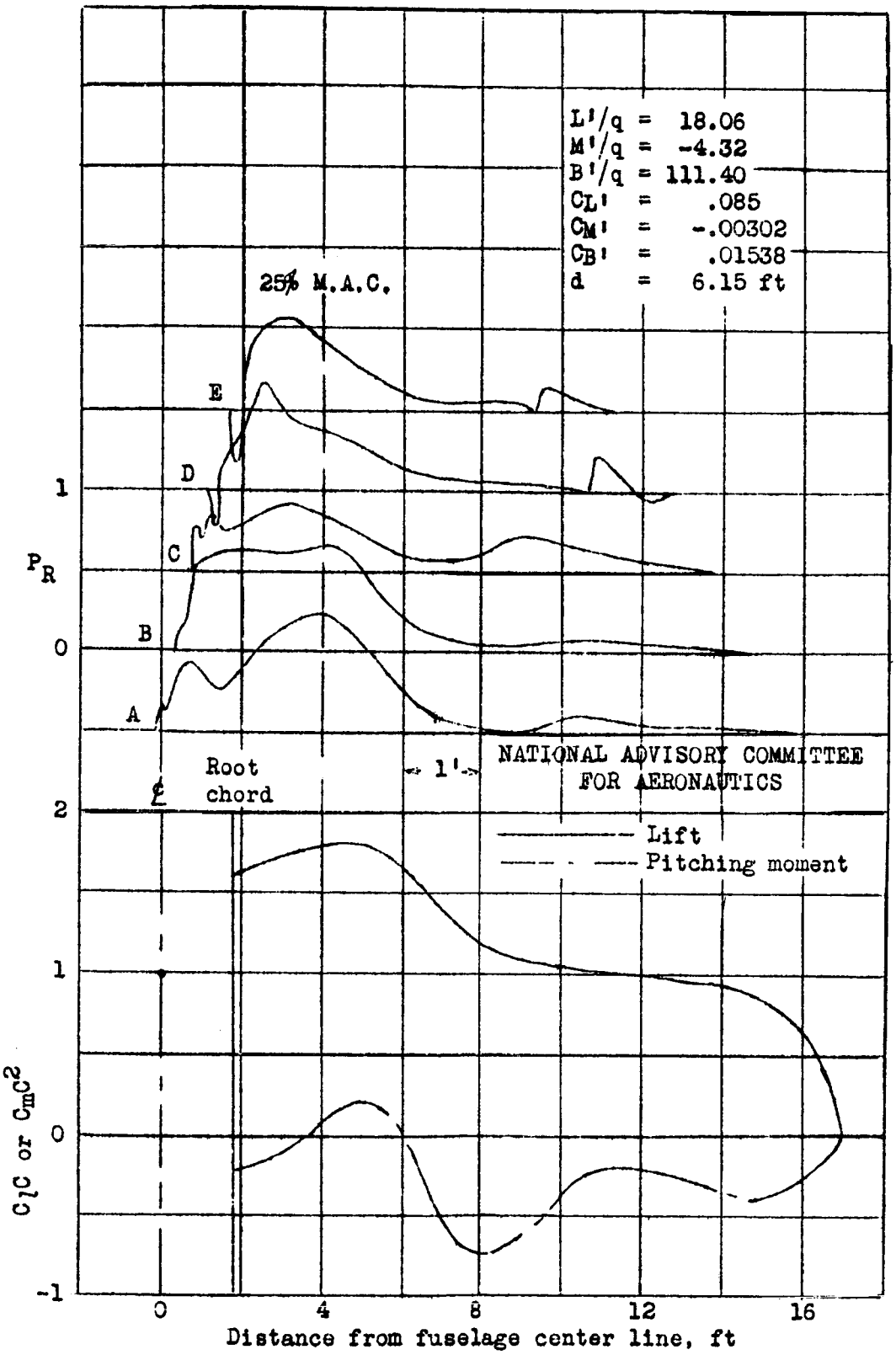

Figure 16. Continued. (k) Lift coefficient = .20, Mach number = .70, P-39N-1.

Fig. 16 1

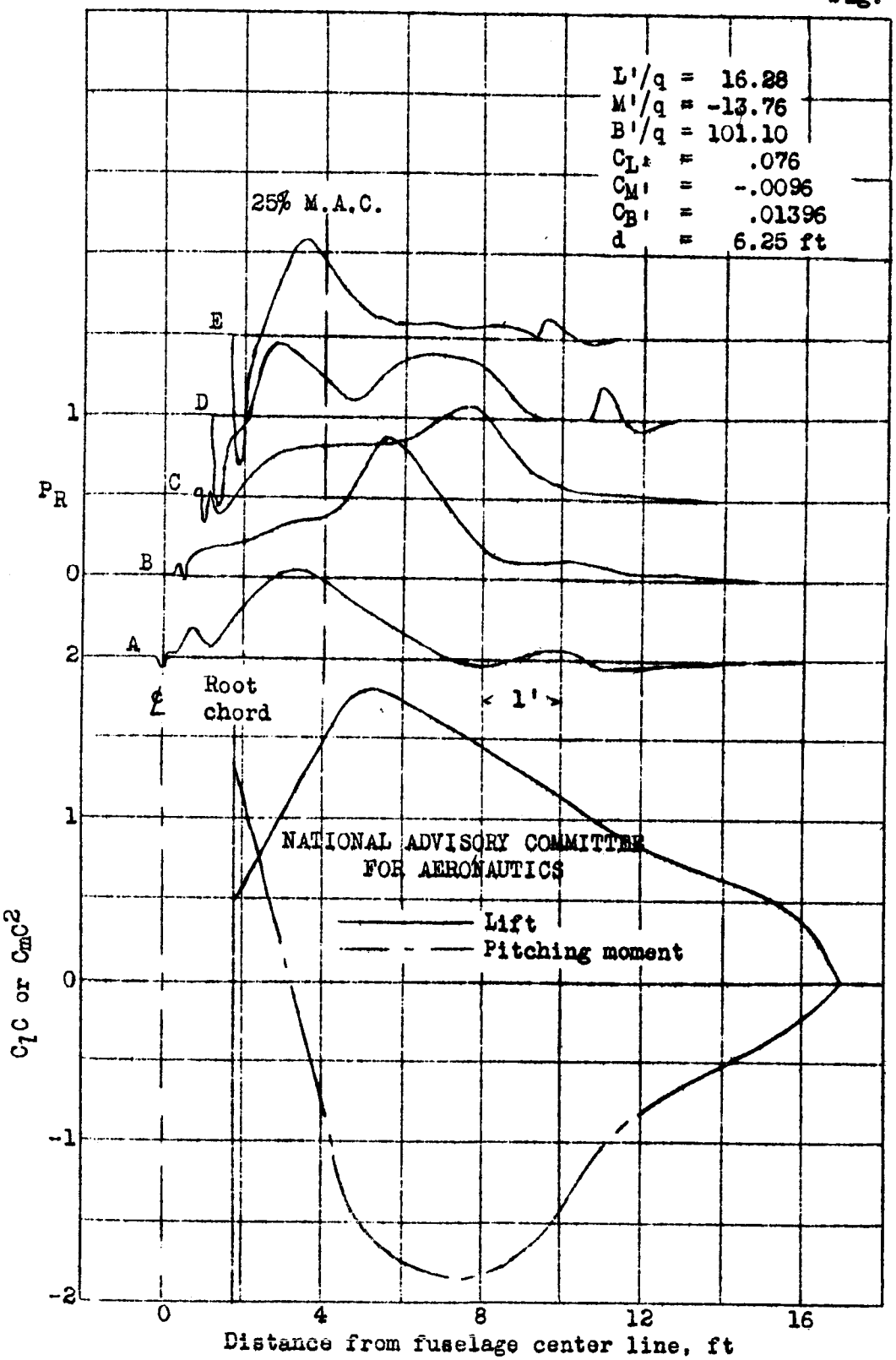

Figure 16.- Continued. (1) Lift coefficient = .20, Mach number = .78. P-39N-1.

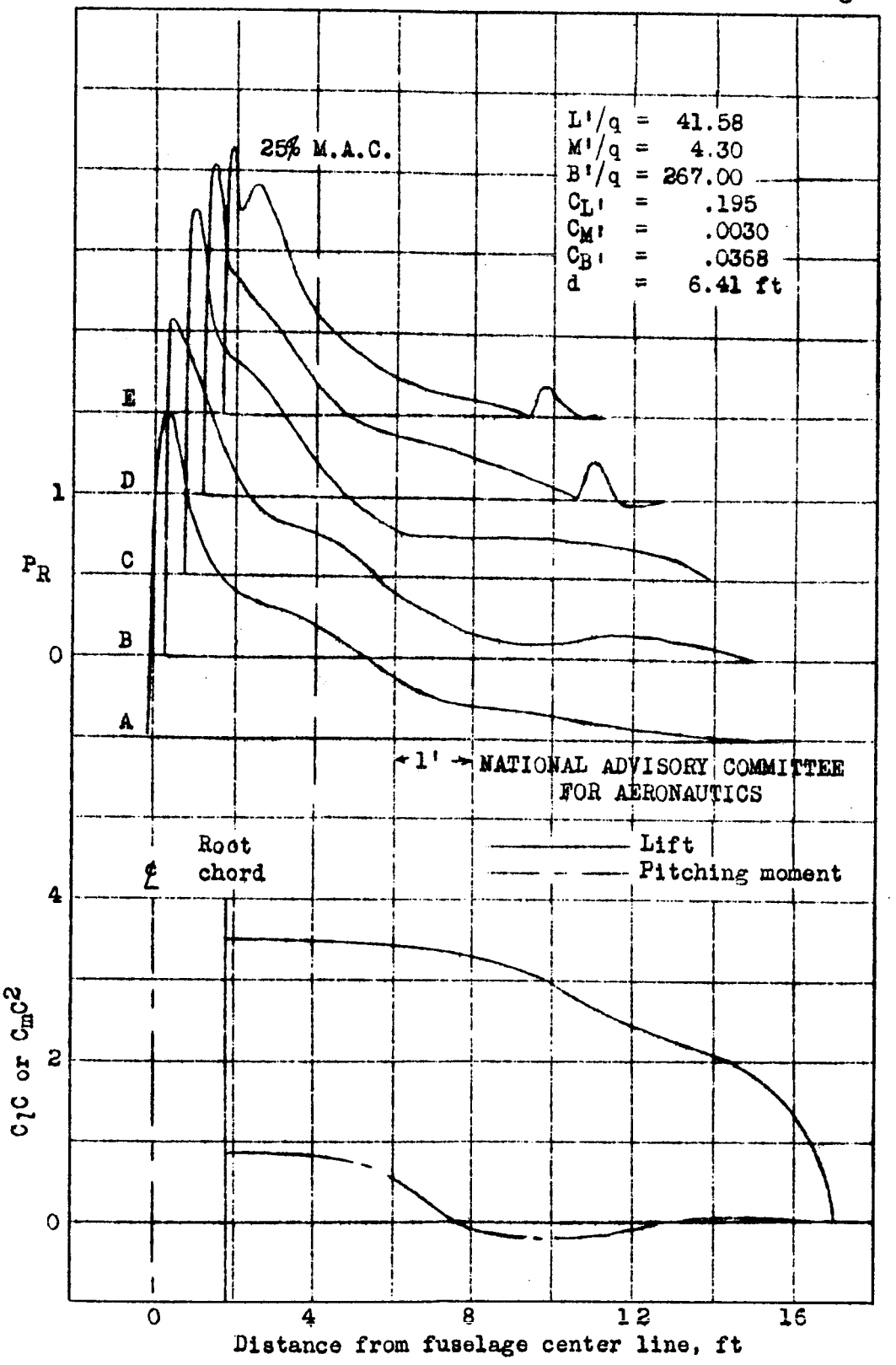

Figure 16.- Continued. (m) Lift coefficient = .50, Mach number = .30. P-39N-1.

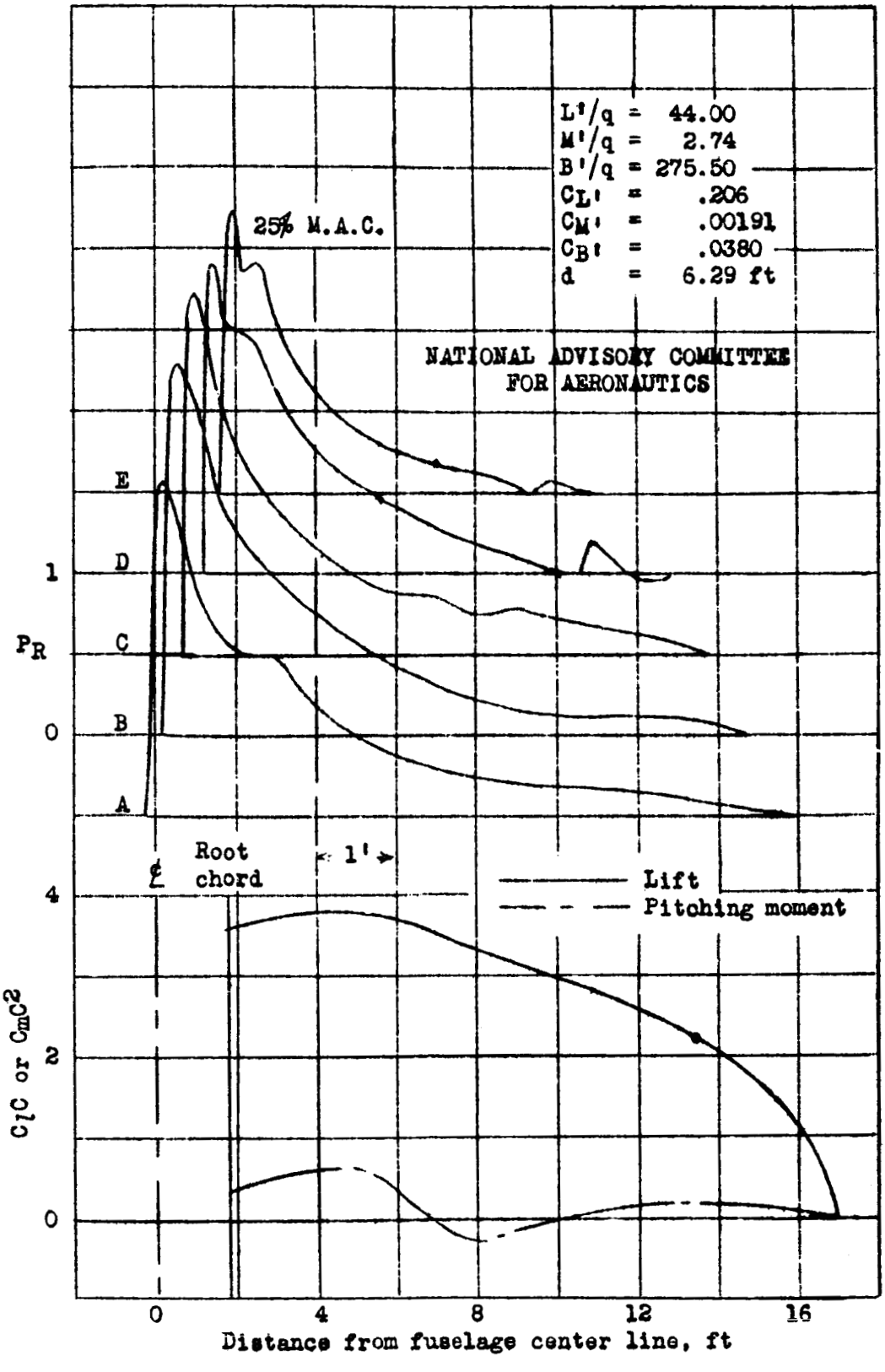

Figure 16.- Continued. (n) Lift coefficient = .50, Mach number = .40. P-39N-1.

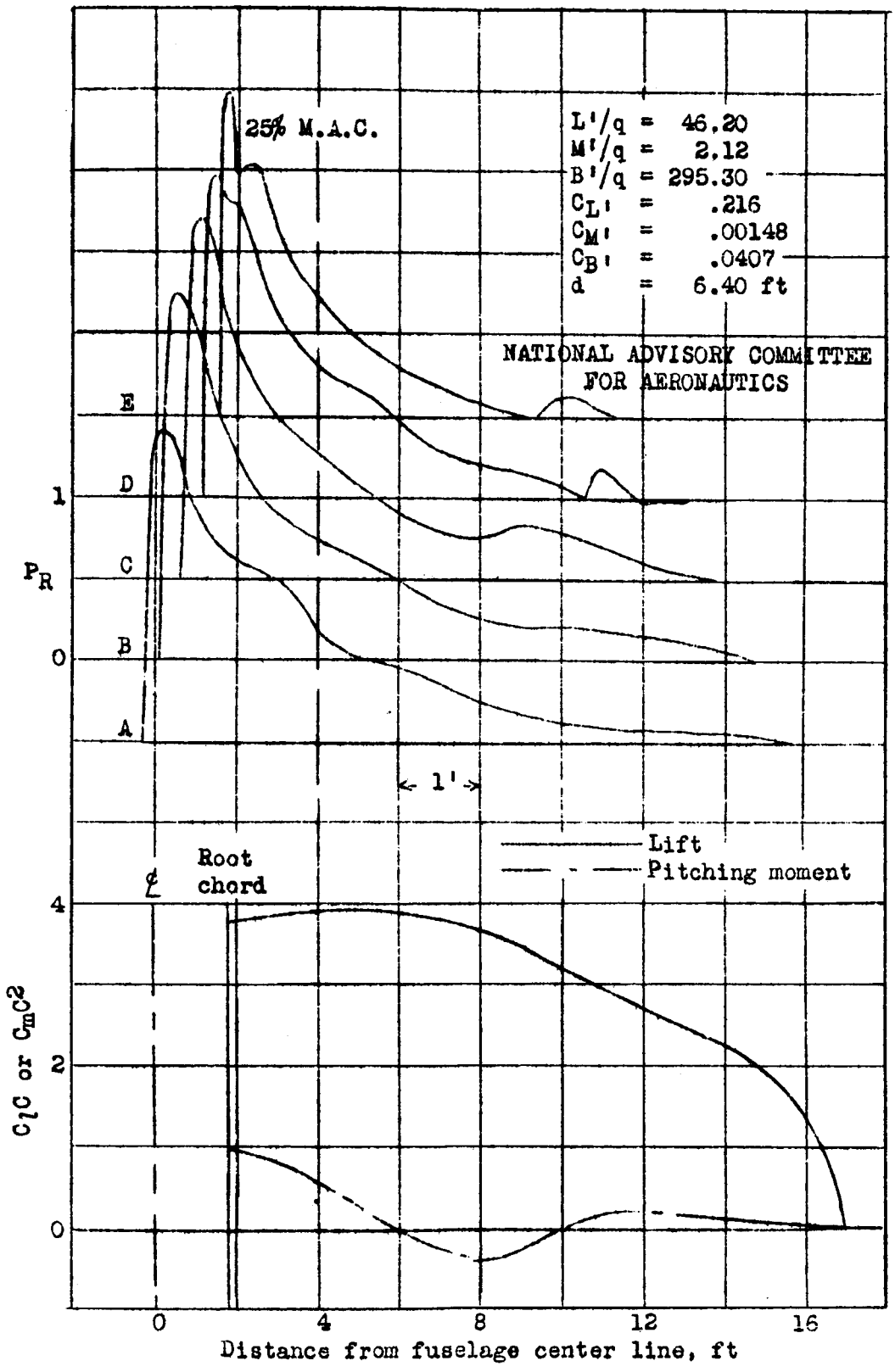

Figure 16.- Continued. (o) Lift coefficient = .50, Mach number = .50. P-39N-1.

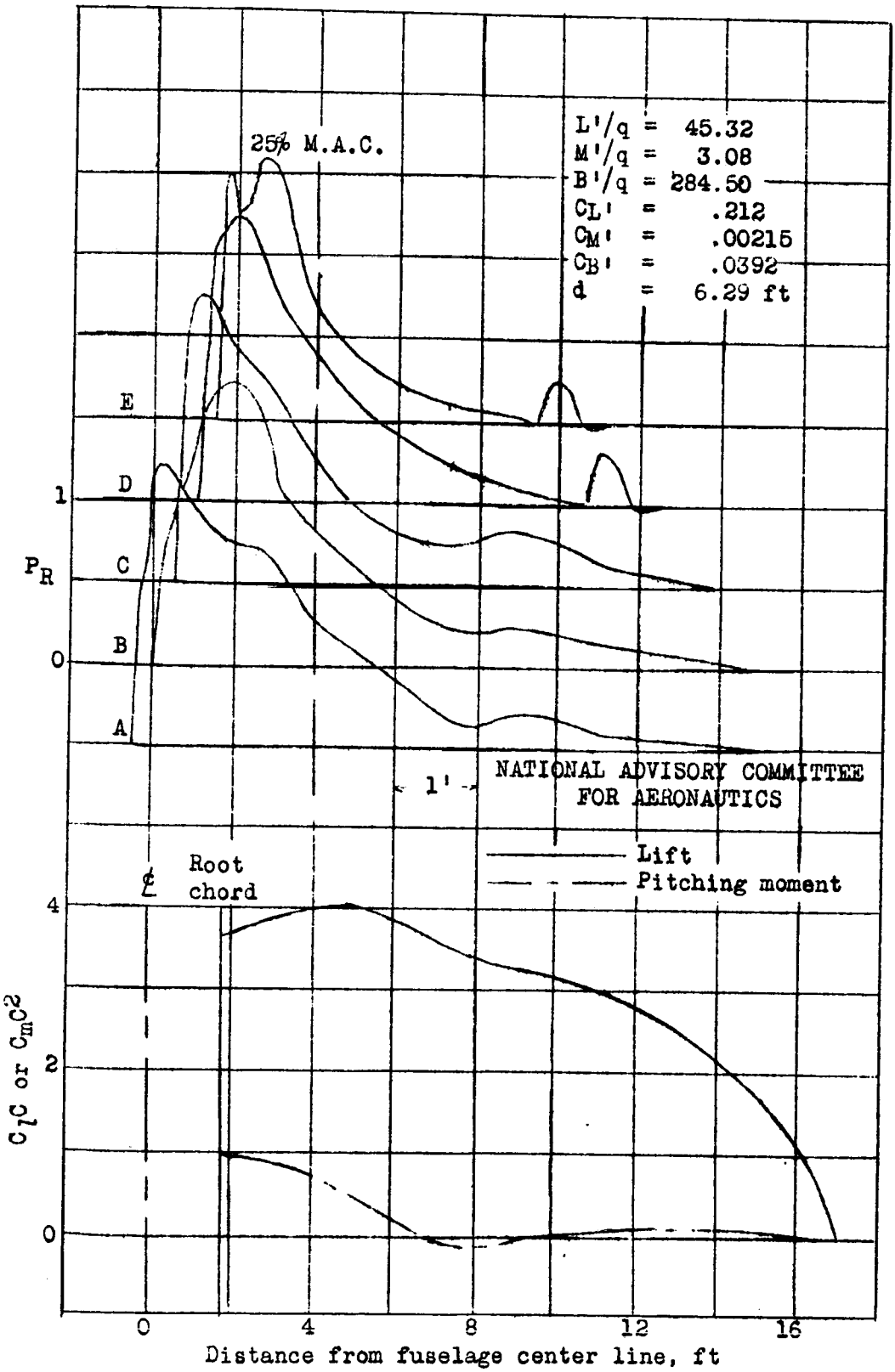

Figure 16.- Continued. (p) Lift coefficient = .50, Mach number = .60. P-39N-1.

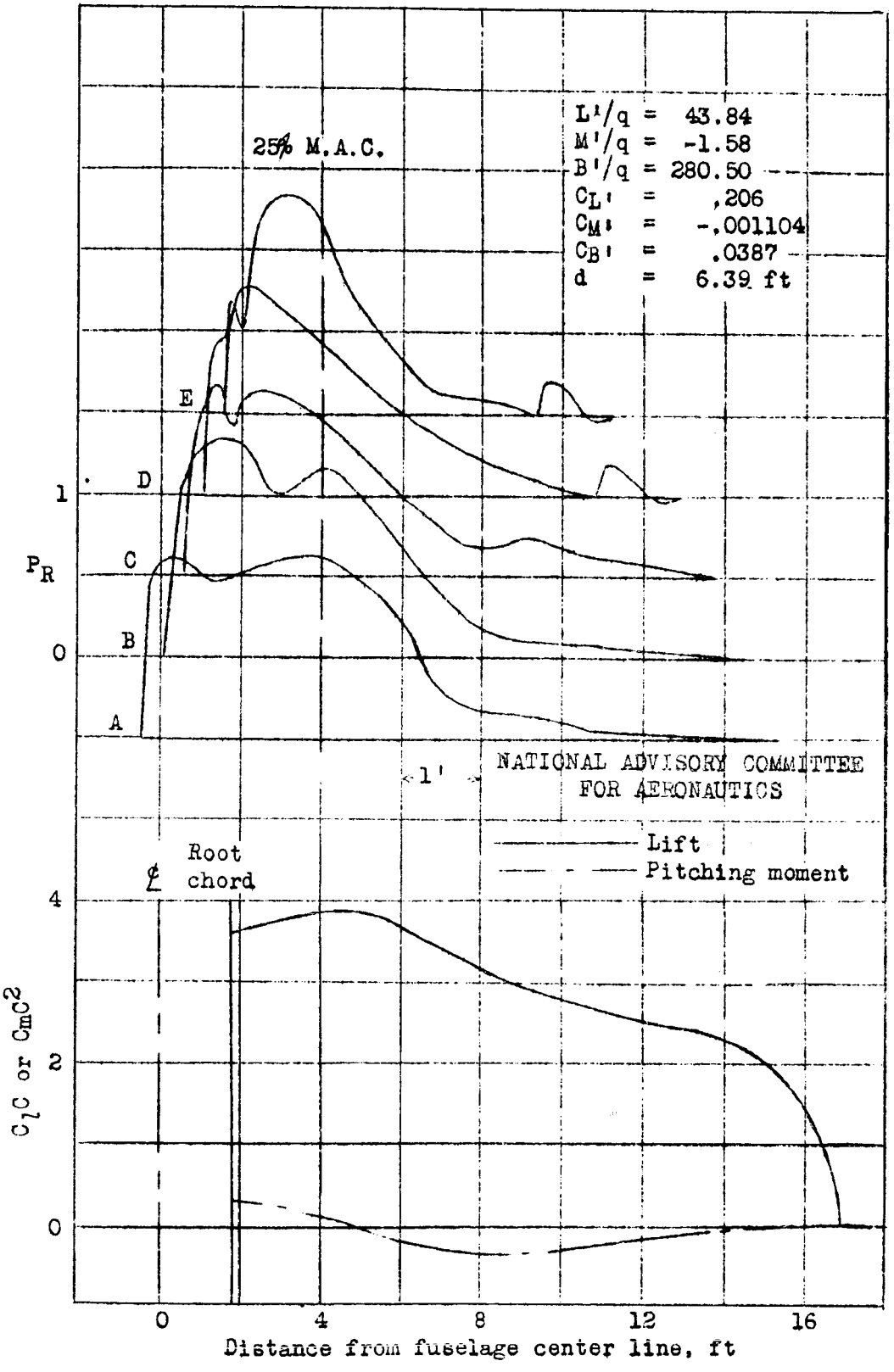

Figure 16.- Continued. (q) Lift coefficient = .50, Mach number = .71. P-39N-1.

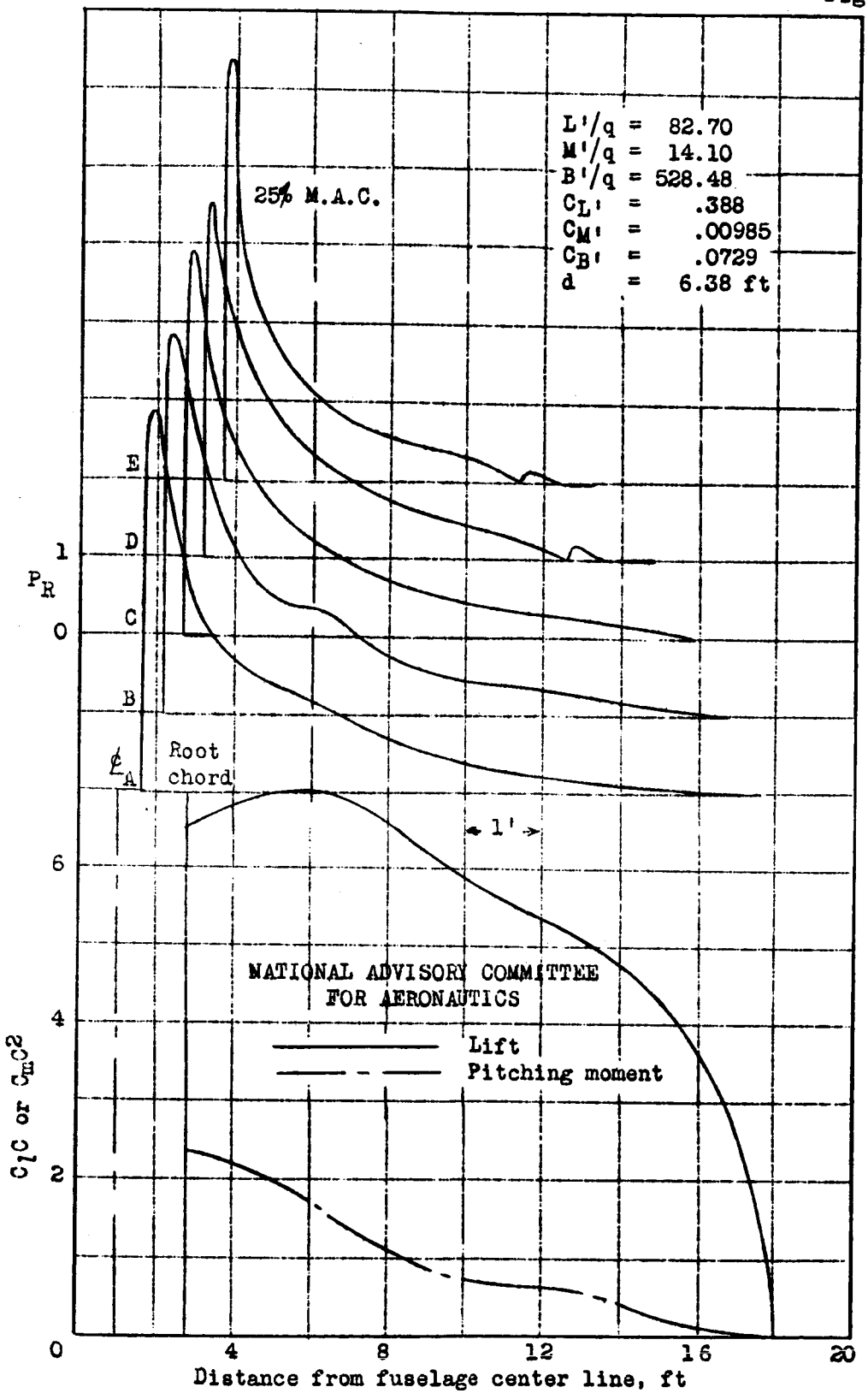

Figure 16.- Continued. (r) Lift coefficient = 1.0, Mach number = .30. P-39N-1.

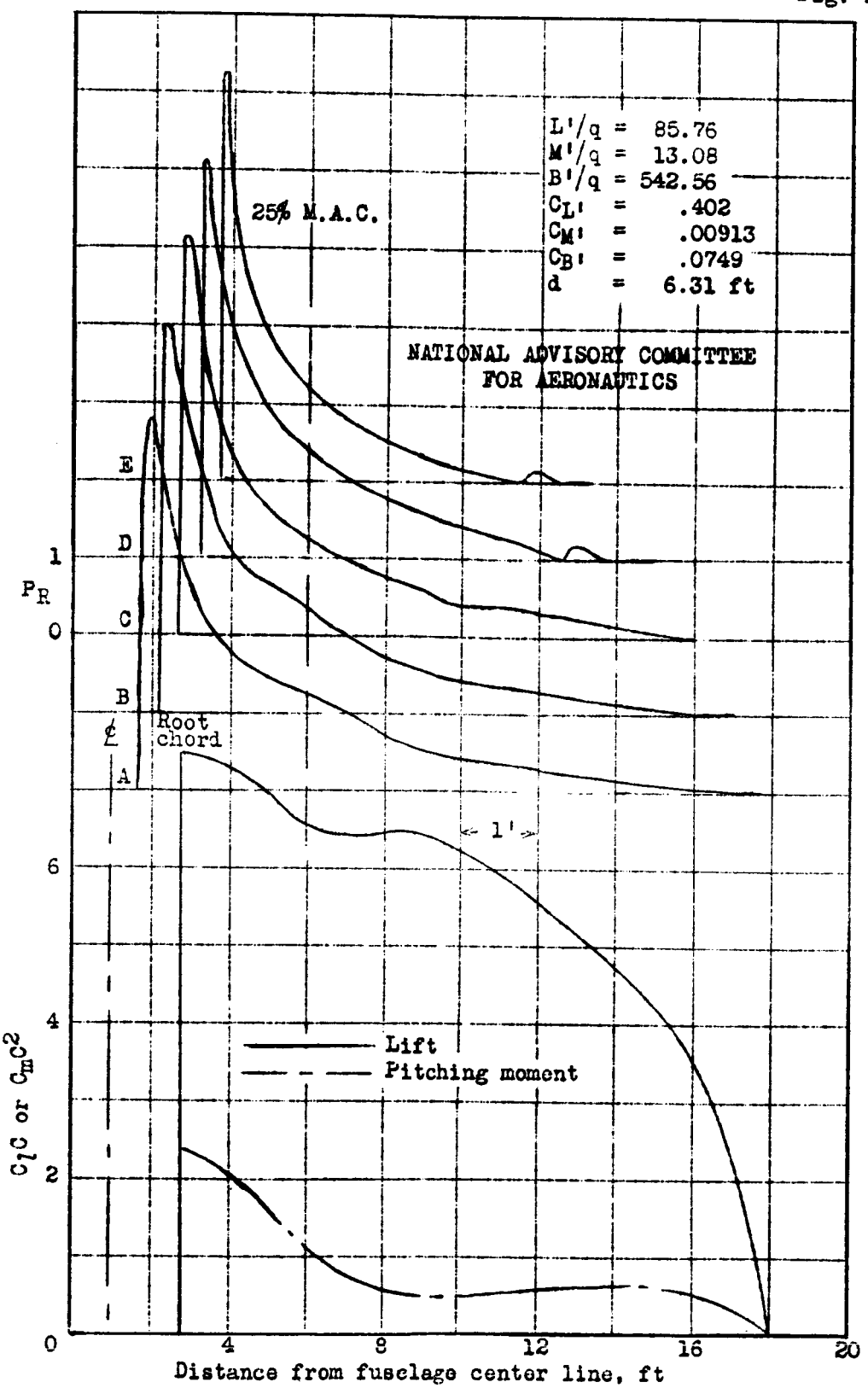

Figure 16.- Continued. (s) Lift coefficient = 1.0, Mach number = .40. P-39N-1.

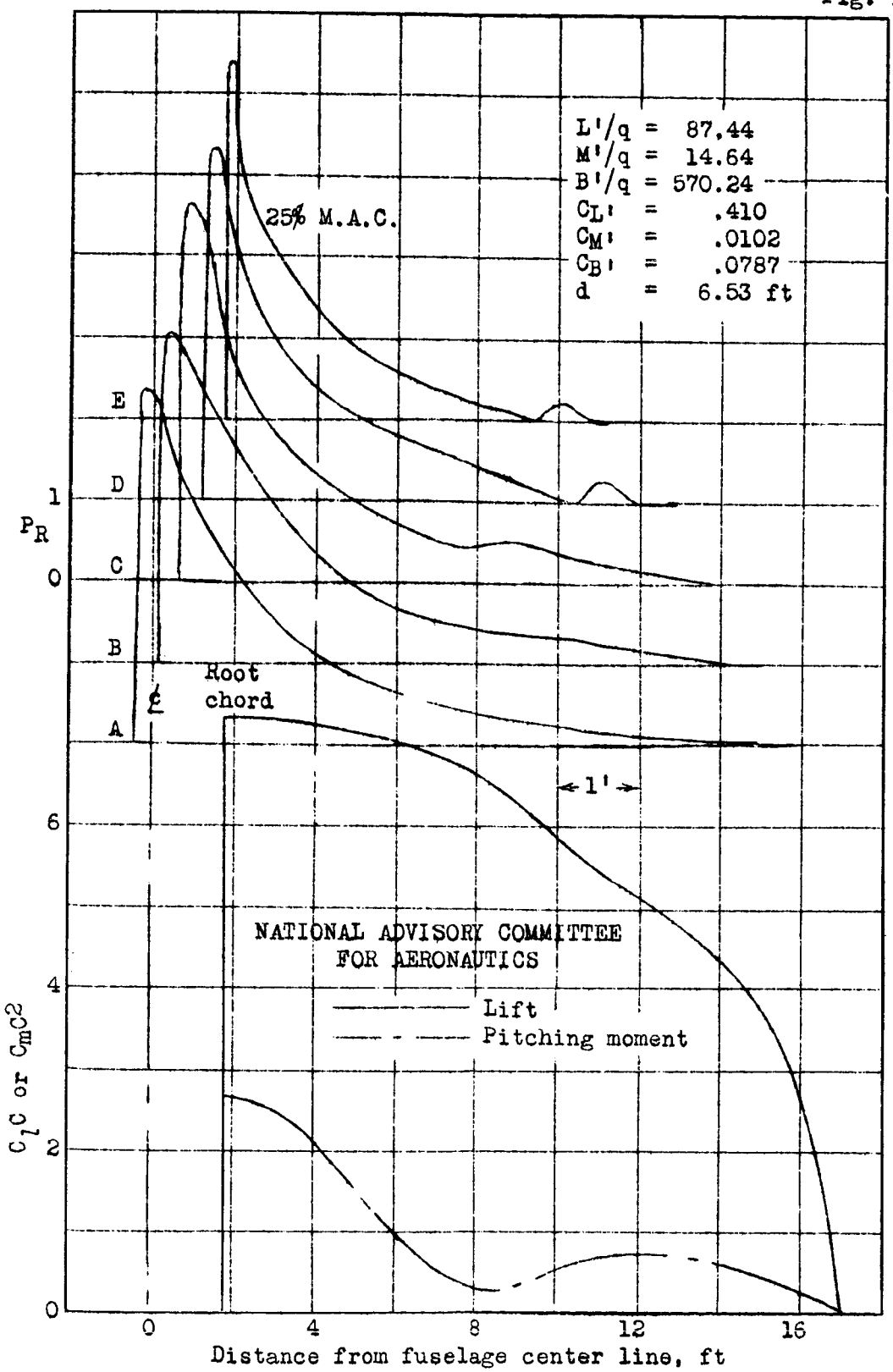

Figure 16.- Continued. (t) Lift coefficient = 1.0, Mach number = .50. P-39N-1.

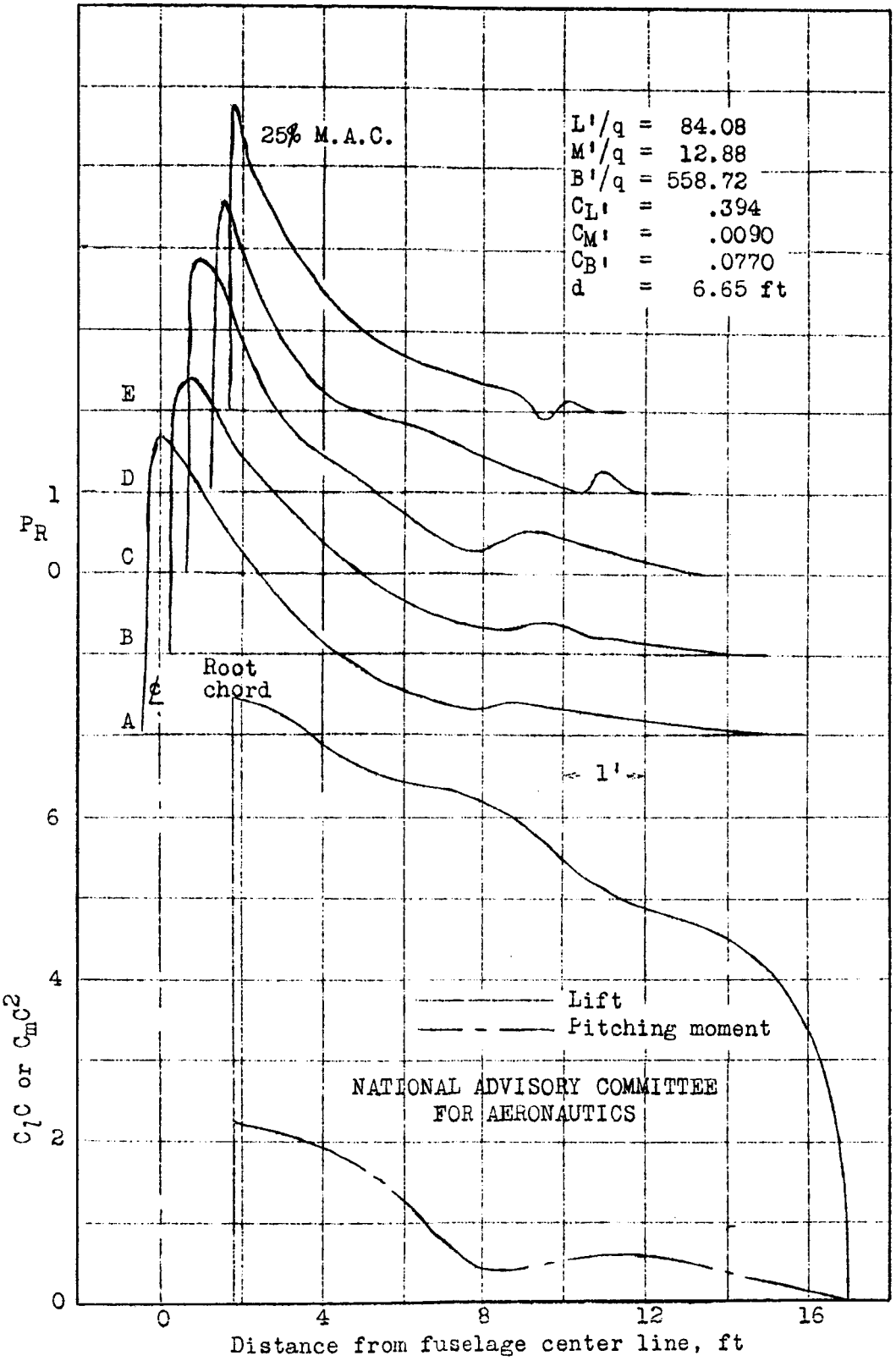

Figure 16.- Continued. (u) Lift coefficient = 1.0, Mach number = .60. P-39N-1.

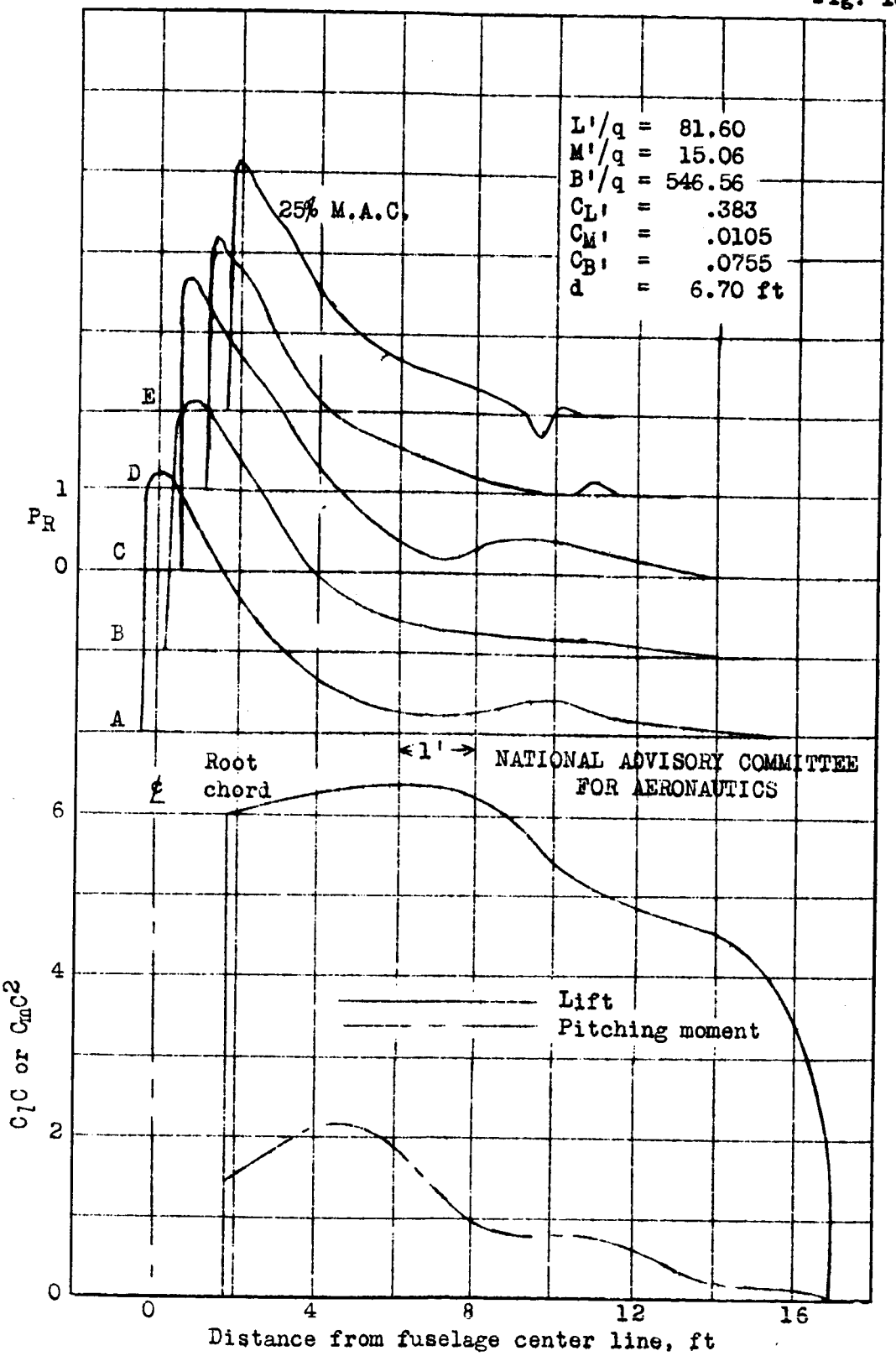

Figure 16.- Concluded. (v) Lift coefficient = 1.0, Mach number = .65. P-39N-1.

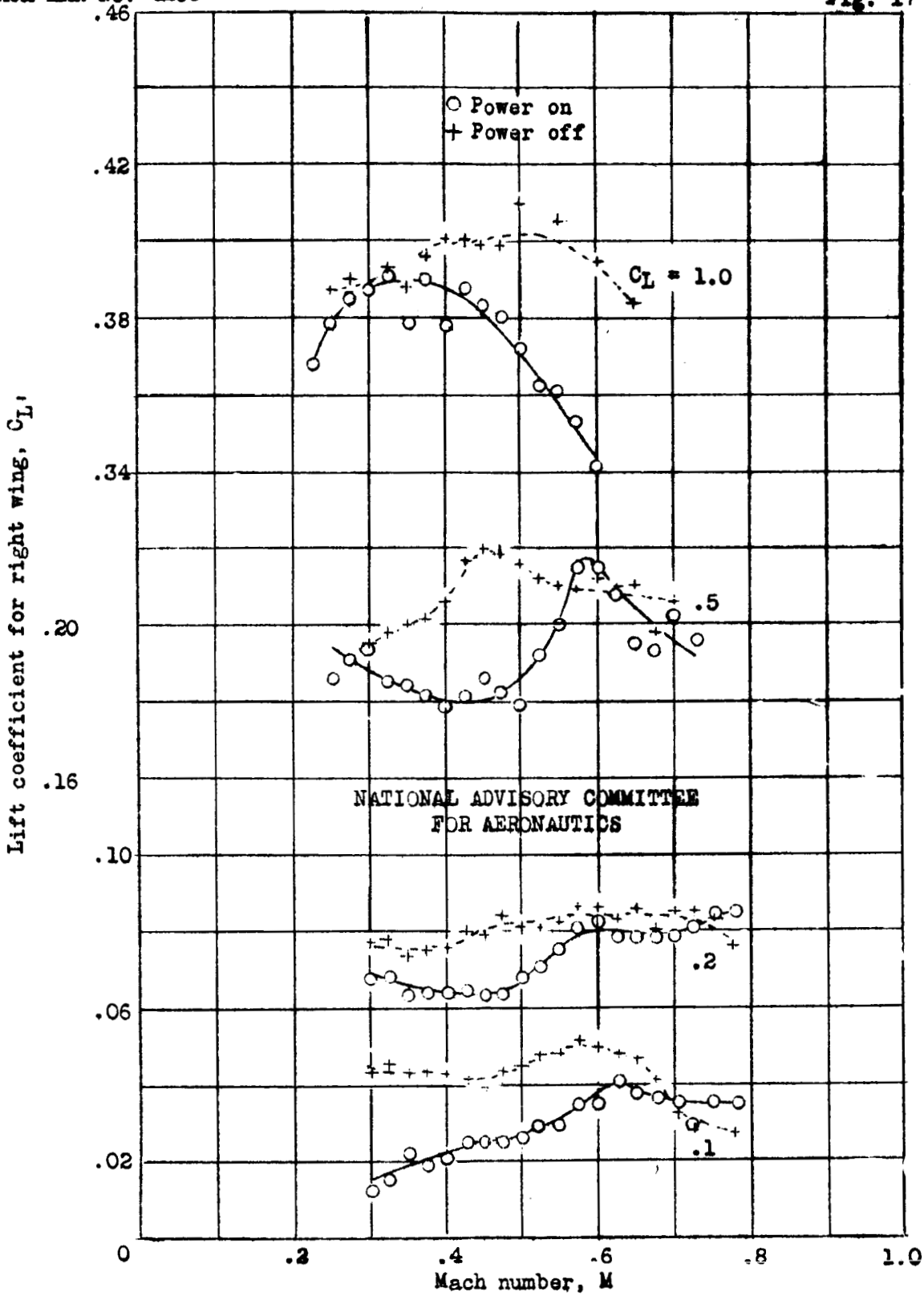

Figure 17.- Variation of right-wing-panel lift coefficient with Mach number. P-39N-1 airplane.

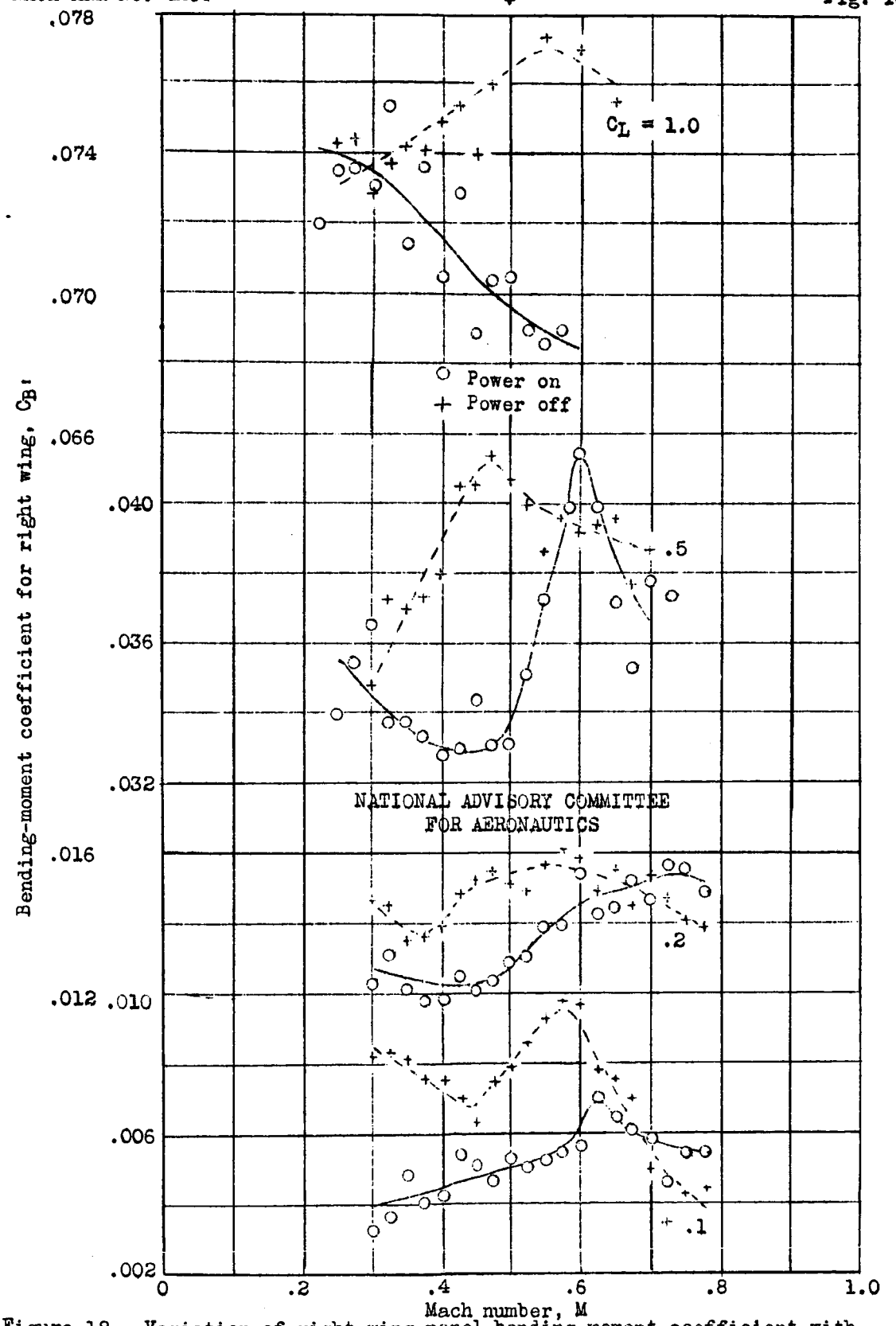

Figure 18.- Variation of right-wing-panel bending-moment coefficient with Mach number. P-39N-1 airplane.

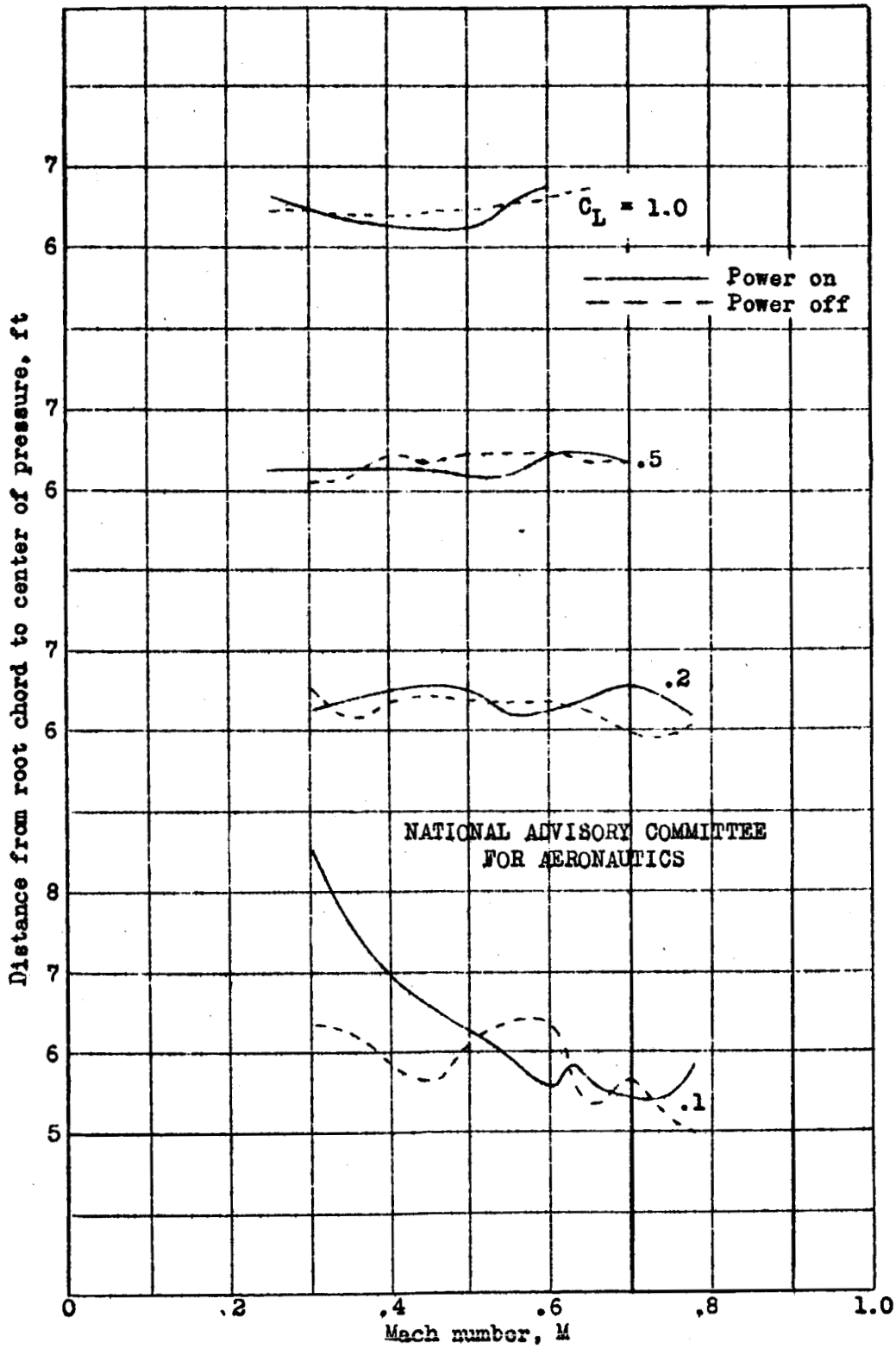

Figure 19.- Variation of lateral distance from root chord to center of pressure of right wing panel with Mach number. P-39N-1 airplane.

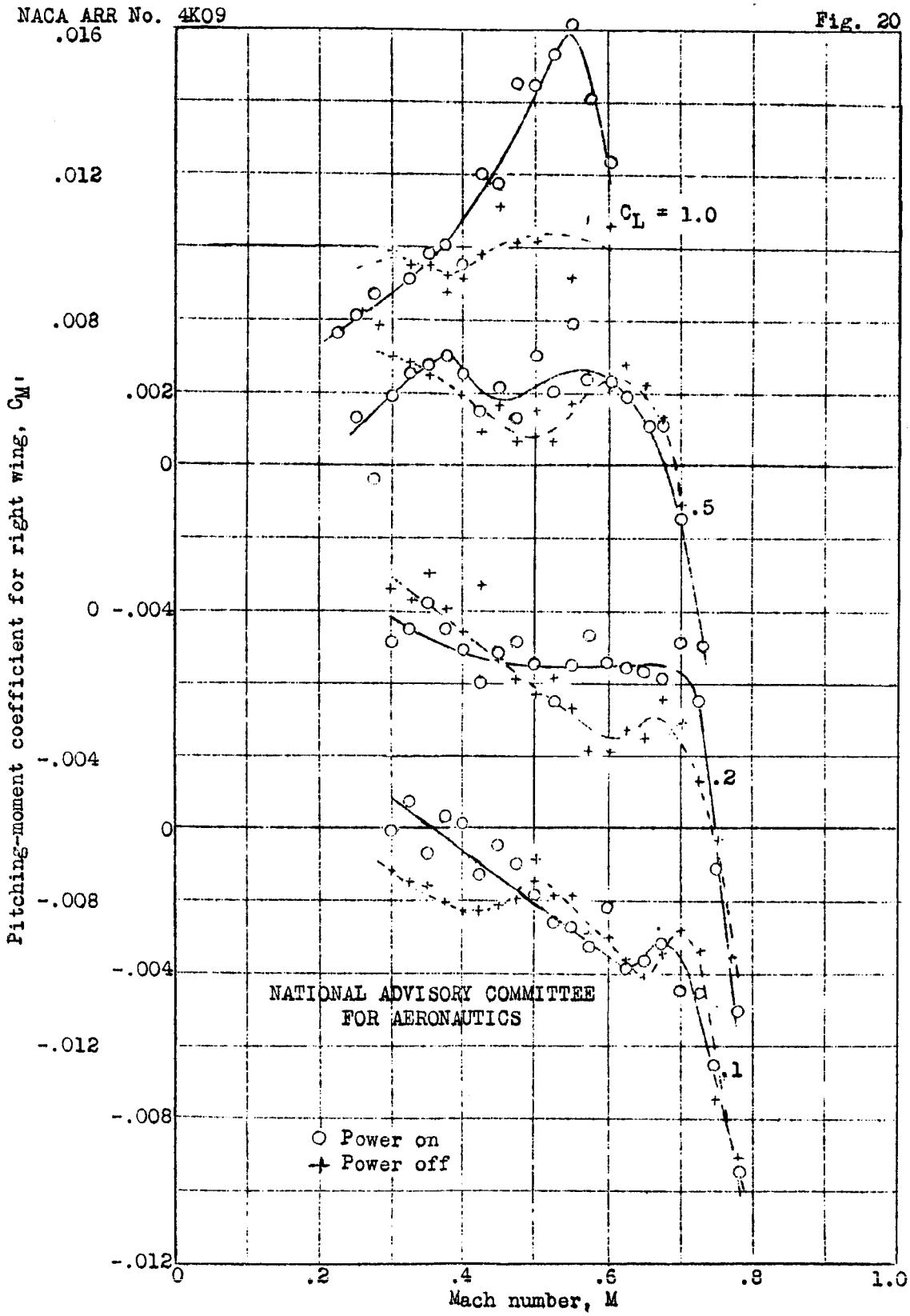

Figure 20.- Variation of right-wing-panel pitching-moment coefficient with Mach number. P-39N-1 airplane.

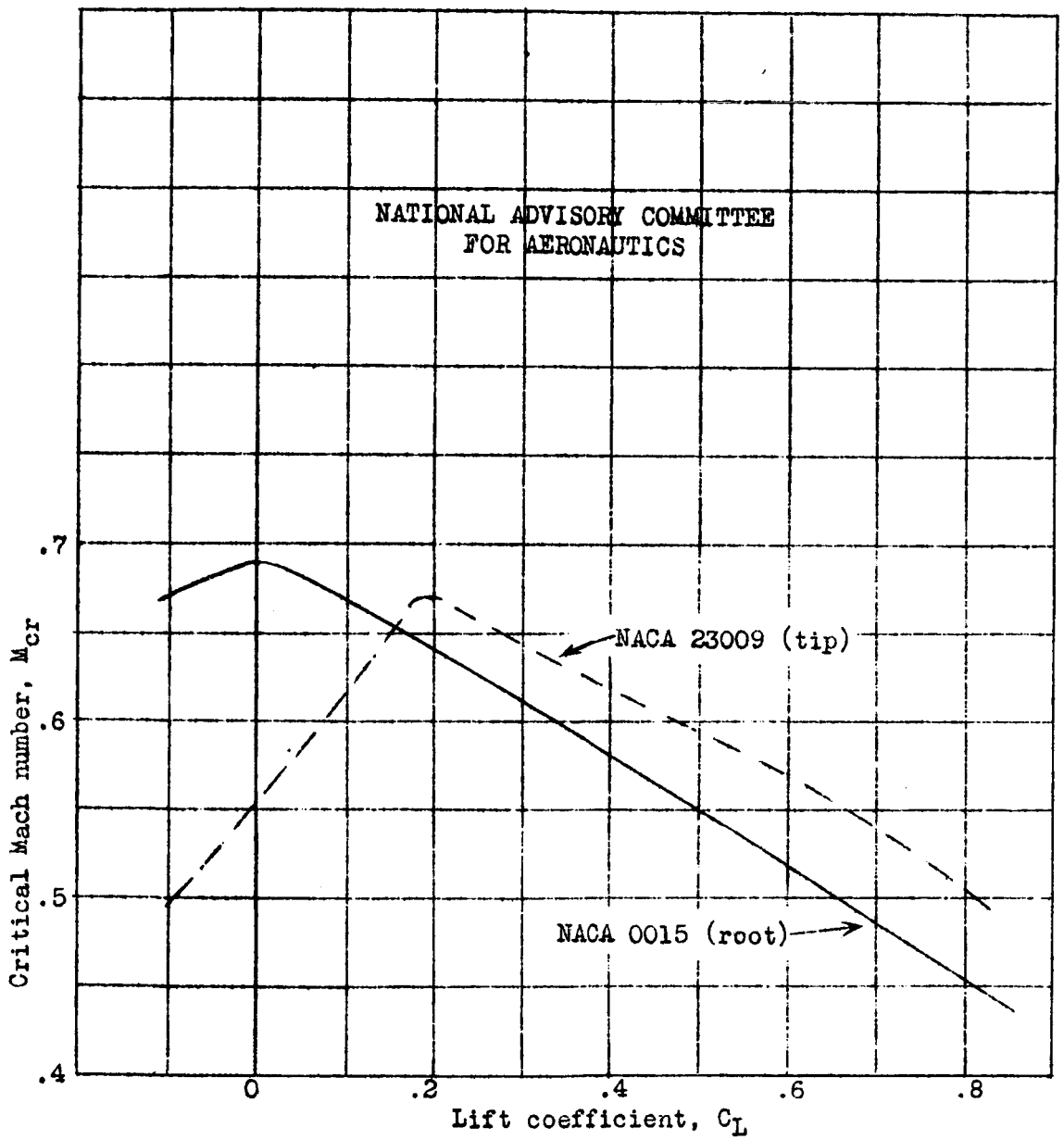

Figure 21.- Calculated values of critical Mach number for the specified root and tip wing sections on the P-39N-1 airplane.

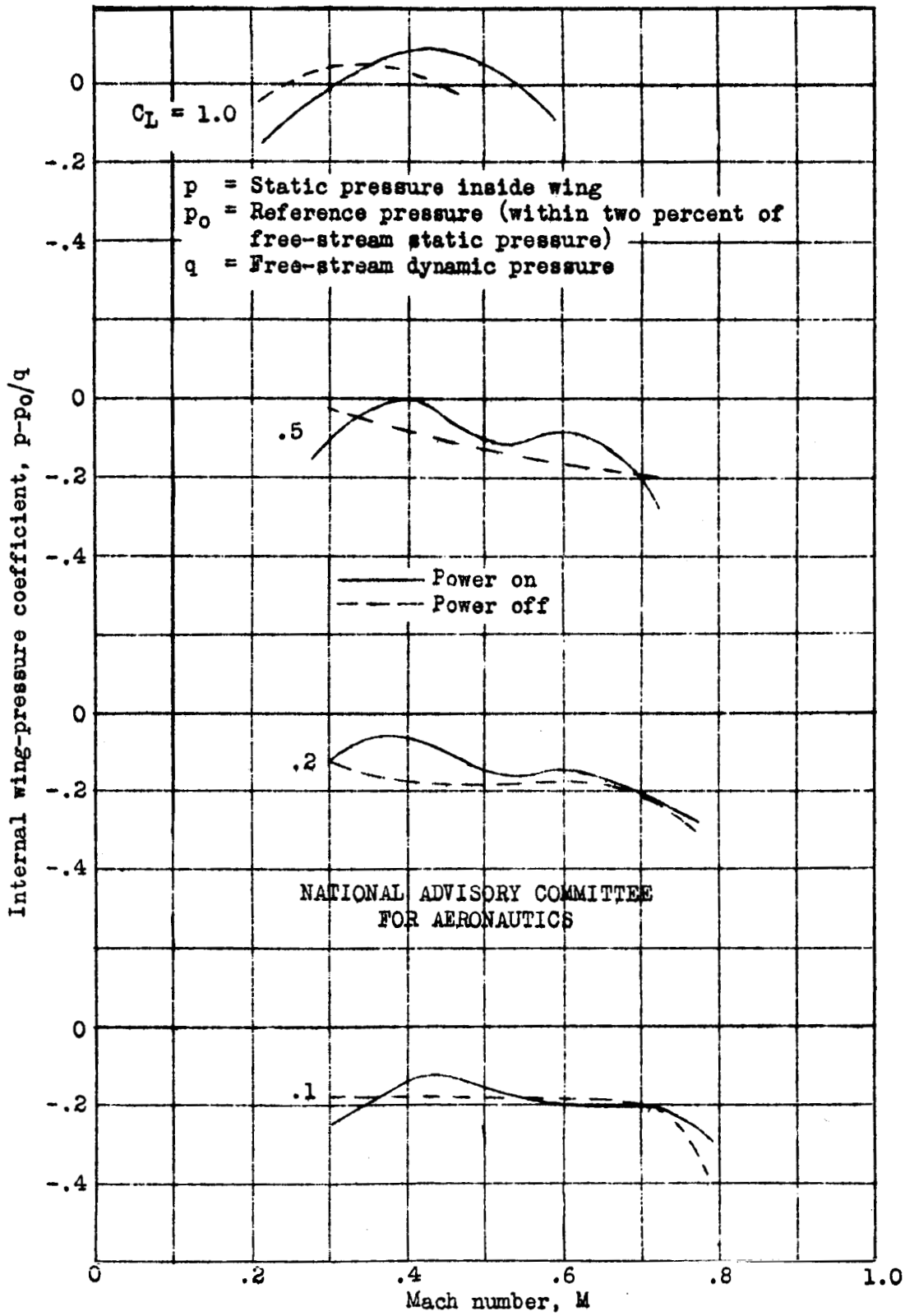

Figure 22.- Variation of wing internal-pressure coefficient with Mach number. P-39N-1 airplane.

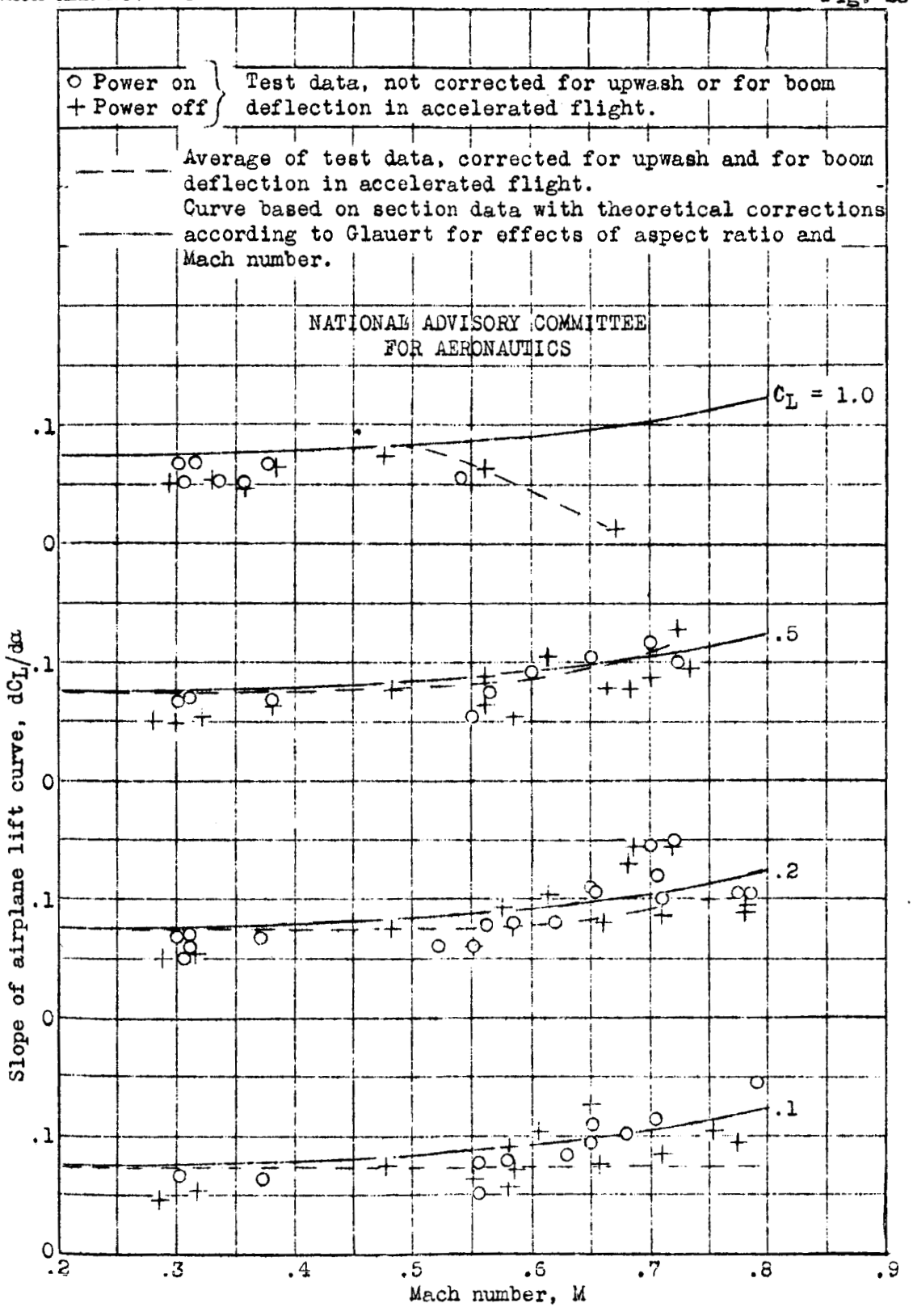

Figure 23.- Variation of slope of the airplane lift curve with Mach number. P-39N-1 airplane.

A-13

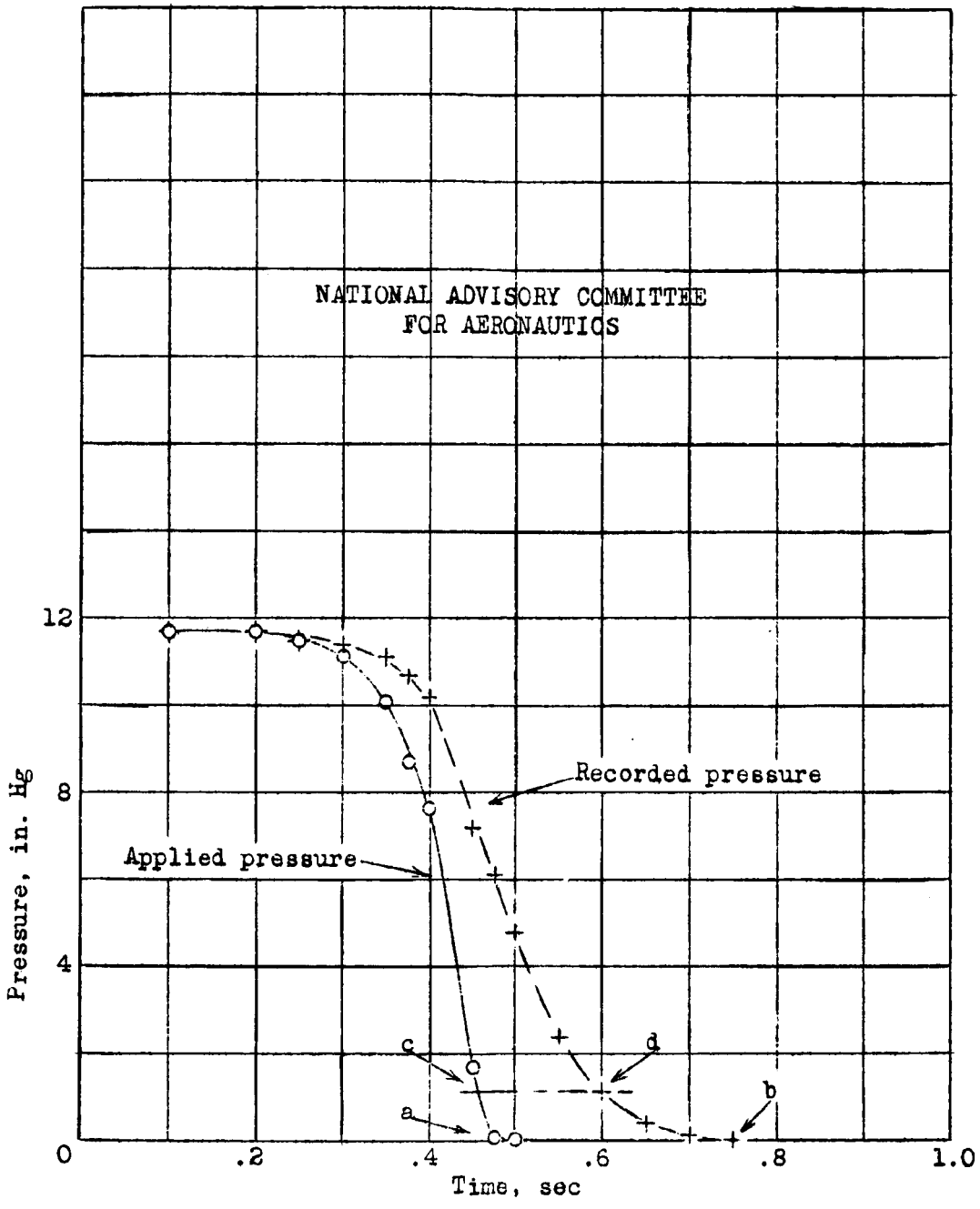

Figure 24.- Time history of pressure lag in typical aileron line. P-39N-1 airplane.

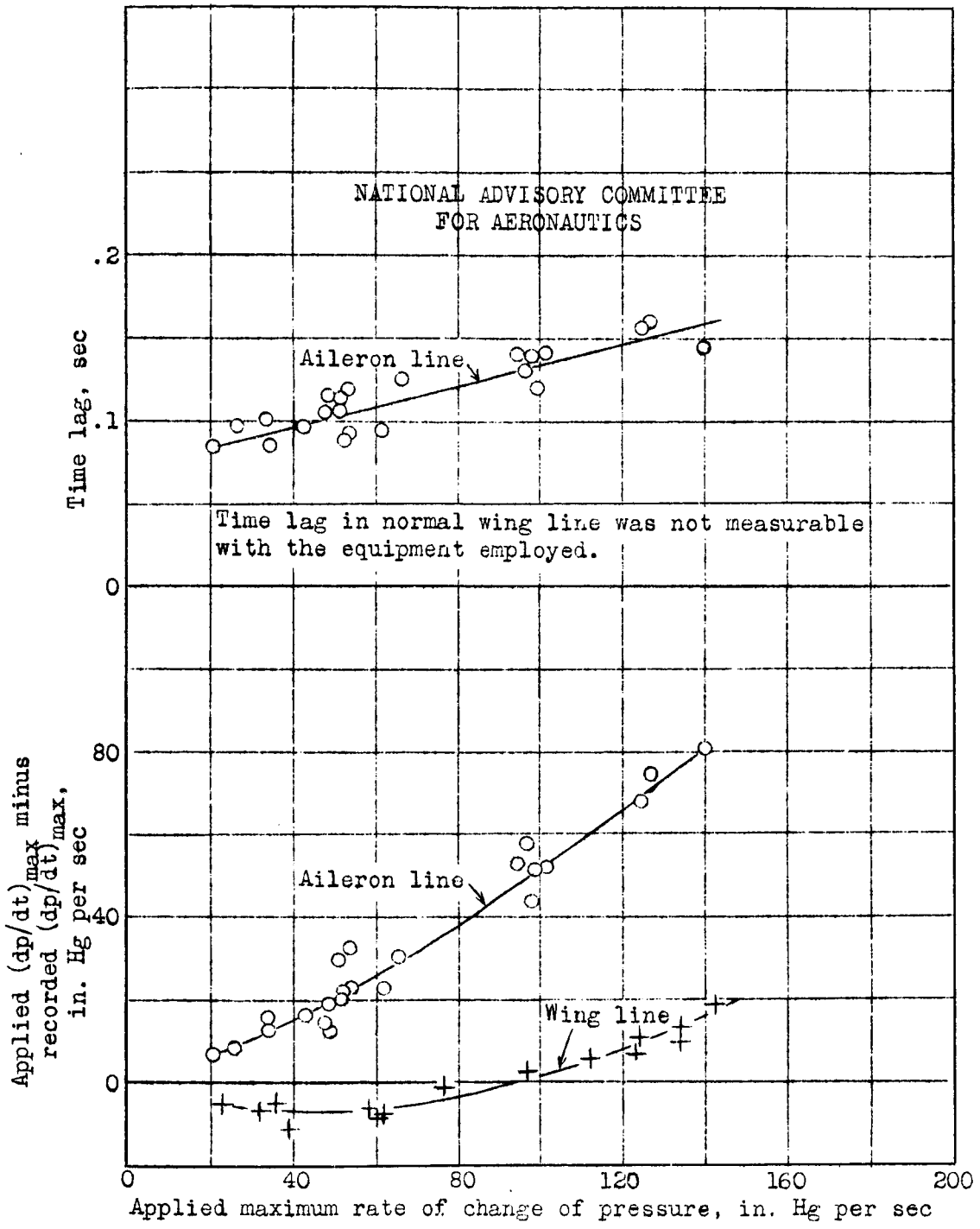

Figure 25.- Lag in typical wing pressure lines. P-39N-1 airplane.